



## Review

**Cite this article:** May PW, Zulkharnay R. 2025  
Diamond thin films: a twenty-first century  
material. Part 2: a new hope. *Phil. Trans. R. Soc.  
A* **383**: 20230382.

<https://doi.org/10.1098/rsta.2023.0382>

Received: 5 February 2024

Accepted: 11 March 2024

One contribution of 8 to a theme issue ‘Science  
into the next millennium: 25 years on’.

**Subject Areas:**

materials science, electrical engineering,  
energy, nanotechnology, quantum engineering

**Keywords:**

diamond, chemical vapour deposition, review

**Author for correspondence:**

Paul W. May

e-mail: [paul.may@bristol.ac.uk](mailto:paul.may@bristol.ac.uk)

Electronic supplementary material is available  
online at [https://doi.org/10.6084/  
m9.figshare.c.7766570](https://doi.org/10.6084/m9.figshare.c.7766570).

Diamond thin films: a twenty-  
first century material. Part 2: a  
new hope

Paul W. May and Ramiz Zulkharnay

School of Chemistry, University of Bristol, Bristol, Bristol, UK

PWM, 0000-0002-5190-7847; RZ, 0000-0002-7420-399X

Nearly a quarter of a century ago, we wrote a review paper about the very new technology of chemical vapour deposition (CVD) of diamond thin films. We now update this review and bring the story up to date by describing the progress made—or not made—over the intervening years. Back in the 1990s and early 2000s, there was enormous excitement about the plethora of applications that were suddenly possible now that diamonds could be fabricated in the form of thin films. Diamond was hailed as the ultimate semiconductor, and it was believed that the few remaining problems would be quickly solved, leading to a new ‘diamond age’ of electronics. In reality, however, difficulty in making large-area diamond wafers and the elusiveness of a useful *n*-type dopant slowed progress substantially. Unsurprisingly, over the following decade, the enthusiasm and funding for diamonds faded, while competing materials forged ahead. But in the early 2010s, several new game-changing applications for diamonds were discovered, such as electrochemical electrodes, the nitrogen-vacancy (NV) centre defect that promised room-temperature quantum computers, and methods to grow large single-crystal gemstone-quality diamonds. These led to a resurgence in diamond research and a new hope that diamond might *finally* live up to its promise.

This article is part of the theme issue ‘Science into the next millennium: 25 years on’.

## 1. Introduction

In the year 2000, we wrote a review paper entitled ‘Diamond Thin Films: A 21st Century Material’ [1] discussing the relatively new subject of diamond chemical vapour deposition (CVD). The review described what was known at the time about the mechanism of deposition—the limitations of the process—and then speculated about how this technology might develop following a few decades of research. It ended by giving a dozen or so promising applications. Nearly a quarter of a century later, the review has accumulated nearly 1000 citations and has become the ‘go to’ paper for new researchers beginning in this field. So, for this special edition of *Phil. Trans. R. Soc. A*, it is timely to update the original review and evaluate whether the technology has advanced as predicted. Through the use of advanced plasma diagnostics and computer simulation much of the fundamental science underpinning the diamond CVD process—some of which was only speculation at the time—has now been confirmed. However, arguably the most important development in this field over the past 25 years is the astonishing diversity of applications that have now emerged for this material, including medical implants, quantum computing, solar energy generation, optics, electrochemistry, particle detectors, ‘everlasting’ batteries and, of course, the capability to fabricate very large single-crystal diamond (SCD) gemstones that are now challenging natural diamonds for the larger share of the jewellery market [2].

Interest and associated research funding for CVD diamond boomed during the 1990s, fuelled by media hype and unrealistic expectations that the next ‘ultimate semiconductor’ material was imminent. However, the crash soon followed. For a decade from about 2000, the failure to achieve *n*-type doping and frustratingly slow progress in the deposition of large-area diamond wafers dampened enthusiasm for the alleged ‘wonder material’. At the same time, competing materials such as SiC and GaN went from strength to strength, and new exciting wonder materials, such as graphene, promised to outshine even diamond in performance. Funding for diamond research dwindled, until around 2010, when scientists and funding agencies began to realize that the competing materials were also having serious problems of their own—graphene, in particular, having been extremely overhyped [3], meaning diamond was back in the game! This was helped by the discovery that the nitrogen-vacancy (NV) centre in diamond (see §9) could act as a single-photon source, which opened up the almost unbelievable prospect of room-temperature quantum computing. Other exciting applications, such as diamond electrochemical electrodes and biosensors, fuelled diamond’s resurgence, and the spectacular success of synthetic diamond gemstones in the worldwide jewellery market [2] drove the long-awaited technological breakthroughs in diamond growth rate, large-area deposition and defect understanding. Diamond has been recently called the ‘Sleeping Beauty’ of semiconductors [4]—showing outstanding properties with respect to other competing materials but never quite matching their performance in actual commercial devices. It may now be the decade that Sleeping Beauty awakens, bringing with it the new hope that diamond may finally live up to its promise.

Currently, there are over 200 research groups studying the growth or applications of CVD diamonds worldwide and as many as 100 commercial companies fabricating diamonds for gemstone or other applications, or utilizing CVD diamonds in novel applications. As a result, the cost of diamonds has fallen rapidly over the past decade. At the time of writing, the typical cost for a freestanding SCD sample ( $4 \times 4 \times 0.5$  mm) from a company such as *Element Six* is approximately \$2000, while that for a larger ( $10 \times 10 \times 0.5$  mm) polycrystalline sample is only approximately \$50–200 depending on quality, while the number of suppliers has increased accordingly (see electronic supplementary material, table S1).

As one might expect for a ‘follow-on’ paper, to avoid unnecessary duplication of content, it is recommended that the reader first become familiar with the original paper [1] before starting this one. It is also worth pointing out that due to page limitations, only a few of the most

important CVD diamond applications are discussed below. However, another recent review covers the vast range of other applications for this material in some detail [5].

## 2. CVD

To recap very briefly, in the CVD process [1,6], a diamond coating is deposited on to the surface of a suitable substrate, for example, a smaller diamond ‘seed’ in the case of gemstone growth, a Si wafer for electronic devices, a quartz window for optics, or a mechanical component for wear applications. This substrate is positioned on a heated stage inside a vacuum chamber and heated to 700–1000°C while process gases are passed over the substrate at a pressure of 20–300 torr. The gas mixture typically consists of a carbon source, such as methane, diluted to a few per cent input mole fraction in hydrogen, although small amounts of other gases such as O<sub>2</sub>, N<sub>2</sub> or dopants such as B<sub>2</sub>H<sub>6</sub> or PH<sub>3</sub> are sometimes added depending on the required product. This gas mixture is energised using either a heated metal (W, Ta or Re) filament placed a few millimetres above the substrate surface or by application of a microwave (MW) discharge in the form of a ‘plasma ball’ that sits above the substrate surface. The thermal or electrical energy deposited into the process gases fragments the molecules to form a chemical ‘soup’ of atoms, radicals, ions and clusters near the substrate surface. Reactive species (mainly H atoms and CH<sub>3</sub> radicals) from this hot gas mixture diffuse to the surface, and if the conditions are correct, they adsorb on to the surface, migrate around and eventually form a continuous layer of diamond. The diamond coating can remain on the surface after growth and be utilized *in situ*, or the substrate can be chemically etched away to leave a freestanding diamond foil or ‘wafer’, or in the case of thick single crystals, undergo further processing (laser cutting and polishing) to produce synthetic diamond gemstones for the jewellery market.

## 3. Methods for production of diamond CVD

In 2000, when the original review was written, the technology required for diamond CVD was only about 10 years old, and four main deposition techniques were in use: hot filament CVD (HFCVD), MW plasma-enhanced CVD (MWCVD), arc-jets (plasma torches) and oxyacetylene welding torches. In the intervening years, both torch methods have largely fallen out of use in the West. Although extremely high diamond growth rates (approx. 1000 μm h<sup>-1</sup>) could be achieved with these systems [7], problems with substrate cooling, poor uniformity over areas greater than approximately 5 × 5 mm<sup>2</sup> and inadequate run-to-run reproducibility meant that these methods fell out of favour compared to the more reliable plasma systems. Nevertheless, the easily accessible, bright, visible emission from these torch systems permitted important fundamental studies to be performed on the gas chemistry and growth mechanisms, using techniques such as optical emission spectroscopy (OES) and cavity ring-down spectroscopy [8–10]. These studies provided early empirical data that would later be essential in developing models of the CVD process (see §4).

In China, it was a different story. Arc-jet plasma deposition systems continued to be developed, and this technology is now considered fully mature and commercialized [11]. A series of direct current (DC) arc jets with powers up to 100 kW [12] were developed for different applications, which are capable of mass-producing polycrystalline diamond wafers of diameters up to 150 mm and thickness of approximately 3 mm. Using this technique, the Chinese company, Hebei Plasma Diamond Technology Co. Ltd, has become the main supplier of freestanding diamond film products in the world.

## (a) HFCVD

This technique remains popular among university research groups, mainly for its low cost, versatility, and especially its ability to deposit diamonds over large areas—something with which most other methods still have difficulty. It is now possible to buy commercial HFCVD reactors that deposit polycrystalline diamond uniformly on to Si wafers of area up to 0.5 m<sup>2</sup> [13], although the low deposition rates (approx. 1 μm h<sup>-1</sup>) mean that thick (greater than 100 μm) large-area diamond films remain rather expensive to manufacture and produce. Smaller HFCVD reactors for sample areas of approximately 100 mm<sup>2</sup> can be built in-house from standard vacuum components for as little as \$20,000, and nowadays many small research groups have their own bespoke diamond HFCVD reactor to study niche research areas. In China, over the past 10 years, HFCVD reactors have been scaled up and modified by biasing the substrate in a technique known as electron-assisted HFCVD [14], together with adopting closely packed filament multi-arrays and short filament-to-substrate distances. As such, HFCVD has become the most important and dominant technique in China for the mass production of thick freestanding polycrystalline diamond films for mechanical and thermal applications [11].

## (b) DC plasmas

These systems were first reported for diamond CVD in 2012 [15], but they remain the ‘poor relation’ among plasma deposition systems, with only a few research groups adopting this as their growth method of choice, mainly at Jilin University in China [16] and in South Korea [17]. DC plasma systems do not require the growth chamber to be a tuned cavity, which is a major drawback with the design of MW plasma systems (see §3d). This greatly simplifies the design of DC reactors and affords the advantage of easier scale-up to larger-area samples. However, the high-power supplies required are expensive, and the growth conditions are not as flexible as those in MWCVD systems, hence their continued relative unpopularity.

## (c) Distributed antenna systems

Rather than use one large plasma source, a number of alternative reactor designs have been developed in the past decade that generate several smaller plasmas distributed in an array or grid over a large area. These distributed plasma reactors have two major advantages over other CVD methods. First, it makes possible very large deposition areas, greater than 1 m<sup>2</sup>. Second, the deposition temperatures (400°C) are typically much lower than those in conventional HFCVD or MWCVD systems, allowing diamond deposition on to substrate materials with low melting points. Indeed, addition of O-containing gases into the feed-gas mixture has been reported to further reduce the growth temperature to 130°C [18]. There are downsides however, the lower deposition temperatures mean that the diamond quality is poor, being mostly nanocrystalline, and growth rates are extremely low (a few 10s of nm h<sup>-1</sup>). Nevertheless, such systems have enabled thin (less than 100 nm) nanodiamond films to be deposited on to large sheets of glass or plastic for use as protective layers—which would be impossible by other methods.

### (i) Linear antenna plasma deposition

This is the most commonly used of these new distributed plasma growth methods, being first reported by a consortium of research groups based in Prague in 2011 [19]. In a linear antenna plasma deposition (LAPD) system, 2.45 GHz MW power is delivered into the growth chamber via several pairs of linear coaxial antennas enclosed in quartz envelopes. These linear plasma sources are arranged parallel to one another a few cm above the substrate holder (figure 1). The use of high-frequency MW pulses and low pressures (approx. 1 mbar) increases

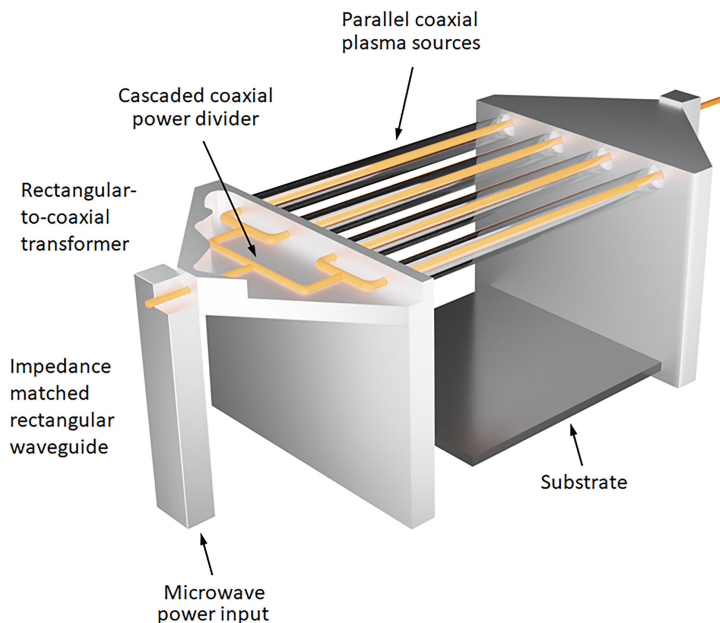


**Figure 1.** Diagram of a LAPD system. Redrawn from [20].

the plasma electron density to  $10^{11} \text{ cm}^{-3}$  [20], while pulsing the plasma power at duty cycles of approximately 30% creates ‘on-off’ cycles that allow the gas dynamics to be altered in a transient manner, while minimising the thermal loads [21].

### (ii) Distributed antenna array MW

A similar deposition process to LAPD, called a distributed antenna array MW (DAAM) system, uses 16 coaxial plasma sources inserted into a square metallic flange in a process chamber and arranged in a  $4 \times 4$  matrix [22]. A 6 kW MW generator is coupled to the system using antennas located in a rectangular waveguide (figure 2). The MW power is divided between the 16 sources, and a discharge is ignited around each source inside the reactor chamber. When the MW power is increased, the plasmas expand and produce a sheet of uniform plasma. The DAAM system allows substrates with sharp edges to be uniformly coated without disturbing the electric field. However, the growth rates and film quality are similar to those deposited by LAPD systems.

### (iii) Surface wave plasma (SWP)

Another new type of system designed for large-area, low-temperature diamond deposition utilizes multi-slot MW antennas and surface wave plasmas (SWPs) [23] (figure 3); SWP reactors use multiple 5 kW, 2.45 GHz MW generators to launch MWs along separate waveguides into which several carefully designed slots have been cut allowing the MWs to access the reactor chamber below. Quartz windows separate the waveguide slots from the vacuum chamber while allowing the MWs to initiate plasmas beneath the slots. Thus, a set of small dense plasmas is formed in a rectangular array allowing substrates of area  $600 \times 400 \text{ mm}^2$  to be coated. The substrate stage is water-cooled, allowing nanocrystalline diamond films to be deposited at temperatures as low as 100–500°C.

Because LAPD, DAAM and SWP systems cannot deposit high-quality diamonds at reasonable rates, they will probably remain niche techniques for researchers primarily focused on large-area, low-temperature deposition of smooth films with high mechanical strength and low residual stress.

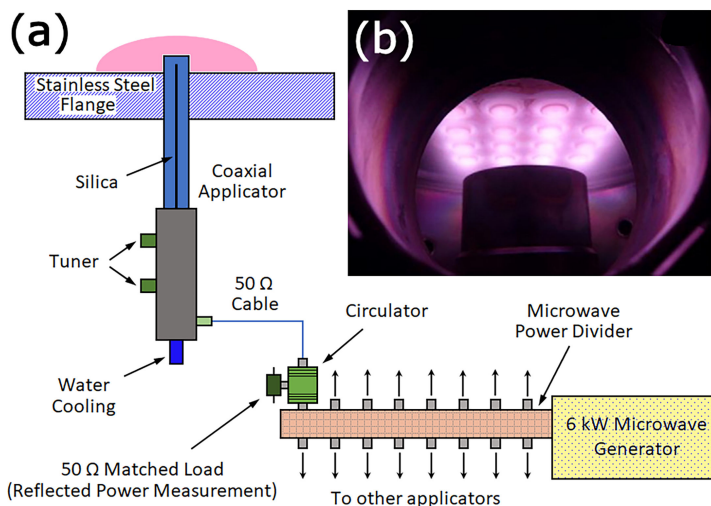


**Figure 2.** (a) Schematic diagram of a DAAM system, redrawn from [22]. MW power is coupled into a rectangular waveguide and is divided equally between 16 applicators (180 W each), which transport the power to the sources within the chamber using coaxial cables. One of the applicators is shown in more detail on the left; the power passes through a matched load into a tuned antenna protected by a quartz coating, igniting a plasma around each source protruding inside the low-pressure reactor. (b) View of the 16 coaxial ignited plasma sources plasma sources inside the DAAM reactor arranged in a  $4 \times 4$  matrix. Photo reproduced with permission from [22].

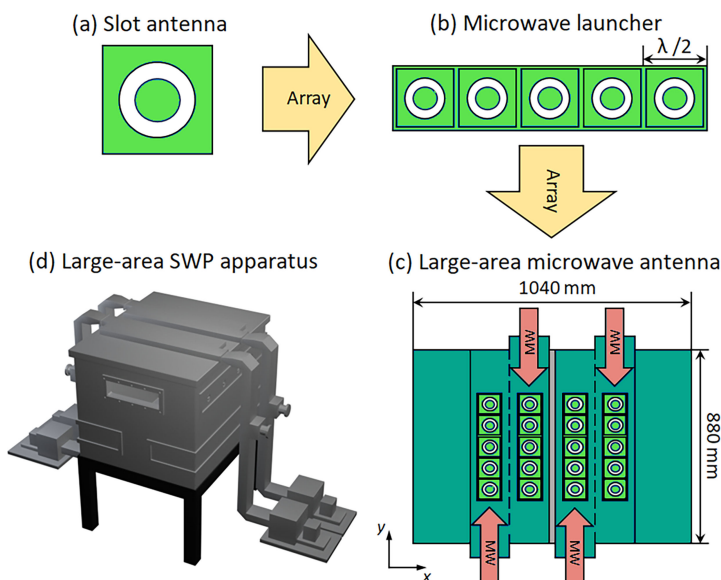


**Figure 3.** Schematic illustrations of components of a SWP reactor, (a) a slot antenna, (b) a MW launcher with five slots, (c) a large-area MW antenna composed of four launchers and (d) large-area SWP reactor. Figure based upon diagram in [23].

### (d) MW plasma reactors

MW plasmas have now become the standard diamond growth technique of choice for most research groups worldwide, despite their high cost. This is due to their compatibility with existing semiconductor fabrication facilities, reproducibility, ability to deposit polycrystalline and SCD with extremely low levels of unwanted impurities (e.g. residual nitrogen

concentrations less than a few parts per billion (ppb) [24,25], ability to use a wide range of process gas mixtures (especially oxygen-containing gases) and the high growth rates that are possible when using high-power reactors. In the past 20 years, driven mainly by the rapid growth in the lab-grown diamond gemstone industry, the technology behind MWCVD has made huge leaps forward [26]. The preferred design of the MW chamber nowadays is the ‘top-hat’ design, formerly known as the ASTEX-style reactor (figure 4), with the older NIRIM-style reactors [1] rarely used nowadays due to issues with Si contamination from the quartz tube. For larger substrates, ‘clam-shell’ reactors are also popular as they provide easier access to the growth chamber. Although most MW systems currently use 5–6 kW power supplies, the commercial requirements for faster growth rates and larger areas have led to greater-volume MW systems being produced with power supplies up to 100 kW [11]. Because MWCVD requires the deposition chamber to be a resonant cavity for efficient transfer of energy from the MWs to the process gases, the chamber size depends inversely on the frequency of MWs used to generate the plasma. To achieve the necessary power densities over larger areas, the MW frequency is often lowered from 2.45 GHz to 915 MHz, allowing the size of the MW resonant cavity to increase accordingly.

The next important and imminent development in MWCVD technology will be the use of MW solid-state power supplies (SSPS), which, although being slightly less energy efficient than the current magnetron-tube technology, offer a number of advantages. First, for a cost approximately 50% higher than a standard MW magnetron tube, SSPSs provide higher stability (fewer fluctuations in the plasma means fewer growth defects) and a significantly longer lifetime (20–30 years compared to approx. 5 years for a magnetron). However, their main benefit is seen in factories with multiple MWCVD reactors in close proximity. As well as the main MW frequency, magnetron tubes also generate unwanted harmonics that vary from tube to tube. These harmonics can perturb the operation of other nearby magnetrons, causing plasma instabilities and fluctuations in all the plasmas in a CVD factory. To overcome this problem, large CVD facilities use special MW filters or costly uninterruptible power supply circuitry on every reactor to block the interference. In contrast, SSPSs generate only a single pure MW waveform with no harmonics and so do not require an uninterruptible power supply. SSPCs began to enter the market from several manufacturers (e.g. Sairem, Muegge) in 2023, with higher power (6 kW and above) promised to become available within a few years.

MWCVD is by far the most widely used deposition technique in China for diamond *films*. It is used for the growth of the highest-quality diamond films required for electronic, thermal, optical and quantum applications. Chinese lab-grown diamond gemstones currently make up approximately 50% of the worldwide market for synthetic diamond jewellery—and although the high-pressure high-temperature (HPHT) method [11] is the technique of choice for the majority of industrial mass production of SCD in China, MWCVD is preferred for the largest and purest gemstones [11]. At first, the thousands of MWCVD reactors required for this huge endeavour were imported into China from companies such as Plassys (France), iPlas (Germany) and Seki (Japan). But cheaper home-made MWCVD diamond deposition systems were quickly developed by Chinese manufacturers such as Uniplasma (Shenzhen), DMT-Diamond (Xian), Three Three Zero (Chengdu), Heuray Microwave (Chengdu) and Tanfangcheng (Carbon Equations, Shanxi), and these now comprise 50% of the MW growth systems in China [11].

## 4. The chemistry of CVD diamond growth

The ‘standard model’ for diamond growth that was devised in the 1990s [27,28] has stood the test of time and has proven to be an accurate description of the diamond CVD process. This model still underpins our understanding of diamond growth today. The model assumes that because CVD growth temperatures (approx. 1000 K) are below the Debye temperature of diamond (approx. 2240 K), the bulk diamond lattice cannot spontaneously rearrange itself into the more thermodynamically favourable graphite structure. Furthermore, the carbon atoms at



**Figure 4.** An example of a top-hat MWCVD reactor (Seki model SDS6380). This reactor has power supplies up to 5 kW (at 2.45 GHz) and is capable of depositing polycrystalline diamond films, SCD diamond plates or SCD gemstones at high rates. The chamber is water-cooled, with a substrate platen capable of accommodating samples up to 50 mm in diameter. Photo courtesy of Philippe Bergonzo, Seki Diamond Systems [13].

each surface are (nearly) all terminated with H, which eliminates any ‘dangling bonds’ that would otherwise cause the surface to restructure into more stable, graphitic structures.

In the growth chamber, the thermal energy from the hot filament or MW energy from the MW power supply dissociates  $H_2$  into H atoms, which then react with the hydrocarbons present in the gas mixture to create a complex chemical soup of hydrocarbon species. These include neutral molecules and reactive carbon-containing radicals, in particular  $CH_3$ . The H atoms also react with the hydrogens in the C–H bonds that terminate the diamond surface carbon atoms, abstracting the H (to reform  $H_2$ ) and in doing so creating surface radical sites. The most likely fate for these surface radicals is that another gas-phase H atom will attach to it, reforming the stable surface. Occasionally, however, a  $CH_3$  will attach to the surface radical site instead. If there are other nearby surface radical sites, the adsorbed  $CH_3$  can migrate across the surface until it finds a diamond step-edge, to which it attaches, thereby adding one more carbon to the diamond lattice. Any non-diamond  $sp^2$  carbon species that adsorb are quickly etched back into the gas phase by the H atoms that continually strike the surface. H atoms etch  $sp^3$  carbon approximately 20 times slower than  $sp^2$  carbon, so all non-diamond carbons are swept off the surface, while  $sp^3$  carbons survive long enough to propagate the diamond structure.

Although the standard model is still fundamentally valid, our understanding of the mechanisms involved in diamond CVD has advanced greatly over the past 20 years, as reviewed in detail by Butler *et al.* [29]. This is mainly due to the use of sophisticated *in situ* diagnostics of the growth environment, using various non-invasive spectroscopic techniques such as optical emission [30], cavity ring-down [31] and direct line-of-sight absorption methods [32,33], as well as more intrusive methods such as mass spectrometric sampling from the plasma [34]. Studies such as these provided key quantitative data about the spatial distribution and concentrations of many of the gas-phase species within hot-filament, MW-plasma and DC arc-jet reactors. These values enabled the development of accurate three-dimensional (3D) models of the chemical processes and gas dynamics in the growth chamber under CVD

conditions, which, in turn, made it possible to estimate similar data for the species that are less amenable to spectroscopic analysis (such as the key  $\text{CH}_3$  radical).

In addition, individual gas-phase and gas-surface reactions, particularly for the diamond  $\text{C}(100):\text{H}$  ( $2 \times 1$ ) surface, were simulated at the molecular level by quantum-mechanical codes such as density functional theory (DFT) [35]. These enabled potential reaction pathways to be studied (figure 5), determination of the relative stability of surface adsorbates [36], the role of dopants in the growth process [37–39] and the function of different reactants and mechanisms in growth [40]. The data from these various experimental measurements and computer simulations were then combined into macro-scale computer models of the whole CVD process, enabling processes such as surface migration, nucleation and step-edge growth to be predicted [41]. More recent kinetic Monte Carlo (kMC) models [42,43] (figure 6) have predicted growth rates, crystallite morphology, etch-pits and the role played by an immobile ‘critical nucleus’ in the initiation of a new diamond layer.

Although the standard growth model is well accepted, there are still some aspects of the mechanism that remain controversial or unresolved. A detailed discussion of two of these issues is given in the electronic supplementary material, but a summary of the important points is provided in the next two sections.

### (a) The $\text{C}_2$ controversy

The first controversial issue concerns the importance, or otherwise, of the  $\text{C}_2$  radical as a growth species. Key to the standard model is the idea that the main growth species are  $\text{CH}_x$  ( $x = 0\text{--}3$ ) and, in particular, the methyl radical,  $\text{CH}_3$  [28], which is supported by a wide range of direct and indirect evidence. These ideas were challenged, however, in 1994, when a paper reported that diamond films could be grown in a MW plasma using a mixture of Ar and vapourised  $\text{C}_{60}$ , i.e. with apparently no H present [44]. The new type of diamond film, termed ultrananocrystalline diamond (UNCD), consisted of approximately 4 nm diamond crystallites, and it was suggested that with allegedly no H present, a different growth mechanism must be operating to that for normal CVD diamond. In the absence of  $\text{CH}_3$ , the  $\text{C}_2$  radical was suggested as the growth species. Indirect evidence was presented for this contentious view in that the plasma was bright green in colour due to emission from the bright Swan bands of the  $\text{C}_2$  radical [45], in contrast to the lilac colour of traditional  $\text{CH}_4/\text{H}_2$  plasmas, while DFT calculations showed that  $\text{C}_2$  radicals were able to insert directly into surface dimers [46].

However, in the few years following these first reports of ‘H-free diamond growth’, no research groups were able to reproduce the results using the Ar/ $\text{C}_{60}$  recipe. In all cases, UNCD films were successfully deposited *only* when trace amounts of  $\text{H}_2$  were added to the Ar/ $\text{C}_{60}$  gas mixture, or alternatively using Ar/ $\text{CH}_4$  mixtures that produce H atoms upon fragmentation—otherwise the films were graphitic. This suggested that maybe there were trace amounts of  $\text{H}_2$  from an unknown source present in the original Ar/ $\text{C}_{60}$  experiments. Cavity ring-down spectroscopy was used to measure the absolute concentration of  $\text{C}_2$  in the plasma during UNCD growth, and this was found *not* to correlate with the film growth rate [47]. Experimental and modelling results of the gas-phase concentrations during UNCD growth showed that, although the concentration of  $\text{C}_2$  was high in the centre of the plasma (and gave rise to the bright green emission), its concentration fell by many orders of magnitude close to the cooler diamond surface [48] and was insufficient to account for the observed growth rate.

Nowadays, the  $\text{C}_2$  growth mechanism has largely been discounted as a viable mechanism for UNCD growth—or for the growth of any form of diamond [49]—although it is still sometimes cited in papers! However, the role of  $\text{C}_2$  (and the more abundant  $\text{C}_2\text{H}$ ) in renucleation and defect formation is still very much a possibility.

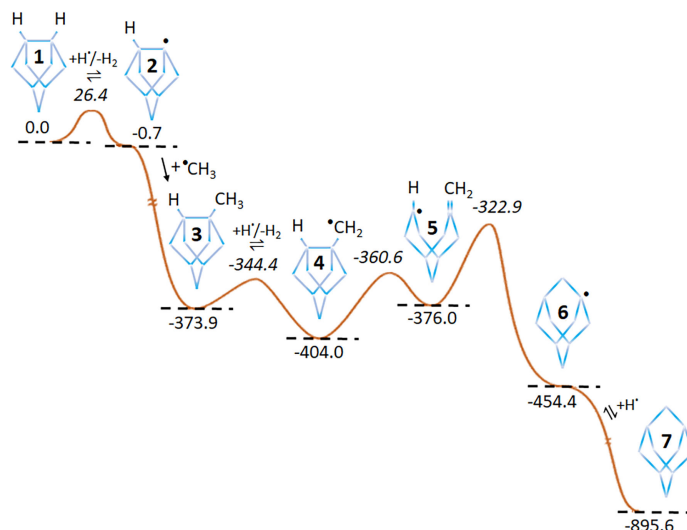


**Figure 5.** Series of elementary steps by which an incident  $\text{CH}_3$  radical can insert into a C–C dimer bond on the C(100):H ( $2 \times 1$ ) surface. The respective minima (normal font) and transition state (in italics) energies are in  $\text{kJ mol}^{-1}$  relative to that of structure 1. The dots indicate the location of a radical group, i.e. a ‘dangling bond’ with an unbonded electron. Redrawn using data in [29].

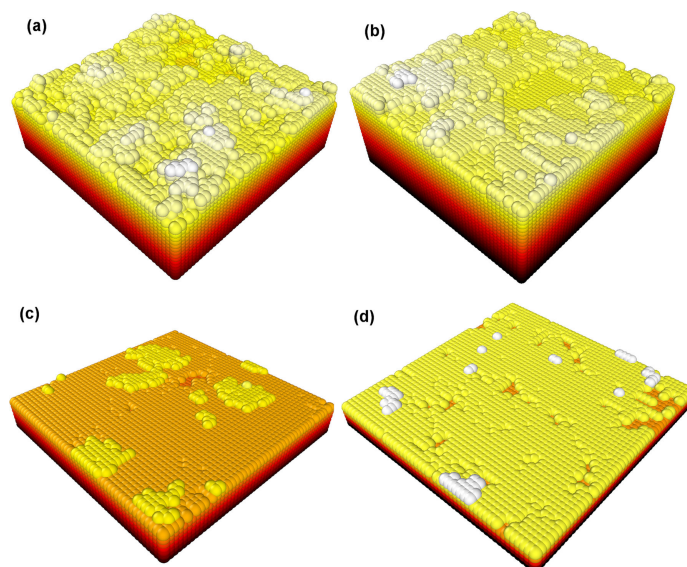


**Figure 6.** 3D projections of the surfaces generated by a 3D kMC model representing the different types of diamond growth resulting from different process conditions. More details of these diamond film varieties can be found in §5. (a) UNCD, with no crystal faces visible as a result of continual random renucleation. (b) Nanocrystalline diamond (NCD), with some small terraces appearing (i.e. nanocrystallites) as a result of a layer-by-layer growth coupled with renucleation. (c) Microcrystalline diamond (MCD), where layer-by-layer growth dominates leading to large micron-sized faceted crystallites. (d) SCD, where growth is now entirely by layer-by-layer growth. The layers have been coloured to make it easy to distinguish individual layers. Reproduced with permission from [42] under the Creative Commons CC BY 3.0 licence.

## (b) The nitrogen effect

The second controversial issue regarding diamond growth involves the so-called catalytic role played by nitrogen. Many studies have shown that even *trace* amounts of  $\text{N}_2$  in the process

gas mixture significantly increase the growth rate from MW-activated  $\text{CH}_4/\text{H}_2$  gas mixtures, sometimes by a factor of 10 or more [50,51]. The morphology of the growing diamond surface is also modified by the presence of nitrogen in the gas mixture, which encourages the preferential formation of flat, square {100}-faceted crystals in the case of polycrystalline diamond films. Excess nitrogen in the process gas mixture, however, produces smaller and less well-oriented surface facets. With further increases in gas-phase nitrogen concentration, the films become nanocrystalline or even graphitic [52,53]. For homoepitaxial growth of SCD, nitrogen in the input gas mixture has been shown to promote macroscopic step-bunching (as shown in figure 7) and disrupt growth on all but the {100} face of an SCD seed [54].

To avoid these issues, in the interests of process control and reproducibility, diamond researchers are now far more careful to control unwanted  $\text{N}_2$  (and other) impurities in the gas mixture. It is now common to add high-vacuum turbopumps to CVD reactors to reduce the chamber base pressure to less than  $10^{-6}$  mbar prior to diamond growth, along with the use of process gases with extremely high purity. Such careful control has allowed electronic-grade SCD films to be fabricated which contain N concentrations of less than 0.1 ppb [24].

This so-called ‘nitrogen effect’—the addition of tiny amounts of  $\text{N}_2$  to the process gas mixture causing dramatic changes to the growth rate and morphology—is still not fully understood. Indeed, nitrogen has sometimes been described as acting as a ‘catalyst’ in the growth, due to a small concentration causing a large effect, but this term is not strictly correct as the gas-phase nitrogen is not unchanged in the reaction—some small fraction ends up incorporated in the film. So how does the usually inert  $\text{N}_2$  molecule cause such huge effects?

To answer this, a combination of experimental studies (such as laser absorption and OES) and computer modelling of MW-activated  $\text{N}_2/\text{H}_2$  and  $\text{NH}_3/\text{H}_2$  plasmas revealed that the hot plasma environment could create excited-state  $\text{N}_2$  species [55,56]. Some of these excited-state  $\text{N}_2$  molecules have sufficient energy that their reactions with other gas-phase species or with the diamond surface break the strong  $\text{N}_2$  triple bond. Thus, unreactive  $\text{N}_2$  is converted to more reactive N-containing radical species such as N atoms and  $\text{NH}$ ,  $\text{NH}_2$  and  $\text{CN}$  radicals, which can now participate in the diamond CVD process.

Theory suggests that these reactive N-containing species should be able to insert into a C–C dimer bond on the  $\text{C}(100):\text{H}$  ( $2 \times 1$ ) surface via a ring-opening/ring-closing reaction mechanism [57] analogous to that shown earlier in figure 5 for the case of  $\text{CH}_3$  addition. These reactions provide viable routes for N incorporation into substitutional sites in the diamond lattice, but they do not explain the unusually large effect that N has on growth rates and morphology.

Theoretical calculations have been used to investigate a number of possible mechanisms. The first suggests that adsorbed  $\text{NH}$  species at different step edges on the  $\text{C}(100):\text{H}$  ( $2 \times 1$ ) surface enhance the binding of gas-phase  $\text{CH}_3/\text{CH}_2$  groups at these locations [58]. A second suggestion is that the additional electron density provided by a buried near-surface N atom weakens any nearby surface C–H bonds. This enhances the rate of the H-abstraction step that creates the surface radical site necessary for  $\text{CH}_3$  radical addition [59]. Other mechanisms explain the apparent ‘catalytic’ nitrogen effect as a consequence of a layer-by-layer growth mechanism growth model in which the rate-limiting step is the nucleation of a new layer. Initiation of a new layer requires the creation of a ‘critical nucleus’—an immobile surface feature with a low etch rate, which acts as a starting point for subsequent rapid lateral growth. Indeed, Monte Carlo models using step-flow growth conditions that include such critical nuclei have demonstrated tenfold enhanced growth rates [42,60]. Butler & Oleynik [61] suggested that adsorbed  $\text{CN}$  might act as just such a critical nucleus because it cannot undergo the  $\beta$ -scission reaction responsible for trimming longer-chained hydrocarbons from the diamond surface (see electronic supplementary material, fig. S1). Hence, it only takes a single  $\text{CN}$  adsorbate across an entire surface composed of billions of carbon atoms to initiate a new layer, which explains the apparent catalytic effect. A similar mechanism involving the critical nucleus being a lone C–N dimer sitting among the thousands of C–C dimers on the flat (100) surface was recently

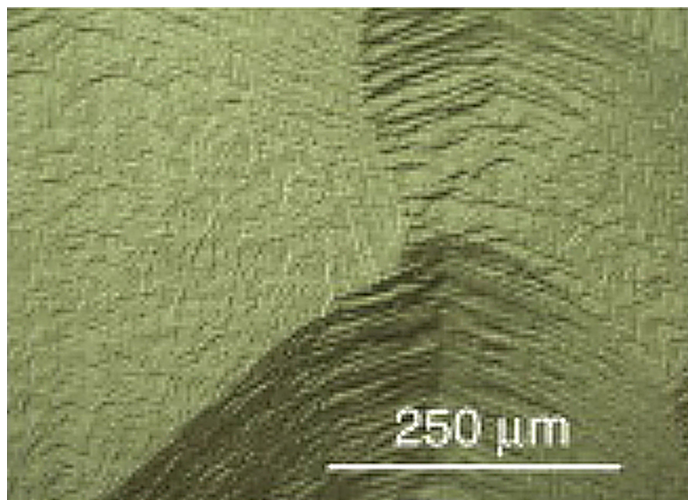


**Figure 7.** SEM image showing macroscopic step-bunching on the surface of an SCD sample grown using nitrogen-containing gas mixtures. Reprinted with permission from [51].

proposed by Oberg *et al.* [62]. It remains unclear which of the many proposed mechanisms is responsible for the nitrogen effect, or whether it is a combination of several of them.

### (c) Remaining issues in CVD diamond growth

Despite the continued success of the standard model of diamond growth and the updates and improvements made to it over the past 20 years, there are still a number of details about the growth mechanism that remain elusive. Unfortunately, research has almost stopped in this fundamental area, partly as a result of the community and funding agencies believing (incorrectly) that the growth mechanism was essentially ‘solved’, but also because, after 20 years of research, funding agencies are now focusing on applications of diamond technology that can produce demonstrable commercial products, rather than fundamental understanding. However, in many cases, it is the ignorance of the basic science that is inhibiting progress with many applications. Some of the unsolved problems are as follows:

- What is the role in growth (if any) of larger hydrocarbon species, such as  $C_2$  or  $C_2H$ ? If their role is detrimental to growth rate or diamond purity, can the plasma conditions be modified to reduce or eliminate these species?
- What causes renucleation? It is clear that as the concentration of  $C > 1$  hydrocarbons in the gas phase increases (e.g. by increasing the  $CH_4:H_2$  ratio), the rate of renucleation increases, leading to twinning and smaller crystallites. But exactly which species cause renucleation, and by what mechanism, is still not known.
- The reaction rate for a  $CH_3$  radical attaching to a surface radical site is limited by a temperature-dependent sticking factor,  $P$ . The value of  $P$  results from a combination of factors that reduce the reaction probability, such as a geometrical factor ( $g$ ) due to unfavourable collision orientation and a steric-electronic factor ( $s$ ), arising from the electron spin selection rules involved in bond formation. Also, only a fraction,  $F$ , of the total surface radical sites will be accessible for adsorption, and the value of  $F$  will depend upon the surface temperature and local H-atom concentrations. Thus,  $p = g \times s \times F$ , and the three factors can be estimated for different growth conditions [63,64]. For example, electronic-spin statistics show that for  $CH_3$ , on average, three collisions out of four will be on the triplet surface and will not lead to reaction at the high temperatures of diamond CVD [65], i.e.  $s \sim 0.25$ , while typically  $F \sim 0.5$  for CVD conditions [63]. The value for  $g$ ,

however, remains little more than a ‘best guess’. As is clear, the uncertainties in these estimates are large, leading to predicted growth rates from computer simulations that can differ from experiment by an order of magnitude. Molecular-dynamics calculations of the reaction process may provide more accurate, or at least more justifiable values [66,67], but nevertheless, the value of  $P$  and its variation with growth conditions and surface orientation remain key inputs to various growth models that urgently need refining.

- Although many macroscopic simulations of diamond CVD confirm the role of surface migration in step-edge growth and surface smoothing [41,42], the exact mechanism by which this happens remains somewhat vague. In particular, the rates with which adsorbed  $\text{CH}_2$  ‘bridge’ species migrate across adjacent dimer reconstructions, or into vacant trough sites, or down atomic steps, are all unknown and yet are key to the quantitative modelling of diamond CVD.
- Trace amounts of nitrogen in the gas phase are known to significantly increase the growth rate and change the surface morphology. There are many suggested mechanisms for this (see earlier), but none have yet been confirmed experimentally.
- Are there strategies, other than simply increasing MW power, that might be used to improve growth rates or uniformity, such as addition of trace gases ( $\text{O}_2$ , halogens, noble gases,  $\text{D}_2$ ), or improved gas injection configurations [68] or tuning the substrate position [69]?

## 5. The CVD diamond film

When diamond is grown *homoepitaxially* [24] on to an existing SCD seed crystal (which can be a natural diamond or one grown by CVD or HPHT methods), then the product is an enlarged SCD that can either be cut and polished into a gemstone (which is the basis for the flourishing CVD diamond gemstone market [2]) or laser cut into flat SCD substrates usually a few millimetre in size, suitable for advanced applications or further seeds.

In contrast, *heteroepitaxial* growth (diamond grown on to a non-diamond substrate) begins from numerous individual isolated nucleation sites, e.g. from microdiamond or nanodiamond seed crystals scattered on the surface, or surface defects such as scratches, impurities or dislocations [6]. The individual diamond nuclei enlarge as gas-phase carbon species adsorb on to them, and new carbon atoms add to the diamond lattice. The nuclei grow in three dimensions until they meet their immediate neighbours, whereupon they fuse together to form a coalesced (or closed) two-dimensional (2D) film that then continues to grow normally to the surface. The resulting material will usually be polycrystalline, composed of almost pure diamond crystallites (or grains) joined together by grain boundaries that contain varying amounts of impurities and non-diamond carbon. The morphology and the average crystallite size, and hence the resulting film properties, can be tuned [70] simply by choosing the appropriate process conditions [71], as shown in figure 8.

Diamond films are usually grouped into categories depending on their crystallite size and morphology.

### (a) SCD

Figure 8a is a near-perfect diamond crystal lattice with sizes that can approach several centimetres. It is usually deposited by templating on to an existing SCD seed, which can be later removed by laser cutting. Minimizing any remaining defects in the SCD layer (dislocation density, impurities, vacancies, etc.) is currently the goal for both the gemstone industry and for electronic device applications, as in both cases, ultra-high-purity SCD is the ‘billion-dollar prize’.

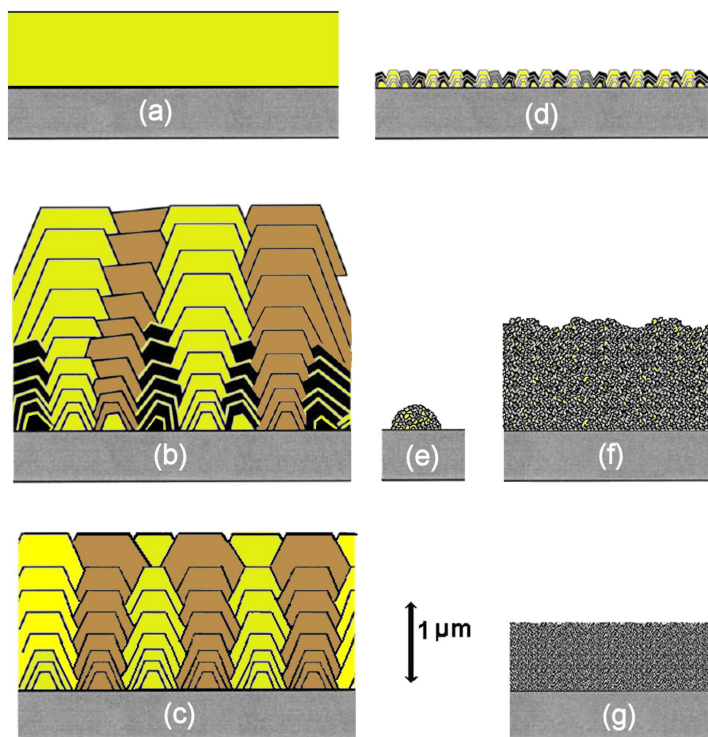


**Figure 8.** Schematic representation of various types of CVD diamond film deposited on a substrate (grey). The colours yellow, brown and black are used to allow the reader to discriminate between different diamond crystallites (grains) and their growth evolution. (a) SCD film grown epitaxially on an SCD substrate. (b) MCD columnar growth from randomly located nuclei, where the slowest growth face determines the overall film texture, in this case (100). (c) Highly oriented textured MCD obtained following special nucleation procedures, such as BEN (see §7). (d) Faceted NCD, which is really just thin MCD with high nucleation density. (e) ‘Cauliflower’ (or ‘ballas’) NCD before it has coalesced into a continuous film. (f) Cauliflower NCD film. (g) UNCD. Computer simulations of some of these diamond-film types were shown previously in figure 6.

### (b) Microcrystalline diamond

These films (figure 8b) exhibit faceted crystallites of size  $0.5\ \mu\text{m}$  to a few  $100\ \mu\text{m}$ , with a columnar growth structure that produces anisotropic properties that vary with film thickness. The grain boundaries between crystallites, which contain non-diamond carbon, are typically only a few angstroms thick. The crystallites in microcrystalline diamond (MCD) films are usually randomly oriented, as a result of the nucleation being from seeds or surface scratches that were themselves randomly located and oriented. As the film grows, the fastest growing surface (110) grows out via the van der Drift competitive growth model [72], leaving only the slowest growing facets, (100) or (111), visible at the film surface. The ratio of square (100) to triangular (111) facets in the film depends upon the growth conditions and is quantified by the  $\alpha$ -parameter [73]. So-called ‘textured’ MCD films can be made using seeds that are arranged to be oriented all in the same direction, or by using specialized seeding nucleation strategies such as BEN [74] (see §7). These films grow preferentially in the (100) orientation, and as the growth islands merge, the resulting continuous film can appear as near single-crystal over large areas (figure 8c).

### (c) Nanocrystalline diamond

These films [75] contain crystallites ranging in size from approximately 10 to 100 nm. Unfortunately, there are two types of diamond film that are often labelled 'NCD' (nanocrystalline diamond) in the literature. Diamond films grown with high nucleation density but for short periods of time, such that the films are less than 1  $\mu\text{m}$  thick, have a faceted morphology and grain boundaries, just like MCD, except the crystallites are 10–100 times smaller. These NCD films have almost identical properties to MCD, except their ratio of grain boundaries to crystallites is larger due to their smaller size (figure 8d). Alternatively, NCD films can also be made by increasing the hydrocarbon concentration in the CVD gas mixture. This changes the growth chemistry, increasing the rate at which renucleation occurs and promoting the growth of secondary crystallites as 'off shoots' of the original nucleus. The greater the C:H ratio in the gas mixture, the higher the rate of secondary nucleation, resulting in a larger number of smaller crystals. This type of diamond growth leads to more rounded crystallites, which form into hemispherical agglomerates (figure 8e), sometimes referred to as 'cauliflower' or 'ballas' diamond (figure 8f). The grain boundaries in cauliflower diamond films can be several nanometres thick and contain  $sp$ ,  $sp^2$  and  $sp^3$  hybridised carbon bonded in variety of configurations, along with impurities such as H and N. Although NCD films have properties that are generally inferior to MCD, their nanometre-scale surface roughness often makes them useful as wear-resistant protecting coatings in mechanical applications [76].

### (d) UNCD

UNCD films [77,78] have crystallite sizes less than 10 nm embedded in an  $sp^2$ -carbon matrix, and although their properties are less extreme compared to MCD and NCD, they have the advantage of being smooth on the nanometre scale (figure 8g) so that they can be used as vacuum pump seals [79] or medical applications [80]. UNCD is deposited using gas chemistries that have a much lower hydrogen concentration than for standard CVD conditions, for example, 1%  $\text{CH}_4$  in Ar, where the H:C ratio is only 4 compared to greater than 200 in standard 1%  $\text{CH}_4/\text{H}_2$  mixtures. The grain boundaries in these films can be several nanometres wide, making them almost the same size as the diamond crystallites. These boundaries (especially when doped with N [81]) can form electrically conducting pathways through the film, allowing them to be used in electronic device applications [82].

## 6. The substrate material

A major goal in the field of diamond CVD is the lowering of substrate temperatures required for growth, as this would permit the use of a much wider range of substrate materials of industrial importance. Das & Singh recently published a comprehensive review [83] of the many attempts to deposit CVD diamonds at lower temperatures. These included methods such as varying the composition of the gas mixture (in particular by addition of O-containing gases or halogens) or by alteration of the processing conditions, such as by coating the substrate with another material, pulse modulation of the MW plasma or cyclic modulation of the  $\text{CH}_4$  flowrate. Many of these techniques succeeded in lowering the deposition temperature by 100–200°C, but usually at the cost of greatly reduced growth rates, poorer quality diamonds and/or significantly added complexity to the CVD process. Most researchers now grudgingly acknowledge that for high-quality diamonds, there is no option but to deposit at temperatures greater than 700°C and accept the substrate limitations this entails.

The major problem associated with such high-temperature growth is that many common industrial materials, such as plastics, glass, semiconductors (GaAs, CdS and CdSe) and metals (Al, Zn, Sn, Pb, Mg and many of their alloys) have melting points lower than the diamond

deposition temperature and so cannot be used as substrates. Many remaining materials (e.g. Ti, Fe (including steels [84]), Ni, Co and Cr) either have a solid-state solubility for carbon that is too high at standard CVD process temperatures, such that most of the deposited carbon reacts to form a metal carbide rather than a diamond film, or are unreactive towards carbon (Cu and Ge), such that the deposited diamond film grows but does not adhere to the substrate. Moreover, some materials when heated to CVD diamond temperatures (greater than 600°C), notably Fe, Co and Ni, catalyse the conversion of  $sp^3$  carbon into  $sp^2$  phases, promoting graphitization over diamond deposition.

Of the remaining materials, thermal expansion mismatch is then often the major problem. The substrate expands at the high growth temperature, and the diamond film then grows upon this expanded substrate. The sample is then cooled back to room temperature, whereupon the substrate contracts back to its normal size while the attached diamond film—with a much lower linear coefficient of thermal expansion (CTE)—contracts significantly less. The stresses cause the sample to bow with the diamond side outermost, the diamond film to crack or delaminate or the entire sample to fracture into pieces, depending on the strength of the adhesion between the substrate and the diamond layer.

These problems highlight another of the ongoing problems with diamond CVD technology, which has been around since the 1990s—there remain only a few materials upon which high-quality diamond films can be deposited. Apart from the diamond itself, silicon remains the substrate of choice due to its high melting point, low cost, availability as flat, polished wafers, low(ish) CTE (only about three times higher than that of diamond compared to those for most metals which are typically 10–20 times higher) and propensity to form a thin (a few nanometres) carbide to enable the diamond layer to adhere. Other ‘diamond-friendly’ materials are given below.

### (a) Oxides and nitrides

It is possible to grow thin layers (a few micrometres) of diamond on to thin (a few micrometres) layers of  $\text{SiO}_2$  and  $\text{Si}_3\text{N}_4$  on a Si substrate. But if the diamond layer or the oxide/nitride layer becomes too thick (e.g. for *bulk*  $\text{Si}_3\text{N}_4$  or  $\text{SiO}_2$ , or quartz), the CTE mismatch often causes the diamond film to delaminate. The same problem occurs with other oxides and nitrides, such as  $\text{Al}_2\text{O}_3$  [85], sapphire [86],  $\text{Ga}_2\text{O}_3$  [87],  $\text{MgO}$  [88] and  $\text{TiO}_2$  [89], which in some cases can be minimized by optimizing the growth conditions. In contrast, many metal oxides can be deposited on to diamonds for use as gate oxides [90], heterojunctions [91] or as surface transfer doping layers [92] (see §12b(ii)).

Diamond can be successfully deposited on to hexagonal [93] and cubic boron nitride [94], although, as for oxides, more work has been reported for the flipped approach—deposition of boron nitride on to diamond [95]. GaN has been of particular interest as a substrate for diamond growth due to its use in high-power electronic devices [96], such as base stations for transmitters used in 5G mobile phone networks [97]. A diamond heat-spreader thermally bonded to a hot GaN device would rapidly dissipate the heat to a remote heat sink or cooling system, enabling the GaN device to operate at higher power loads with a longer lifetime [98]. The room-temperature CTE of GaN is 28% larger than that of diamond [99]; however, the bigger problem is the diamond growth chemistry. Although its normal melting point is approximately 2500°C, GaN reacts with hydrogen at temperatures around only 800°C, decomposing to volatile  $\text{NH}_3$ ,  $\text{N}_2$  and  $\text{GaH}_3$  resulting in etching of the GaN [100]. Moreover, the interface between GaN and diamond is rather weak because Ga does not readily form a carbide. Thus, the as-grown diamond adheres to the GaN mainly via weak non-covalent interactions, rather than strong covalent bonds, making it prone to delamination. Reasonable quality diamond films have been deposited on to GaN at lower temperatures or using a thin SiC or SiN barrier layer [101], but these tend to have poor adhesion and poor thermal conduction across the GaN/diamond interface—which is a crucial failure for heat spreading

applications [102]. Recent work has shown that thick diamond layers can be grown on to AlN [103], which can also be used as a relatively high-thermal-conductivity barrier layer on GaN.

## (b) Metals

For pure metals, diamond grows well on Mo, W, Re and Ir, with the latter being used for growth of heteroepitaxial SCD layers (see §7). Beryllium has also been reported to be a suitable metallic substrate for diamond growth for films less than 30  $\mu\text{m}$  thick, so long as the growth temperatures exceed approximately 750°C required to convert the native oxide (BeO) into carbide (Be<sub>2</sub>C) [104]. For Cu, its inability to form a carbide combined with its very high CTE has meant that diamond films that grow on its surface delaminate upon cooling. This has led to it being used to fabricate freestanding diamond plates [105].

## (c) Carbides

Diamond also grows well on many carbides, in particular, WC [106] and SiC [107], due to the fact they are already saturated with C. This means none of the depositing carbon is lost by dissolving into the substrate or reaction to form a carbide. Their low CTE values also help prevent delamination.

## (d) Silicides

Very little work has been reported about deposition on to these materials, but some silicides have been shown to meet the criteria for diamond growth, such as Ni<sub>3</sub>Si [108] and CoSi<sub>2</sub> [109], but less so on Fe<sub>x</sub>Si ( $x = 0.5, 1, 3$ ) [110].

## (e) Graphite

Diamond growth on to graphitic or  $sp^2$ -carbon-rich materials is tricky because the CVD conditions are designed to etch  $sp^2$  carbon. Diamond has been deposited on to bulk graphite [111,112], but this usually requires careful control of the CVD conditions to reduce the possibility of etching. The trick here, at the start of the deposition process, is to use a very high seeding density—almost a continuous monolayer—together with low deposition temperatures and high CH<sub>4</sub>/H<sub>2</sub> ratios. These conditions aim to make the initial growth rate exceed the graphitic etching rate, thereby rapidly creating a protective continuous layer of diamond over the whole surface, which protects the graphitic substrate from the hydrogen atmosphere before it has a chance to etch. Once this protective coating is continuous, the CVD conditions can revert to normal, to grow higher-quality diamonds at higher rates. More recently, similar growth techniques have been used to diamond coat carbon fibres [113], carbon-fibre composites [114] and carbon nanotubes [115].

Depositing diamonds at much lower temperatures (200°C) has recently become possible using LAPD, DAAM or SWP systems (see §3). These systems have very low deposition rates, but the films they deposit have high  $sp^2$  carbon content and are best described as NCD or even UNCD. Nevertheless, they are hard, smooth diamond coatings that can be deposited as thin (less than 10 nm) layers on many substrates that are impossible to coat with conventional high-temperature CVD. These substrates include glass [23,116], fibre optics [117], plastic [118] and infrared optics [119].

## 7. Nucleation

For heteroepitaxial growth of diamond on to non-diamond substrates, the long initial induction period before which diamond starts to grow can be significantly reduced using a suitable

pre-treatment prior to deposition (see the excellent review of nucleation by Mandal [120]). Many different types of pre-treatments have been reported to realize high uniform nucleation density leading to good quality diamond film growth. The list includes mechanical abrasion/scratching, seeding, electrical biasing, covering/coating with Fe or amorphous C, ion implantation, pulsed laser irradiation and carburization, all reviewed in detail in [83]. Mechanical abrasion and seeding were well-known in the 1990s [1]. But many of the other techniques in that list are used rarely, or only for specialized substrates. Perhaps the most important advance relevant for diamond nucleation in the last 20 years has been the discovery and commercial production of detonation nanodiamond (DND) [121].

DND particles typically have sizes 2–10 nm [122], and their most common production method is via detonation of explosives (such as trinitrotoluene and hexogen) in an inert atmosphere or in water/ice, inside a steel chamber [123]. The detonation produces a supersonic shockwave within which the prevailing high pressures and temperatures are sufficient to crystallize carbon into diamond. However, after the transient shockwave passes, the conditions revert to less extreme pressures and temperatures, favouring other forms of carbon. Thus, the explosion produces a mixture of nanodiamond particles, soot and other  $sp^2$  carbon material.

The powdery mixture of detonation products is cleaned with various acids and reagents to remove unwanted metallic impurities and soot, and the diamond component is extracted. The resulting DND material is now commercially available from many suppliers worldwide (see electronic supplementary material, table S1) as a powder or as a suspension in water and is currently produced at a rate of several tons per year and sold for as little as \$100/kg. Unfortunately, the DND particles tend to fuse into aggregates approximately 100 nm in size, and thus the as-supplied material usually requires de-aggregation before subsequent processing. This can be achieved in many ways, including ball milling, pulverization, high-power sonication, acid treatments, controlled heating in  $O_2$  or  $H_2$  or combinations of these methods [124]. The DND particles that are finally obtained are often described as having a diamond core surrounded by a (partially) graphitic or fullerene-like shell—and are sometimes called ‘bucky-diamonds’ [125].

Following the various cleaning processes, the surfaces of DND particles are usually terminated with oxygen-containing groups, which makes them hydrophilic and helps their stability in aqueous suspensions (see §1c in the electronic supplementary material). This oxygenated surface can be modified by standard chemical methods, replacing the O-containing functional groups with H (producing a mildly hydrophobic surface), with F (which is superhydrophobic) or with  $NH_2$  (which permits further chemical functionalization) or with a host of organic molecules [126].

Functionalized DND particles are currently of great scientific interest in their own right for a range of applications, e.g. as carriers for targeted drug delivery [126] and as luminescence biomarkers [127,128]. However, in terms of diamond CVD, their main utility is in seeding. Due to their small size, an aqueous or ethanolic suspension of DND particles can be drop-cast on to a substrate surface; after drying, a near monolayer of seeds is formed with extremely high density ( $10^{12}$ – $10^{13}$   $cm^{-2}$ ), which is close to the theoretical maximum [120]. Alternative DND seeding methods are also popular—the substrate can be dipped into the DND suspension (with or without sonication), spin-coated or submerged, and the DND particles are left to settle on to the surface. A DND suspension can also be electrostatically sprayed on to a surface enabling complex 3D microstructures to be conformally coated in a layer of seeds [129]. More details about the application of DND seeding can be found in the electronic supplementary material.

Bias-enhanced nucleation (BEN) was considered rather a niche method for nucleation in 2000. However, in the last few years, BEN has come to prominence due to it being used to make freestanding SCD wafers that are 92 mm in diameter [74]. BEN works by applying a negative bias of approximately  $-100$  V to the substrate plate during MWCVD for a short nucleation step. The bias accelerates positive hydrocarbon ions from the plasma bulk, which then strike the single-crystal substrate with energies around 100 eV sufficient to implant C just beneath the

surface (a process called subplantation). As time goes on, the concentration of sub-planted C reaches saturation, and the C atoms precipitate out of the surface as diamond—but crucially the diamond islands that form are aligned with that of the underlying substrate lattice. After a few minutes, this nucleation step is complete, the bias is turned off and conditions revert to those for standard CVD growth. The diamond islands continue to grow and then coalesce with very little mismatch at the boundaries, eventually producing a near SCD film across the whole substrate.

The original BEN work used Si (100) substrates, and the diamond films produced were called textured diamonds as they were composed of large SCD (100) plates all closely aligned with the substrate lattice [130]. This work was pioneered, among others, by Matthias Schreck from the University of Augsburg, and the big breakthrough was the realization that the nucleation density afforded by BEN was far denser and the crystal orientation distribution much narrower on single-crystal iridium metal substrates. This was partly due to the close lattice match of Ir to diamond [131], but also due to a unique mechanism in which buried lateral growth occurs within an approximately 1 nm-thick carbon matrix induced by the intense ion bombardment, described in detail in [74]. Unfortunately, using freestanding single-crystal Ir substrates is not practicable due to their astronomical cost. However, thin single-crystal Ir layers can be deposited on to various oxides, such as  $\text{Al}_2\text{O}_3$ ,  $\text{SrTiO}_3$  and  $\text{MgO}$  [132], with the best being yttria-stabilized zirconia (YSZ). YSZ substrates are available and reasonably inexpensive, but in its bulk form, the CTE mismatch between YSZ and diamond is still rather high. The method of choice, therefore, is to use a triple-sandwich structure by depositing thin layers of YSZ on to a standard cheap Si (001) wafer, followed by a layer of single-crystal Ir, to produce Si/YSZ/Ir substrates. The diamond films grown on these sandwich substrates using BEN followed by MWCVD are near-perfect, transparent single-crystal layers up to 92 mm in diameter by 1.6 mm thick [74] (figure 9).

Large-area freestanding diamond films fabricated by this method are now available commercially from the German company Audiatic [133]. Such heteroepitaxially grown SCD films currently suffer from higher defect densities than their homoepitaxially grown counterparts, as well as significant bowing from the remaining CTE mismatch, but the hope is that SCD wafers with substantially larger diameters and fewer defects can be routinely fabricated by this method in the near future.

## 8. Doping

Undoped CVD diamonds of any grain size are highly electrically insulating. However, doping by incorporation of a suitable impurity atom, usually from Group 3 or 5, can increase the conductivity of the film in a controllable manner. The dopant atoms are usually added to the input gas mixture in gaseous form, e.g.  $\text{B}_2\text{H}_6$  for boron,  $\text{NH}_3$  or  $\text{N}_2$  for nitrogen,  $\text{SiH}_4$  for Si and  $\text{PH}_3$  for phosphorus, or by exposing a solid compound containing the intended dopant (e.g. rods of solid Si or B) to the plasma during deposition. Alternating layers of doped and undoped diamond can be fabricated by switching the doping gas on and off. Dopants in the form of solid rods can be retracted and inserted into the plasma extremely rapidly, allowing very thin (less than 1 nm) dopant layers to be made for so-called ‘delta-doping’ applications (see §12b(ii)).

Adding boron to diamond changes the conductivity in a reproducible and reliable manner (figure 10) [134]. At low-to-medium concentrations, B doping creates a *p*-type semiconductor [135], while at high concentrations (greater than  $1 \times 10^{20} \text{ cm}^{-3}$ ), the conductivity becomes near-metallic, and for B concentrations above approximately  $3 \times 10^{21} \text{ cm}^{-3}$ , the films become superconducting at temperatures less than 10 K [136,137]. The *p*-type conductivity in B-doped diamond (BDD) results from hole carriers, and SCD exhibits the highest hole mobility at room temperature of any wide-bandgap semiconductor [138]. A higher-mobility material has a higher frequency response because the carriers can travel through the device faster. Also, materials with higher mobility transport more carriers per second, which means they can operate at

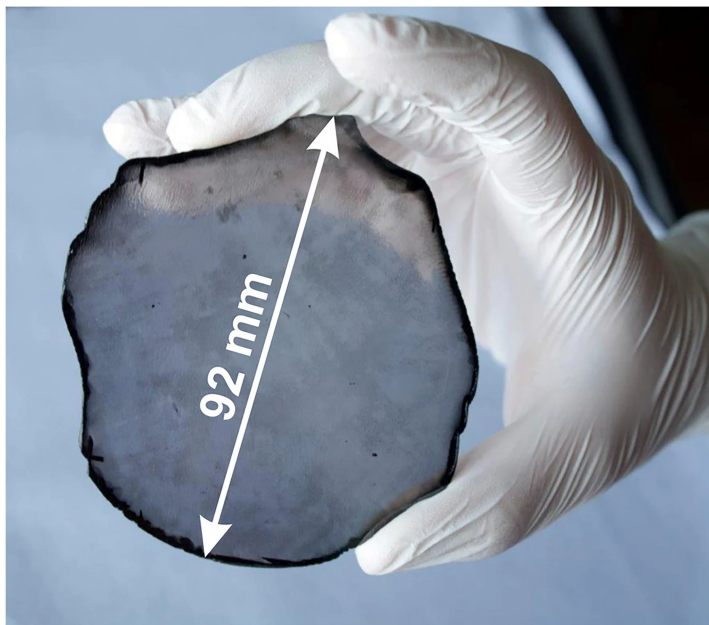


**Figure 9.** Freestanding unpolished large-area SCD wafer synthesised by heteroepitaxy on Ir/YSZ/Si(001). The thickness of the disc is  $1.6 \pm 0.25$  mm and its weight is 155 carat. Reproduced from [74] under the Creative Commons Attribution 4.0 License.

higher currents and therefore higher powers. Although this high hole mobility in BDD drops considerably with increasing temperature and B concentration, it nevertheless remains high enough for BDD to be used in a variety of simple electronic devices (especially those operating at high frequencies and high powers), sensors and electrochemical electrodes [139].

In contrast, *n*-type semiconductivity—with electrons now acting as carriers—is much harder to achieve, because most potential *n*-type dopants (P, As and Sb) are too large to easily substitute for a small C atom in the rigid diamond lattice and thus have a low solid-state solubility in diamond [140]. Despite diamond exhibiting high values for electron mobilities similar to the hole mobilities seen in BDD, the low dopant concentration leads to low electrical conductivity and limited device performance. The exception is nitrogen for which atoms are small enough to substitute for carbon [50], but unfortunately, the energy levels of the N donor in diamond are too deep [141] (figure 11) and so are electrically useless for most room-temperature applications. Over the past 20 years, some degree of success has been achieved with phosphorus doping [142], but device performance is still poor compared to competing semiconductor materials such as Si, GaAs, GaN and SiC. Experiments with more unusual candidate dopants, such as Sb [143], Li [144], Na [145], S [146,147] and Se [148], have *all* proven disappointing.

Co-doping—addition of both *p*-type and *n*-type dopants simultaneously—has been attempted—again with little success. B + Li doping failed due to the Li migrating through the diamond (especially when grain boundaries were present), possibly forming Li clusters [149]. Calculations for N + Li co-doping suggested that a  $\text{LiN}_4$  defect, with substitutional Li, is *likely* to behave as a shallow *n*-type donor [150]—if it could somehow be realized experimentally. Similarly, computational predictions for B + N [151], B + P [152] and Se + B [148] look promising, but none have yet been proven experimentally to be useful *n*-type doping schemes.

Despite all this effort, the continued lack of a reliable *n*-type dopant with useful electronic properties at room temperature has hindered the use of diamonds in electronic applications more than any other issue. To date, *n*-doping unfortunately remains the ‘holy grail’ of diamond semiconductor research.

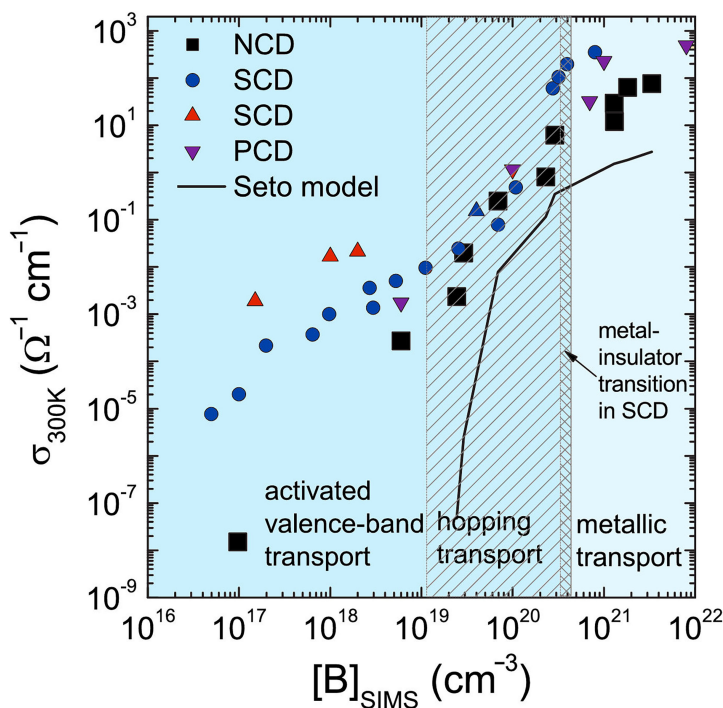


**Figure 10.** Conductivity ( $\sigma$ ) at 300 K as a function of boron content measured by secondary ion mass spectrometry (SIMS) for various boron-doped diamond samples. Different conductivity mechanisms operate at different B concentrations, as shown by the labelled regions on the plot. The curve predicted by the Seto model of conductivity is plotted as a solid line. Figure reproduced from [134] with permission and coloured. For  $[B] > 1 \times 10^{21} \text{ cm}^{-3}$  and temperatures less than 10 K (not shown) the conduction mechanism switches to superconductivity via Cooper pairs.

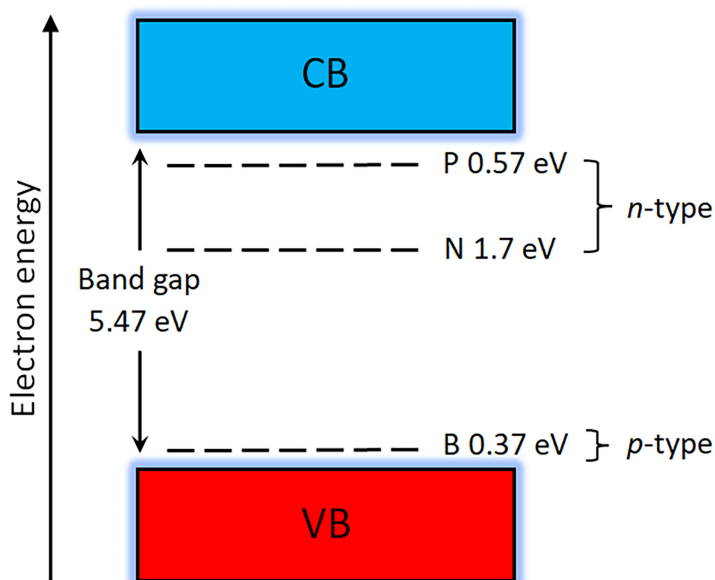


**Figure 11.** The three most common dopant types (e.g. phosphorus, nitrogen and boron) in diamond with the associated energies within the band gap; VB and CB stand for the valence band and conduction band, respectively. The B acceptor level is measured from the top of the VB, while the P and N donor levels are measured from the bottom of the CB.

Another type of conductivity can occur in diamonds, as a result of an unusual property of the diamond surface, called ‘surface transfer doping’ [153,154]. Hydrogen-terminated diamond exhibits a surface dipole due to the difference in electronegativity between the carbon atoms in the bulk and the H atoms on the surface. Electron-accepting molecules from the ambient air adsorb on to this polar surface, and electrons are transferred from the bulk diamond to the adsorbates. As a result, the adsorbates become negatively charged. Similarly, the diamond becomes positively charged, and this takes the form of a stable two-dimensional hole-gas (2DHG) layer a few nanometres thick, which forms just below the surface [155]. This layer is electrically conducting, with both a high hole mobility ( $100\text{--}200\text{ cm}^2\text{ V}^{-1}\text{ s}^{-1}$ ) and a high hole concentration ( $10^{12}\text{--}10^{13}\text{ cm}^{-2}$ ). Unfortunately, the conductivity can be altered or even destroyed by simply changing the atmosphere (pressure, humidity, etc.) above the surface, as this affects the concentration and nature of the adsorbates. To stabilize this fragile conductive layer, the diamond surface can be capped with a protective layer of an electron-accepting oxide, such as  $\text{V}_2\text{O}_3$ ,  $\text{Al}_2\text{O}_3$  or  $\text{MoO}_3$  [156]. This capping layer hermetically seals the surface as well as providing additional surface acceptors helping to generate and stabilize the 2DHG layer. Several groups have recently exploited this process to fabricate novel types of electronic devices (see §12b(ii)).

## 9. The NV centre

Although its usefulness as a dopant is doubtful, N in diamond, when situated next to a vacancy, forms the so-called ‘NV centre’ [157], as shown in figure 12. The negatively charged version of this defect ( $\text{NV}^-$ ) is causing a great deal of excitement in the scientific community because these defects behave as isolated ‘pseudo-atoms’, with a set of energy levels distinct from those of the surrounding diamond. NV centres act as excellent single-photon sources [158], underpinning a host of novel applications involving quantum computing and quantum information processing [159,160] (§12c), as well as quantum sensing and magnetometry [161] (§12c(iii)). When excited by green laser light, the NV centres fluoresce in red, and this gives rise to another set of applications for the study of biological cells [162] (§12c(iii)).

There are a variety of methods to fabricate  $\text{NV}^-$  centres in diamond. The most popular is to implant diamond with N ions, followed by high-temperature annealing. The implantation process adds N to the diamond, with many of the N atoms displacing C atoms from the lattice and taking their place as substitutional atoms. The implantation process also creates damage, such as vacancies and interstitial C atoms. The subsequent anneal then allows the defects to relax into a stable structure, and because the formation energy of an  $\text{NV}^-$  centre is exothermic, these form readily. The difficulty is in not flooding the diamond with too many N atoms such that the density of N atoms is so great they start to cluster. As such, simultaneous implantation of only a few N atoms (less than 5) within a volume of approximately  $1\text{ }\mu\text{m}^3$  is required—which is pushing the limits of current implantation technology. Furthermore, the NV centres need to be within a few nanometres of the surface for them to be affected by the presence of any adsorbates (e.g. for sensing purposes) and for any emitted photons to be able to escape the surface [163]. The NVs also need to be separated from any neighbouring NVs by more than 30 nm to prevent dephasing (signal interference between the two centres) [164]. The substrate must be ‘electronic grade’ or ‘quantum grade’—extremely high-quality SCD, which is transparent at the wavelength of the emitted photon with no optical defects (such as birefringence), contain extremely low N concentrations (less than 1 ppb) and polished to a smoothness of a few nanometres or better. Along with gemstones, these exacting requirements for electronic-grade diamonds for quantum applications remain one of the key driving forces for improvements in diamond growth technology.

As well as the  $\text{NV}^-$  centre, several other diamond ‘colour centres’ have been investigated for quantum applications, including  $\text{NV}^0$  (neutral NV) [165],  $\text{SiV}^-$  [166],  $\text{SiV}^0$  [167],  $\text{GeV}^-$  [168],  $\text{SnV}^-$

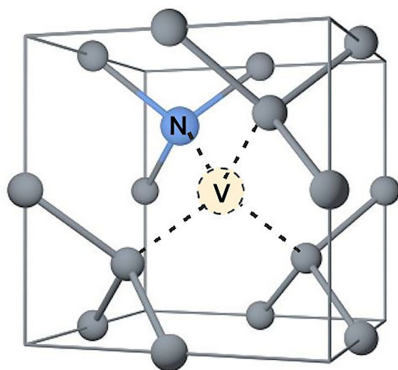


**Figure 12.** Schematic diagram of the NV defect centre in the diamond unit cell.

[169] and  $\text{PbV}^-$  [170], and many more candidate defects are being discovered on a regular basis [171].

## 10. SCD growth

One of the most remarkable success stories in diamond technology over the past 20 years is the development of methods to grow SCD gemstones of sufficient size and clarity so that they can compete directly with natural diamonds in the jewellery market. The market for CVD lab-grown diamonds was valued at \$11.3 billion (USD) in 2022 and is projected to reach \$15.9 billion by 2027, growing at an extraordinary rate of approximately 7% a year [172]. This burgeoning demand for SCD gemstones has been the driving force behind significant improvements to both the growth technology (see §3) and the quality and size of high purity diamonds available as substrates for scientific use (see §11). The three crucial considerations for both the gemstone market and scientific applications of SCD are high growth rate, high throughput (either large surface area or more diamond gemstones per growth run) and high purity.

### (a) High growth rate and throughput

For gemstones, SCDs up to 1 cm in thickness can now be deposited by MWCVD at growth rates up to  $100 \mu\text{m h}^{-1}$  [173], although more typical routine industrial growth rates are approximately  $20 \mu\text{m h}^{-1}$ . For SCD growth, the growth chemistry is modified only slightly from that used for polycrystalline films.  $\text{CH}_4/\text{H}_2$  is still the preferred gas mixture, except that for high growth rates the carbon concentration in the gas phase is often increased from 1% to approximately 15%  $\text{CH}_4$  in  $\text{H}_2$ , while process pressures are also increased to over 200 torr. To prevent build-up of longer-chained carbon radicals in the gas phase, which might cause unwanted renucleation, the plasma density is increased to typically  $70\text{--}300 \text{ W cm}^{-3}$  by using higher-power MW systems. Such high-power (up to 75 kW) 915 MHz reactors can accommodate large substrate platens capable of holding as many as 24 diamond seeds at a time, substantially increasing throughput. Often, small amounts of  $\text{O}_2$  are added to the gas chemistry to further improve the diamond quality, while additions of small quantities of  $\text{N}_2$  improve growth rates significantly (see §4b), leading to diamond with a yellowish or light brown colour. These unwanted colours can be partially or wholly removed using a post-growth treatment to produce a clear colourless gemstone [174]. Indeed, most CVD material sold as jewellery has undergone at least one round of post-growth treatment, such as HPHT annealing or a combination of irradiation and annealing.

After decades of studying colour centres in natural diamonds, it is now possible to engineer the correct impurities into CVD diamonds during growth or in post-growth processing, to produce diamond gemstones with specific colours [175]. These so-called ‘fancy’ diamonds can sell for many times the price of their colourless counterparts, and so some manufacturers concentrate on producing these diamonds exclusively. Fancy diamond colours include brown (attributed to non-diamond carbon inclusions and/or internal extended defects such as dislocations), yellow (due to incorporation of nitrogen), red (from post-growth irradiation), blue (due to boron incorporation) and grey (boron again, plus sometimes carbonaceous inclusions; figure 13) [176]. The most famous natural blue diamond is, of course, the 46-carat Hope Diamond, which is permanently on display in the Smithsonian Museum in Washington DC [177]. If the rapid rate of progress in CVD gemstone growth technology continues, a very large, blue, lab-grown diamond should be possible within a few more years [178] (hence a possible secondary meaning for the title of this paper—a new Hope?).

## (b) High purity

This is achieved in various ways. Ensuring that high-quality vacuum components are used throughout the MWCVD process prevents air leaks. The use of ultra-high purity process gases (99.9999%) and hydrogen generators—which generate extremely clean H<sub>2</sub> gas (99.99999%, i.e. an impurity content less than 100 ppb) by electrochemically splitting high-purity water—ensure that unwanted impurities in the diamond, especially nitrogen, can be reduced to levels below 0.1 ppb [24]. Extremely stable noise-free MW power supplies and control electronics ensure that growth conditions (pressure, gas flows, power and temperature) remain constant to within fractions of a per cent during the many hours or days required to produce thick films or large gemstones.

However, extended defects, such as dislocations, grain boundaries, twins and cracks, remain a significant problem in SCD growth [179], as these can substantially reduce the diamond quality and cause a variety of problems, such as birefringence [180], unwanted luminescence or carrier leakage in diodes [181]. SCD is usually deposited epitaxially on to mechanical-grade HPHT type-Ib seeds due to their low-cost and availability. Unfortunately, these substrates contain large numbers of point defects (impurities such as N and metal atoms) and extended defects, especially dislocations, that significantly affect the CVD films grown upon them. The dislocations in the substrate are a problem because they transfer to the growing CVD film [182] and ‘thread’ through the layer along the (001) growth direction.

The dislocations at an HPHT seed surface can be revealed and their density determined by a short dry-etch process using an H<sub>2</sub>/O<sub>2</sub> plasma. This process preferentially etches the dislocations projecting from the surface and creates micron-sized inverted-pyramidal square-sided etch-pits visible via optical microscopy [183]. Typical dislocation densities in HPHT seeds are 10<sup>2</sup>–10<sup>4</sup> cm<sup>-2</sup>, increasing to 10<sup>5</sup>–10<sup>7</sup> cm<sup>-2</sup> for CVD homoepitaxial SCD, and further to 10<sup>8</sup>–10<sup>10</sup> cm<sup>-2</sup> for heteroepitaxial SCD [182,184]. However, not all defects have the same detrimental effect. Defects that fatally disrupt the operation of the application in question are termed ‘killer’ defects [185]. The exact nature of what constitutes a killer defect differs depending upon whether the application is optical or electronic, as well as between different types of electronic devices. The typical density of killer defects is 10<sup>4</sup>–10<sup>5</sup> cm<sup>-2</sup> for Schottky junction devices fabricated on a Ib type HPHT substrate [186], i.e. killer defects constitute approximately 1–10% of all dislocations in the sample. For comparison, the lowest killer defect density reported in a device to date is approximately 600 cm<sup>-2</sup> [187]. For a particular application, identifying which of the various defects present in the diamond are the killer defects that must be eliminated (or at least minimized) and which are less harmful is currently a major endeavour if SCD devices are to live up to their promise [188].

There are two methods commonly used to significantly reduce the generation of dislocations at the interface between the seed/substrate and the CVD diamond layer. The first involves



**Figure 13.** Examples of fancy-coloured CVD diamond gemstones. Photo reproduced with permission of Infi Advanced Materials Co., Ltd [176].

polishing or etching the seed/substrate prior to deposition to reduce the number and severity of surface defects [189]. The second method involves selecting much higher-quality type-IIa HPHT diamonds with low dislocation density for use as seeds [190]. Other reported methods, which have also been used for heteroepitaxial CVD on Si/YSZ/Ir substrates, include blocking the threading dislocations using thin Au stripes [191], deliberate incorporation of W impurities [192] or a grid of laser-cut holes [193] or Ni etching [182] followed by lateral overgrowth of more diamond. Sometimes the easiest solution is to simply grow the diamond film thick enough that most of the dislocations grow out and disappear [184].

With suitable seed selection combined with substrate pre-treatment and the use of clever growth technology, reports are starting to emerge of CVD SCD films with very low dislocation density ( $400 \text{ cm}^{-2}$ ) [194]. Despite such impressive improvements in defect reduction, current state-of-the-art values are still a long way from those required for realistic commercial SCD devices [188], and this will become one of the major challenges for diamond device fabrication in the coming years.

Since about 2008, CVD diamonds of gemstone quality began to enter the marketplace, but it was not until around 2013 that production really took off, particularly in China, which now manufactures approximately 50% of the lab-grown diamonds used in jewellery worldwide [11]. Gem manufacturers in other countries (see electronic supplementary material, table S1), such as India, Singapore, the UK and the USA, are also ramping up their output of diamond gemstones. The majority of faceted CVD gemstones on the market today are 2 carats or less in size, although the average sizes are increasing each year [175]. The current record for the largest faceted CVD lab-grown gemstone diamond is held by a stone called ‘The Pride of India’ produced by Ethereal Green Diamond (Mumbai) in May 2023; it weighed 34.59 carats and measured  $13.97 \times 13.87 \times 9.56 \text{ mm}$  [195], while the largest equivalent HPHT diamond gemstone weighs slightly less at 20.23 carats and was made in 2019.

Lab-grown CVD or HPHT diamonds can be distinguished from natural diamonds by a number of identifying markers caused by their growth conditions [196,197]. Some differences, such as metal inclusions in natural stones, can be seen in an optical microscope or become apparent from the interference patterns visible using polarised light microscopy. CVD

diamonds also have a different fluorescence signature to natural diamonds and nowadays can be readily detected using portable systems such as the *DiamondView* imaging instrument developed by de Beers in the mid-1990s [198,199]. More details about methods of distinguishing natural and CVD diamonds can be found in §2 of the electronic supplementary material.

## 11. Large-area diamond films

To compete against other materials and for the commercial advantages in price, reproducibility and throughput that accompany larger area growth, it is essential that diamond films are fabricated in the form of large wafers and to thicknesses approaching 1 mm. The Si industry currently uses 12-inch single-crystal wafers as standard, while materials such as SiC and GaN are not far behind and have established commercial products with approximately 6-inch wafers. It seems that SCD substrates—which appear to have been stuck at only  $10 \times 10$  mm for many years—have a long way to catch up. Fortunately, there are a number of strategies proposed for large-area diamond growth described below and reviewed in detail in [4].

### (a) Polycrystalline diamond films

Current MWCVD reactors are limited to substrate areas approximately 4 inches in diameter, although larger areas are possible using lower frequency MW power supplies (see §3). However, the requirement for a tuned cavity in MW systems makes large-area growth problematic. China is currently leading the way in DC arc-jet technology for large-area polycrystalline diamond deposition [11]. In a new type of arc-jet reactor (or plasma torch) developed by the University of Science & Technology Beijing, large-area uniformity is achieved through an externally applied magnetic field that stabilizes the arc jet, combined with careful magnetic and fluid dynamic control to guarantee the dynamic mixing of gases before they strike the substrate [12]. The 100 kW models are available that are capable of depositing diamond films over a substrate of 150 mm diameter with a thickness of 3 mm at growth rates as high as  $40 \mu\text{m h}^{-1}$ . The high rate of gas usage in these types of reactors is mitigated by recycling 95% of the process gases. Such reactors are currently employed in China for the mass production of mechanical, thermal and optical grade (but not electronic grade) diamond film wafers [11]. Plans to scale up to even larger areas are undoubtedly in the pipeline; however, the enormous power supplies that would be required, along with the vast cooling rates and gas flows, may prove difficult hurdles to overcome.

Commercial hot-filament CVD reactors are available that can deposit polycrystalline diamond films on to 12-inch-diameter wafers; however, their low growth rates (a few  $\mu\text{m h}^{-1}$ ) mean they are not practicable for mass-production applications. The various distributed antenna reactors (LAPD, DAAM and SPW) described in §3 have the potential to grow on very large areas, perhaps several  $\text{m}^2$ . However, the diamond quality is poor (NCD at best), and the growth rates are pitifully low. Nevertheless, such systems may find use in coating large-area panes of glass with a thin protective NCD layer.

### (b) Heteroepitaxial SCD

The most promising candidates for SCD films grown on non-diamond substrates to date are those grown upon Si/YSZ/Ir substrates using BEN and MWCVD [74] (see §7). Transparent freestanding SCD diamond films have been grown with diameters as large as 92 mm (figure 9); however, larger areas are proving tricky due to challenges with cracking and bowing resulting from CTE mismatch between the diamond and substrate. The large number of defects that propagate into the diamond from the imperfect interface between the diamond and the Ir is also a problem for electronic or quantum applications. Although improvements in film quality and

size are reported regularly, it remains to be seen if this fledgling technology can compete with the SCD films grown homoepitaxially.

### (c) Homoepitaxial SCD

The problem with growing large-area SCD on diamond substrates is that the seeds are usually made by the HPHT method and are thus limited in size to a maximum of approximately  $12 \times 12$  mm [200]. Even if larger seeds could be fabricated, the other issue is that the substrate size remains limited by the size of the MW chambers (see §3d). For smaller substrates (approx.  $1 \text{ cm}^2$ ), there are a number of options for faster growth rates. Diamond CVD growth rates generally scale with power input [201], so simply increasing the power density of the MW plasma can greatly increase growth rates, although care has to be taken with cooling to ensure the growth temperature remains within the usual limits. Similarly, in HFCVD, increasing the filament temperatures to nearly the melting point of the Ta filament (approx. 3000 K) achieved growth rates of  $10 \mu\text{m h}^{-1}$ , but at the expense of some evaporated metal from the filament contaminating the diamond [202]. Adding a small amount of nitrogen-containing gases to the feedstock can more than double the growth rate and produce flat (100) diamond surfaces (see §4b). Another approach is to grow via the step-flow growth mode on miscut substrates [203]. These substrates have been deliberately cut off-axis by a few degrees such that there are many step-edges present on the growth surface. CVD then proceeds via the step-flow mechanism at these edges, which speeds up the growth rate and reduces hillocks [204], permitting very thick, macroscopically smooth films to be deposited [205].

The ability to rapidly grow large numbers of thick plates of  $10 \times 10 \text{ mm}^2$  SCD in high-power MW systems promises perhaps the most hopeful method for fabricating large-area SCD substrates—'mosaic growth'. In this process, many diamond seed plates are arranged in a grid in the reactor, and diamond is grown laterally, fusing them together into one large SCD plate. The resultant wafer is formed of small tiles, but the plates need to be aligned accurately with each other and have identical off-axis orientation. One method to achieve this is the use of 'cloned' tiles (figure 14). This technique uses a lift-off method first reported by Parikh *et al.* [207], in which a high-energy ion beam implants C ions into a flat SCD seed forming a thin, damaged layer buried beneath the surface. Annealing in vacuum at approximately  $600^\circ\text{C}$  graphitises this layer, making it much more amenable to etching than the surrounding diamond. This graphitic layer can then be etched electrochemically, lifting off the freestanding SCD plate above it. Another CVD growth run then creates a new homoepitaxial layer, which can then be implanted and removed again. This process allows for repeated growth of SCD clone plates that have identical characteristics. These can then be aligned and grown together into a single, large tiled clone [206] (figure 14). Tiled clones still contain imperfect crystal boundaries, so the next step is to use them as an even-larger-area seed crystal for another subsequent homoepitaxial growth. To remove the newly grown larger area layer from the top of the tiled mosaic, the surface is mechanically polished then ion implanted as before, followed by a final electrochemical lift-off process. Although this is a complex multi-step process, SCD wafers of size  $60 \times 40 \text{ mm}^2$  have been produced this way, which consist of 24 SCD plates, each  $10 \times 10 \text{ mm}^2$  [206]. A number of companies (e.g. EDP Corporation in Japan) now sell mosaic diamond substrates with areas approximately  $25 \times 25 \text{ mm}^2$ , and it seems to be only a matter of time before even larger areas become available.

## 12. Applications

One of the most remarkable things that has occurred in CVD diamond technology over the past 20 years is the emergence of an astonishing variety of commercial applications for this material. Diamond has always been seen as 'the biggest and the best' with regard to most physical and

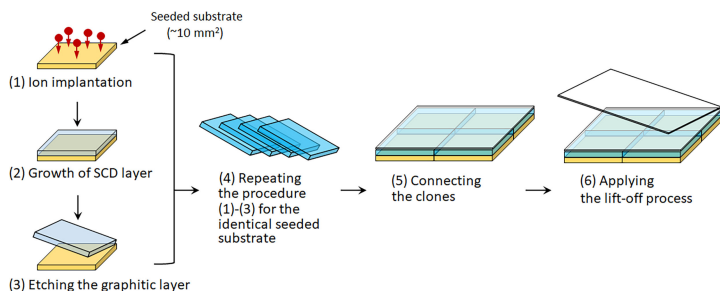


**Figure 14.** Procedure to produce clones and tiled clones. Figure redrawn based upon diagram in [206].

mechanical properties [1], and these extreme properties are now beginning to be exploited in a wide range of exciting new uses. Indeed, the number and variety of applications for diamonds is now so large that they require an entire review article all to themselves [5]. Thus, here we will focus only on the three applications that we believe show the most promise to produce transformative widescale technologies: quantum information, electrochemistry and electronic devices.

## (a) Electrochemistry

Electrodes made from or coated with BDD have a number of advantages for electrochemistry compared to conventional electrodes made from gold, platinum or glassy carbon [139,208,209]. First, BDD electrodes have a wide potential window from  $-1$  to  $+1.8$  V (figure 15), allowing detection of redox species that would normally fall outside the operating range of conventional electrodes [210]. Within this operating window, the response is flat, so there is no background and little to no capacitance, making BDD electrodes highly sensitive. This enables them to detect the presence of compounds at nanomolar (ppb) levels, even in the presence of chemically similar species (figure 16a). Also, BDD electrodes are chemically inert and non-corroding at high temperatures, high pressures and in environments where other electrodes would not survive. These include biological environments in which diamond is bioinert, i.e. its presence does not invoke an unwanted biological response, such as inflammation. Furthermore, BDD electrodes can be nanostructured into various shapes, such as nanowires [212], foams [213] fibres [214] and needles [211], increasing the available surface area by up to 1000-fold, along with an accompanying increase in sensitivity [211] (figure 16b,c). In addition, BDD electrodes are robust, have far less tendency to foul than other electrodes and can be electrochemically cleaned *in situ*.

However, it should be noted that BDD comes in many different varieties, and the electrochemical performance of the electrode depends critically upon grain size, B-doping level, surface functionality (e.g. hydrophilic H-termination or hydrophobic O-termination), surface roughness, number of grain boundaries and their  $sp^2$  carbon content, among other factors [139]. For some applications, particularly those involving high electrical currents such as water purification (§12a(vi)), delamination of the BDD film can be a problem.

There are perhaps 50 electrochemistry research groups worldwide using BDD electrodes, and a number of companies (e.g. Element Six (UK), Windsor Scientific (UK), Adamant Technologies (Switzerland), Condias (Germany), Sumitomo (Japan) and  $sp^3$  Diamond Technologies (USA)) sell BDD electrode material for use as electrodes.

### (i) Electrochemical analysis

One of the most important uses for BDD electrodes is to determine the identity and concentration of unwanted impurities in a solvent, especially those in water supplies such as rivers and lakes. Many toxic compounds and metals have redox potentials that are too high to

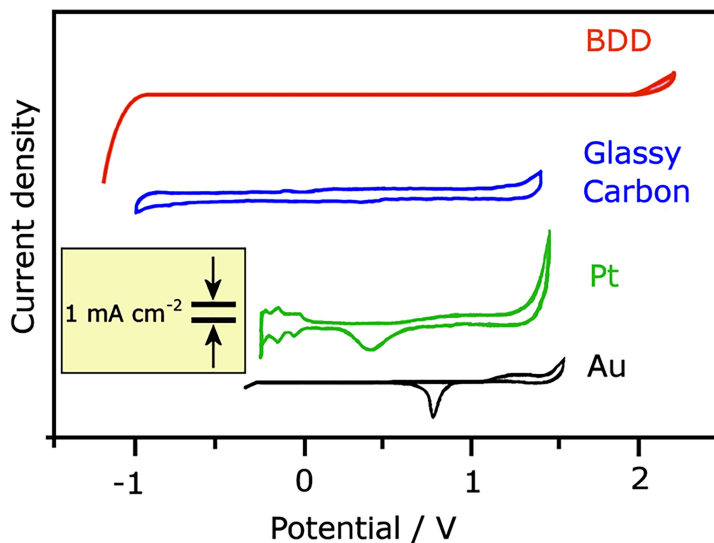


**Figure 15.** The potential windows of several different electrochemical electrodes. Redrawn using data from [210].

detect using conventional electrodes because the oxidation and/or reduction of water occurs at lower potentials than those required to detect the target compound. BDD electrodes, with their wider potential window, have been used to analyse a range of aqueous systems, including detection of heavy metals (mercury [215], cadmium, lead, nickel [216] and arsenic [217]), polycyclic aromatics and pesticides [218], hormones and estrogenic compounds, explosives [219], neurotransmitters such as dopamine [211], drugs (paracetamol, narcotics and pharmaceuticals) [220] and water-soluble nerve agents [219].

### (ii) *In situ* medical diagnostics

An emerging application for BDD electrodes, especially in neuroscience, is for electrochemical measurements made *inside* a living organism. Micron-sized electrodes are required [221], prepared by coating a sharpened metal W or Pt wire with BDD. Such *in situ* methods provide important information about the changes in the concentration of electroactive neuro-signalling molecules near the site(s) of their release and/or action. BDD microelectrodes have been used to measure the release of norepinephrine from sympathetic nerves (a process that regulates the diameter of arteries and veins) [222], as well as serotonin release from enterochromaffin cells in the small and large intestine [223]. One issue with using BDD for *in vivo* sensing is the rigid structure of diamond that is undesirable for sensors implanted into soft tissue. To overcome this, Fan *et al.* [224] have created a flexible BDD microelectrode using parylene C as a soft substrate. This flexible sensor is capable of electrochemical detection of dopamine in the presence of ascorbic acid and has been used to record the *in vivo* neural activity of a rat. Although such studies are still in their infancy, they hold great promise for future medical diagnostics.

### (iii) Modified B-doped diamond electrodes

Although diamond electrochemistry using planar macroscopic diamond films has been widely investigated, the use of diamond nanostructures such as nanotextures, nanowires, networks, porous films, nanoelectrodes and undoped/BDD nanoparticles is also a thriving field of study (reviewed in detail in [225]). Similarly, BDD electrodes decorated with metal nanoparticles are another important field, as the metal nanoparticles can be utilized to study specific analytes

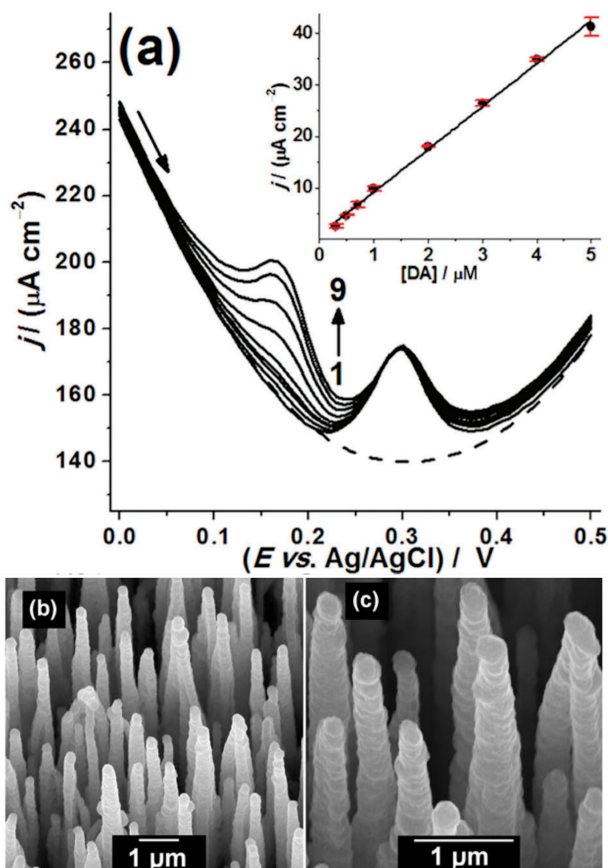


**Figure 16.** An example of the sensitivity and selectivity of BDD electrodes used for electrochemical trace analysis in water. (a) Differential pulse voltammograms recorded for different concentrations of dopamine (DA) (1–9 =  $0.0$ – $5.0 \times 10^{-6}$  M) in the presence of a chemically similar analyte ( $3.0 \times 10^{-5}$  M uric acid). Inset: current density  $j$  ( $\mu\text{A cm}^{-2}$ ) versus concentration of dopamine (mM) showing a linear response with concentration. (b,c) SEM images of ‘black diamond’, nanostructured BDD needles on the surface of an electrode, with electrochemically active area 220 times larger than that of a flat diamond electrode. Figures reprinted under CC BY 4.0 licence from [211]. (Published by The Royal Society of Chemistry).

while the BDD electrode acts as an electroactive but chemically inert support. There are many examples of the use of nanoparticle-decorated BDD electrodes for a variety of analytical applications (reviewed in [208,226]), but some recent representative examples include the use of Pt (biosensors [227]), Ag (analysis of ceftizoxime [228]), Au (proton detection [229], tumour-marker sensing [230], Hg detection [231]), Ni (immunosensor [232]) and Bi (Zn, Cd, Pb ion detection [233]).

#### (iv) $\text{CO}_2$ reduction

BDD electrodes can also be used to expedite useful electrochemical reactions [208]. To improve efficiency, often the bare BDD electrodes are decorated with metal or metal-oxide nanoparticles to exploit the catalytic activity of the high-surface-area nanoparticles and to make the reaction more selective. Also, the low background current of BDD electrodes suppresses the production of  $\text{H}_2$  gas, which might otherwise compete with the electrochemical reaction of interest. For example, there is a lot of interest currently in capturing  $\text{CO}_2$  from the air and converting it into chemically useful compounds, such as formic acid, formaldehyde or methanol [234]. Besides reactivity (especially at low overpotentials) and stability, the major issue is the catalyst’s ability to selectively produce a single compound with high efficiency. A recent example [235] reported

that CeO<sub>2</sub>-decorated BDD electrodes allowed CO<sub>2</sub> electrochemical reduction at overpotentials below 50 mV, yielding formic acid with a Faradaic yield higher than 40% and with stable performance for many hours. Electrolyte composition and concentration also has an effect upon the efficiency of the CO<sub>2</sub> reduction reaction, as reported by Jiwanti & Einaga [236], who used Pt-decorated BDD electrodes with NaCl and KCl cathode electrolytes. Ir-decorated BDD electrodes were used to produce formic acid with a Faradaic efficiency of approximately 50% and a low overpotential of  $-1.7$  V [237]. Other C<sub>2</sub>- and C<sub>3</sub>-containing molecules, such as ethanol (main product), acetaldehyde and acetone, were produced from the electrochemical reduction of CO<sub>2</sub> at the surfaces of Cu-modified BDD electrodes in aqueous media at room temperature, with the product distribution being dependent upon the amount of deposited Cu and the applied potential [238].

#### (v) Electrochemical water splitting

Electrochemical water splitting (EWS) is electrochemically converting water into H<sub>2</sub> and O<sub>2</sub> gases. The H<sub>2</sub> can then be reacted with oxygen in fuel cells to produce electrical power. Thus, development of a cheap and efficient EWS process is key to hydrogen power generation and the 'hydrogen economy' [239]. Unfortunately, the wide potential window of BDD electrodes, which is so useful in electroanalysis, is detrimental to EWS, as it means a high overvoltage is required for water splitting [240]. The two key processes involved in EWS—the hydrogen-evolution reaction (HER) and the oxygen-evolution reaction (OER)—are both inner-sphere reactions that consist of multi-step electron-transfer processes that involve the adsorption on to the electrodes of various reaction intermediates [241]. Diamond's chemical inertness means that these intermediates are reluctant to adsorb; consequently, the catalytic effect for HER and OER on bare BDD electrodes is weak [240].

However, the situation changes when the BDD electrodes are decorated with nanoparticles, as these now act as the catalyst, lowering the overpotential needed for EWS, while the BDD electrodes serve as robust, corrosion-resistant, fouling-resistant but electrically active supports. For example, BDD electrodes treated with CuO and ZnO nanoparticles have been reported to increase the efficiency of the EWS process [242], while Ir-black powder on BDD electrodes has been shown to be particularly suitable for the OER [243].

An alternative approach is to use the energy from sunlight to photocatalytically split water. For example, Ashcheulov *et al.* [244] reported that Si photoelectrodes were able to convert sunlight into electrical current; however, the Si gradually degraded when in contact with the electrolyte. To prevent this, the photocurrent was passed into the aqueous electrolyte via a protective BDD coating decorated with a cobalt phosphate catalyst, and this current was sufficient to drive EWS. Similarly, nanostructured BDD electrodes covered by an *n*-type TiO<sub>2</sub> thin film have been shown to develop a high photocurrent suitable for EWS [245]. Cu<sub>2</sub>O nanoparticles on BDD electrodes also act as efficient photocathodes for solar hydrogen generation [246]. There are a large number of possible metal and metal-oxide catalysts that can be used alongside BDD electrodes for solar-energy-driven photoelectrochemical water splitting [247], most of which are yet to be studied—so this is definitely an area to watch over the coming years.

#### (vi) Water purification

As well as detecting possible toxic compounds and ions in water sources, BDD electrodes can be used to clean up the water, removing organic toxins (chemical agents [248] or bacteria/viruses [249]) by electrolytic destruction [250]. This is an electrochemical technique that involves passing a high current (often many tens of amps) through the contaminated water via a series of electrodes. The current breaks apart any dissolved or suspended molecules, converting the organic components into CO<sub>2</sub> and rendering the toxins harmless and the water

safe. Unfortunately, the high currents sustained for long periods of time cause degradation and erosion of most electrodes, which must be replaced periodically at a high cost in money and time. BDD electrodes have proven to be more robust than most alternative materials, allowing higher currents to be used for longer periods between replacements [251].

One of the most environmentally important and timely water-purification challenges being tackled by BDD electrodes is to oxidatively destroy endocrine-disrupting chemicals (EDCs) in wastewater effluents [252]. EDCs are compounds that interfere with the function of the endocrine system that synthesises various regulatory hormones in mammals, fish and birds. The most common EDCs are used as pesticides (chlorpyrifos and dichlorodiphenyltrichloroethane), plastics (bisphenol A), plasticisers, industrial chemicals and solvents (dioxins, polybrominated biphenyls and polychlorinated biphenyls), surfactants (per- and polyfluoroalkyl substances) and preservatives (parabens) [253]. BDD anodes in water samples have been shown to be effective in the destruction of many of these EDCs with very high removal efficiencies, although scale-up is still an ongoing major problem [252].

A number of companies currently offer commercial water-purification systems based on BDD electrode technology, e.g. Proaqua (Austria), CSEM (Switzerland) and WaterDiam (France). The technology has recently been miniaturised, by a company called Enozo [254], to produce micro-ozone cells, which have been commercialized into household cleaning sprays, replacing bleach, alcohol or other cleaning fluids. At present, the available water-purification systems are suitable for household supplies, or perhaps a small factory, but not yet for large-scale use, e.g. to clean up rivers or reservoirs. However, in principle, to do so, this technology just needs to be scaled up and made portable.

### (vii) Solvated electrons

If diamond is illuminated with ultraviolet light at photon energies greater than the diamond band gap of 5.5 eV ( $\lambda < 225$  nm), electrons are excited from the valence band into the conduction band, from where they may be ejected from the surface. For H-terminated diamond, the surface dipole formed by the electronegativity difference between H and C, gives rise to negative electron affinity (NEA). This NEA surface means that no potential barrier needs to be overcome for these conduction-band electrons to escape the surface. If a liquid (rather than air or a vacuum) is present above the surface, the high-energy ejected electrons can interact with the liquid molecules to form 'solvated electrons'—complexes where isolated electrons are surrounded and stabilized by polar solvent molecules [255]. These solvated electrons are extremely reactive reducing agents ( $-4.6$  V compared to a normal hydrogen electrode) that can be used to drive chemical and biological reactions that are not accessible through conventional methods.

In 2013, Hamers' group at the University of Madison–Wisconsin reported the use of transient absorption spectroscopy to detect solvated electrons arising from emission of electrons from diamond into water [256]. The diamond sample was irradiated with a pulsed 213 nm UV laser while the change in intensity of a second laser beam (633 nm) parallel to the diamond surface was detected. A decrease in intensity of the transmitted 633 nm light was seen as a result of absorption by the newly created solvated electrons.

Solvated electrons generated by diamond surfaces or nanoparticles have been reported to expedite a number of reactions [257]. An example is the reaction of  $N_2$  gas and  $H_2$  gas to form  $NH_3$ , which is normally very demanding and expensive due to the high-energy intermediates involved and the reluctance of the two reactants to adsorb on to a solid catalyst or electrode. Using solvated electrons by-passes these problems [258].  $NH_3$  production has also been demonstrated using this approach in both single-compartment and dual-compartment cells [259]. This photo-electrocatalysis reaction has been further improved by using  $NH_2$ -terminated diamond [260] and also by embedding 100 nm Ag nanoparticles into the BDD electrodes [261]. Reduction of  $CO_2$  to CO was also demonstrated with 95% efficiency using solvated electrons generated from diamond electrodes [262]. However, to sound a note of caution—after

the initial excitement about the possibilities of solvated electron chemistry in the early 2010s, in the decade following, surprisingly few reports of new reactions using solvated electrons from diamond electrons have appeared, although a few intriguing publications still appear occasionally [263].

## (b) Electronic devices

Diamond has a number of advantages when compared to other wide-band-gap semiconductors, such as SiC or GaN, due to its high hole and electron mobilities (greater than  $2000 \text{ cm}^2 \text{ V}^{-1} \text{ s}^{-1}$ ), high critical electric field (greater than  $10 \text{ MV cm}^{-1}$ ), extremely high thermal conductivity (approx.  $22 \text{ W cm}^{-1} \text{ K}^{-1}$ ) and very wide band gap (5.4 eV) [264]. As a result, there is a large variety of applications in the medium-to-high-power regime for which diamond would be the ideal semiconducting material (see the excellent reviews by Donato *et al.* [265] and Araujo *et al.* [266] and the comprehensive book by Koizumi *et al.* [267]). At the moment, many of these applications might be considered niche and are limited to high-power, high-frequency and/or high-temperature operations. Nevertheless, improved efficiency in power electronics is becoming increasingly important as countries become more environmentally aware. This is because processing electricity along the chain from primary sources (power stations, solar farms, etc.) to end-users (factories, houses) loses approximately 9% of the generated energy [268], the majority of which comes from the use of inefficient Si-based power-conversion systems. Replacing Si power converters with diamond ones, which can switch higher power loads with fewer losses and at higher frequencies, could reduce the energy wastage significantly.

There are several problems that have held back progress in diamond electronics for over 30 years. The most important and frustrating of these is the continued lack of an effective room-temperature *n*-type conductor (see §8), which is crucial for fabrication of many important types of devices. Progress has also been hindered by the painfully slow progress in commercializing large-area SCD wafers. In comparison, the standard size SiC wafer produced today is 150 mm (6 inches), and many fabrication facilities are already moving to 200 mm (8 inches) wafers. Similarly, GaN-on-Si wafers can be purchased relatively inexpensively at all sizes up to 200 mm, and even the relative newcomer, gallium oxide, can be purchased at sizes up to 100 mm (4 inches). Although in recent years a lot of progress has been made with increasing the size of diamond wafers (see §11), the SCD substrates that are commercially available now are approximately 1 inch (25 mm), which is significantly smaller than competing materials, and are considerably more expensive. Sizes will increase and prices will fall, but the question remains whether the semiconductor industry will wait for diamond to catch up, or ‘make do’ with the existing materials because they are available now and ‘good enough’ for most applications.

### (i) Schottky diodes

Attendees at any international conference about diamond science and technology will find that there will be several sessions devoted to devices, and maybe half of the presentations will describe diamond Schottky diode (SD) devices [269]. The reason for this focus on SDs results from the lack of a suitable *n*-type dopant for diamond—SDs only require *p*-type diamond and so are the obvious candidate to demonstrate workable, commercial diamond devices.

An SD is a semiconductor diode formed by the junction of a semiconductor with a metal. As a diode, it conducts current primarily in only one direction where it has low electrical resistance and therefore a low forward voltage needed to pass current. In the reverse direction, there is a high resistance that prevents backward current flow. If the semiconductor is *p*-type diamond, then the forward voltage can be very low, while the reverse voltage is extremely high, allowing efficient switching of high-power systems operating at up to 20 A (equivalent to a current density of  $100 \text{ A cm}^{-2}$ ) at 500 K [270].

The vertical structure (as shown in figure 17) is one of the best geometrical configurations used for diamond SDs due to its low serial resistance. This structure is characterised by vertical electrical current transport through a layered stack comprising an active layer and a highly conductive substrate.

The problems with obtaining large-area SCD have resulted in the development of pseudo-vertical diamond SDs (figure 17b), where heavily doped  $p^{++}$  diamond layers are grown on top of a diamond substrate. A range of metals (W, Zr, Cu and Pt) and surface treatments have been studied to improve the uniformity of the diamond-metal junction, as well as to reduce leakage currents which result in premature breakdown of the device. Using Zr metal, a pseudo-vertical diamond SD has been demonstrated operating at  $1000 \text{ A cm}^{-2}$  at 6 V and a high reverse breakdown field greater than  $7.7 \text{ MV cm}^{-1}$  [271].

Despite the difficulty with  $n$ -type doping, it is still possible to make diodes using  $n$ -type diamond; however, the high resistance of the  $p$ - $n$  junction often limits the efficiency of these types of devices [272]. Nevertheless, various so-called PIN devices and Schottky PN diodes (figure 17c,d) have been fabricated with reasonable performance figures [265].

## (ii) Field effect transistors

Field effect transistors (FETs) are devices that control the flow of current from one electrode (the source) to another (the drain) by the application of a voltage to a third electrode (the gate). The applied voltage alters the conductivity between the drain and source, allowing the FET to be used as a digital on/off switch for binary electronics or as a current amplifier. FETs are unipolar transistors because they only involve single carriers, i.e. either electrons or holes, but not both. This means FETs can be fabricated using only  $p$ -type diamond, and the lack of an  $n$ -type dopant is not so critical. There are many different types of FET devices, but the three which have been applied most to diamond are surface-channel devices,  $\delta$ -doped devices and two-dimensional hole-gas devices.

### Surface-channel FET devices

The most common type of FET device uses the metal-oxide-semiconductor (MOS) structure for the gate electrode, where a metallicly conducting gate electrode sits upon a very thin oxide layer on top of a semiconductor (in this case, doped diamond) substrate (figure 18). Thus, the gate has a capacitor structure with the oxide preventing direct electrical contact between the metal and semiconductor. When an appropriate voltage is applied to the gate, current flows from the source to the drain through a thin conducting channel that has been temporarily created close to the diamond surface beneath the gate oxide.

A number of MOSFET devices have been fabricated using diamond as the semiconductor, with varying degrees of success. However, the lack of a solid oxide for diamond often results in highly defective interfaces, which negatively affects the carrier mobility through the source-drain channel. Numerous diamond-metal-oxide interfaces have been studied over the past few years [273], with  $\text{Al}_2\text{O}_3$  exhibiting the best performance [274]. The difficulty in making standard MOS devices has led to new designs such as finFETs operating in so-called deep-depletion mode [275], with reasonable device performance but a rather high negative threshold voltage, suggesting that a high level of interface defects remained.

The gate-oxide problem can be eliminated by using different types of device designs that do not require a gate-oxide layer, such as junction FETs, metal-semiconductor FETs and bipolar transistors. The performance of all these devices is reviewed in detail in [265], and improvements are continually being made at a slow and steady pace. However, competing materials, in particular SiC, have more than a decade's head start and may well capture the market for high-power, high-temperature devices *before* diamond devices become commercially viable.

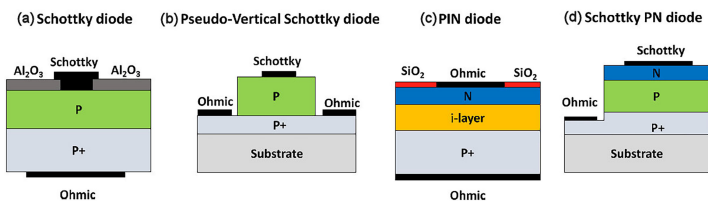


**Figure 17.** Different vertical device structures for diamond diodes. (a) Vertical SD using only  $p$ -type diamond. (b) Pseudo-vertical SD that uses only  $p$ -type diamond but no back contact. (c) PIN diode composed of a sandwich of  $p^+$ -type diamond, an undoped intrinsic diamond layer and an  $n$ -type diamond layer, with Ohmic contacts on either side. (d) Schottky PN diode. Figure reproduced from [265] and modified under the Creative Commons Attribution 3.0 licence.

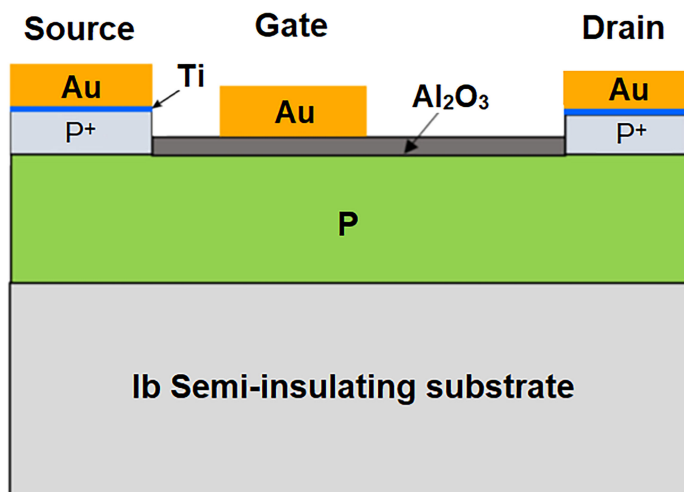


**Figure 18.** A typical design for a diamond lateral deep-depletion MOSFET-style device. The type-1b diamond substrate (usually HPHT) has a  $p$ -type BDD layer (green, labelled 'P') deposited homoepitaxially on to it. The source and drain electrodes are composed of heavily BDD (grey, labelled  $P^+$ ) capped with a highly conducting metal such as Au (gold), with a thin Ti layer (blue) at the interface allowing a good electrical contact to be formed with the underlying diamond. These are patterned using standard photolithography and dry etching methods. The Au gate electrode is electrically isolated from the BDD layer by a gate oxide (grey), in this case made from insulating  $Al_2O_3$ . Image reproduced and modified from [265]. Creative Commons Attribution 3.0 licence.

### *$\delta$ -Doped devices*

So-called 'delta doping' requires the epitaxial growth of a very thin (less than 2 nm), heavily boron-doped diamond layer with B concentration above the metallic transition point (see figure 10 earlier). This doped layer is called a 'delta-doped layer' from its similarity to the abrupt ' $\delta$ -function' in mathematics because it has atomically sharp and atomically smooth interfaces between itself and the undoped diamond layers above and below it. Although a number of research groups have attempted to make  $\delta$ -doped FET devices [267,276], attempts at achieving a true monolayer doping profile with significant mobility enhancement have generally been disappointing, mainly due to the difficulty of controlling the dopant concentration profile to such precision.

### *Two-dimensional hole-gas field effect transistor devices*

Research groups, such as those at the University of Glasgow [154] and Waseda University (Tokyo) [277], have been exploiting surface transfer doping in hydrogenated diamond

(described earlier in §8), to produce novel FET devices in which the conduction from source to drain, moderated via a gate electrode, is through the 2DHG conductive layer, rather than through the semiconducting substrate (figure 19). Not only do these 2DHG FETs exhibit excellent device performance, but because they are fabricated directly on to an insulating diamond substrate, they should be considerably more radiation hard compared to standard Si-based devices.

For all the SD and FET devices mentioned above, the comprehensive analysis conducted by Donato *et al.* [265] has suggested that diamond may remain a niche device material for quite some time and be limited to devices with high junction temperatures (greater than 450 K), medium-high frequency (greater than 20 kHz) and high voltage (greater than 3 kV) where they should outperform SiC and GaN commercial alternatives. More specialized diamond electronic devices, such as radiation-hard architectures, surface acoustic wave filters and micro/nanoelectro-mechanical systems, are discussed in the electronic supplementary material.

### (c) Quantum applications

Diamond-based quantum technologies revolve around optically active atomic-scale defects in the diamond lattice [278]. The most studied is the NV defect (see §9) [279], although various other defects with similar properties have also been investigated [280]. The electrons associated with these defects have a spin that is sensitive to external magnetic fields, and due to diamond's transparency, the electrons can be manipulated using light. Moreover, these spins possess long coherence times (i.e. the duration for which the spin remains stable and predictable) due to their exceptional isolation from other nearby NV-centre spins by the diamond lattice. This isolation has another important consequence; because the NV centre acts like a single isolated pseudo-atom, it can only absorb or re-emit *one* photon at a time. So, when a laser beam is used to probe the defect, only *one* photon from the billions of laser photons is absorbed, and its energy is used to excite *one* electron. After a short delay, the electron relaxes to a lower state, emitting *only one* photon (usually of lower energy than the original laser photons). In the case of the NV centre, usually, the pumping photons are green ( $\lambda = 532$  nm), while the emitted fluorescence is red ( $\lambda = 637$  nm) [281].

The process by which the spin is measured is called optically detected magnetic resonance. The NV defects have a remarkable set of energy levels, in that no matter what ground-state spin an electron has originally, if the diamond is illuminated with green light the electron will cycle through all the allowed energy levels, absorbing green photons and then relaxing and re-emitting red photons. Due to quantum selection rules and the relative lifetimes of the states involved, eventually, the electron is statistically more likely to end up in the ground state with spin  $m_s = 0$ . For multiple NV centres, if the electrons are cycled around this loop enough times, nearly all their electrons will end up in the same  $m_s = 0$  state, and the spins of each NV centre will be aligned. This effectively 'resets' the system, ensuring the starting point is always identical.

Once reset like this, the readout from a quantum experiment is observed as a change in the red fluorescence after shining green light on a single NV defect, or on to a group of them, while scanning an applied MW field. When the MW frequency hits resonance with an  $m_s = 0$  to  $m_s = \pm 1$  transition, a decrease in fluorescence intensity is observed. So, by measuring the intensity of the fluorescence, the spin state of the defect can be read out.

The quantum-mechanical nature of spin means that the red fluorescence photon will be emitted with spin properties based on those of the original electron, for example, either 'up' or 'down'. The single photons emitted from different NV centres can be captured in fibre-optic waveguides and then combined to create quantum superpositions and entanglement. Such entangled photons form quantum bits (qubits) that are the key to quantum communication and computing.

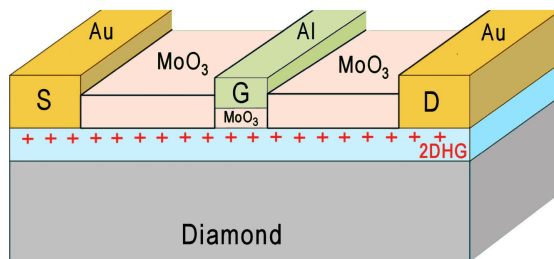


**Figure 19.** Schematic cross-sectional view of a diamond-based MOSFET device utilizing the 2DHG conduction channel in H-terminated diamond protected by a MoO<sub>3</sub> capping layer, based on the design proposed in [156]. S, G and D refer to source, gate and drain, respectively.

### (i) Quantum computing

In standard binary computing, a ‘bit’ is either 1 or 0. If spin-up is a 1 and spin-down is a 0, then two entangled photons in a qubit would be both 1 *and* 0 at the same time, until one of the pair is examined (figure 20). At the instant the spin of the examined photon is revealed, the spin of the other photon is also known, even though that second photon had never been examined and may now be a very long distance from the first photon. (In fact, quantum theory states that there is *no* limit to this separation—the two photons might be on different continents, different planets or even different galaxies—yet the communication between them remains instantaneous.)

The power of quantum computing lies in the fact that changing one of the states of *one* of the qubits immediately changes the states of *all* of its entangled partners. This means that the number of calculations that can be performed scales as  $2^n$ , where  $n$  is the number of qubits. So, entangling only 20 qubits together enables the equivalent of over a million calculations to be performed instantly. This means that a calculation performed linearly by a normal computer, which requires multiple steps (additions, multiplications, carrying values, etc.), can be done in *one* fast step by a quantum computer. Thus, quantum computers have the potential for unprecedented computing speeds and, coupled with artificial intelligence, may truly be world-changing.

At the time of writing, the World’s most powerful quantum computer is reported to be the *Google* Sycamore processor with 70 (non-diamond) qubits. In 2019, an earlier version of Sycamore with only 53 qubits completed a calculation in 200 seconds that *Google* claimed [282] would take a normal state-of-the-art supercomputer 10,000 years to finish. Although astonishing, current quantum computers do not yet use diamond defects to create qubits and so need to be cooled by liquid helium to temperatures a few degrees above absolute zero to attain coherence times sufficient for complex calculations. Diamond-based quantum computers should work at *room temperature*, making them vastly cheaper and easier to operate.

Progress in the field of diamond quantum computing has been fairly rapid since the first demonstration of entanglement between an NV spin and a photon was reported in 2010 [283]. In 2013, entanglement was reported between two separated NV centres using lenses patterned into the diamond surface acting as amplifiers [284]. Later that year, the distance between the qubit photons (i.e. the ‘node’ separation) was extended to 3 m [285]. In 2015, the node separation was extended to more than 1 km [286]. In 2019, a group at Delft University reported a 10-qubit register that could store quantum information for up to 75 s [287]. Such long timescales provide sufficient time for controlled logical operations (AND, NOR, etc.) to be performed between different spin qubits [288]. The initialization and manipulation of the diamond NV centre spins can now be performed with single-shot measurements, making them ideal systems for scaling up into multi-qubit quantum registers [289].

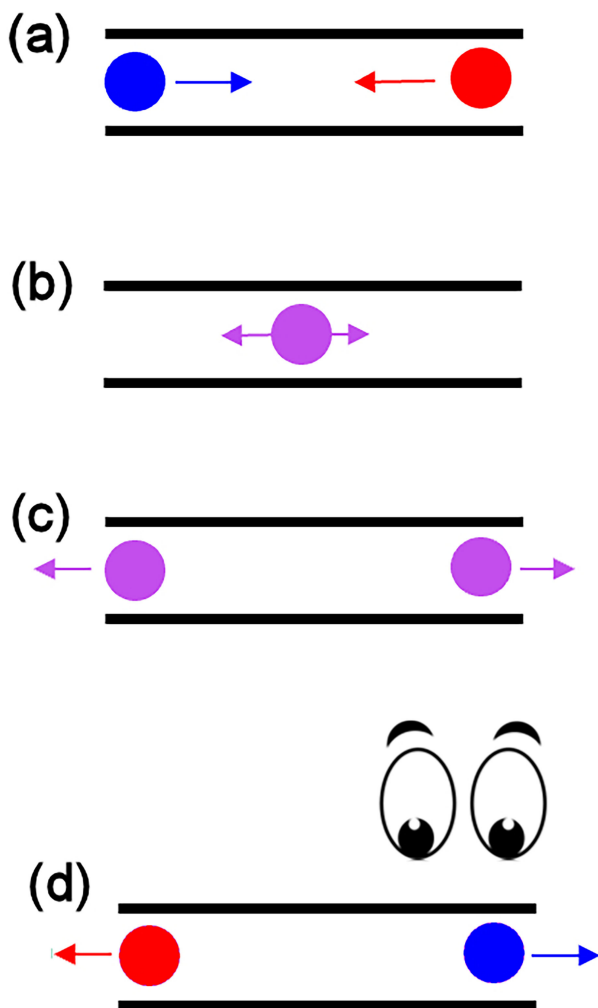


**Figure 20.** A simplistic representation of quantum entanglement of two photons. (a) Two independent photons with opposite spin (depicted as red and blue) emitted from different NV centres approach each other inside a fibre-optic waveguide. (b) When they meet, their wavefunctions entangle, and they both share the same superposition wavefunction—i.e. the photons are now both red *and* blue simultaneously (depicted as purple). (c) When they separate, both photons remain entangled in the same shared quantum state. (d) If one of the photons is observed, the superposition wavefunction collapses, and the spin of that photon is fixed at that instant as being either up or down (red or blue, in this case red). At that same instant, the spin of the other photon is also known (blue), even though it was never observed and might now be thousands of kilometres from its partner.

Research in this area is now following two approaches. The first aims to further improve the quality of the diamond, reducing defects and developing methods to control the density and positioning of NV (or other) centres, along with maximizing the efficiency by which photons are extracted from individual NVs [290]. The second approach involves developing the new software required to control these quantum systems. In particular, code that enables errors in qubit states to be detected and corrected has already been realized in small qubit networks [291]. The key challenge for the future is to scale up to quantum networks of tens or hundreds of qubits. Such work is now proceeding rapidly; however, it may be many more years before we see a fully functioning diamond quantum computer [292].

## (ii) Quantum cryptography

Another application of the control and entanglement of photon spins from the NV centre is to enable perfectly secure communications [293]. To do so, the information being sent would be encrypted using an entangled quantum key known only to the sender and receiver. If the message were to be intercepted by a third party, the wavefunction of the quantum key would collapse and the attempted eavesdropping event revealed. Such secure communications should, in theory, make copying or modifying confidential data (e.g. a PIN number sent over the internet or medical records) almost impossible [278].

## (iii) Quantum sensing and magnetometry

Electronic spins in NV centres are sensitive to temperature, electric fields and magnetic fields and can be used as highly sensitive sensors that operate at room temperature. Most of the work in this area concerns magnetometry and describes the measurement of tiny magnetic fields at the nanometre scale, for example, in the study of new superconductors or semiconductor materials.

Quantum sensing is achieved in practice by placing or depositing on to the substrate a diamond sample with a high-density, thin layer of near-surface NV centres. The NV centres can also be incorporated into nanostructures, such as DND particles, to achieve nanometre proximity to the site of interest, or attached to fibres to make magnetic endoscopes. For instance, DND particles containing NV centres have been ingested by biological cells enabling *in situ* sensing and tracking [162], while the local temperature inside a living cell has been monitored providing information about the cell's metabolism and transport pathways [294]. Indeed, since the first reports of NV-based magnetic sensing in 2008 [295–297], this technique has been used to detect a range of other physical quantities, such as electric fields, charge, voltage, current, orientation, strain, temperature and pressure. A summary of different sensor types with their related sensitivities is listed in table 2 of Nebel's detailed review paper [279].

Looking to the future, there is a growing number of companies developing diamond quantum technology, including large companies such as Lockheed Martin, Bosch and Thales, as well as many start-ups such as Quantum Diamond Technologies [298], NVision [299] and Qnami [300]. In parallel with the development of high-purity substrates within which NV centres (or other suitable defects) can be fabricated, quantum technology could well become one of the killer applications for diamond technology in the second half of this century.

## 13. Conclusions

The advances in CVD diamond technology which have occurred over the past decade have mostly been driven by the upsurge in the market for lab-grown diamond jewellery, which has seen huge increases in the number of SCD gemstones produced, their size, quality and throughput. Countries including, Israel, the US and especially China, and more recently, India, have invested heavily in the technology and equipment necessary for mass-market production of lab-grown diamonds. The market for CVD lab-grown diamond jewellery is still increasing at a rapid rate and may exceed 20% of all global diamond jewellery sales by the end of the decade. Lab-grown HPHT and CVD diamonds are already available in a range of colours [197] and at sizes previously only affordable by the very wealthy.

However, the next few years will probably witness the maturing of the CVD diamond gem industry, driven by (i) nearly limitless supply, (ii) uniform and reproducible high quality, (iii) branding and proprietary design and (iv) even more unusual custom shapes and colours [301]. With the market for smaller gemstone diamonds eventually becoming saturated, manufacturers may switch tactics from quantity to size. It has been estimated [301] that by the end of the

decade, a customer with a typical \$6500 budget may be able to purchase a 6- or even 7-carat lab-grown diamond with a diameter greater than 1.2 cm.

An alternative strategy to ‘bigger is better’ may be to use lab-grown diamond gems in a way that is impossible with natural diamonds. With advances in growth and laser-cutting technology, manufacturing an ‘all-diamond’ ring or bracelet may become possible. The conventional cuts (such as the well-known ‘brilliant’ cut) that have been used for centuries to enhance the sparkle of natural stones may find new rivalry in the form of complex 3D custom cuts or shapes that differ considerably from those traditional ones. Similarly, by treating the diamonds post-deposition using HPHT annealing or radiation exposure, diamonds might be fabricated in a range of exotic colours that do not exist in nature.

The developments in the gem industry so far have fed into the scientific sector in terms of ultra-pure SCD substrates with increasingly larger wafer sizes for electronic and quantum applications and at progressively lower costs. But increased supply means that prices of CVD diamond gemstones are falling year-on-year [302], although the ‘green’ credentials of lab-grown diamonds combined with the consumer’s certainty that they do not come from conflict zones or are mined by an exploited labour force should prevent the price dropping too low. If that predicted trend continues, profit margins will eventually drop, possibly leading to a decrease in investment in diamond technology by the gem manufacturers. The knock-on effect for scientific diamond research may be less research funding, potentially leading to a much slower delivery time for many of the more ambitious applications mentioned in §12. It is somewhat ironic that a material with so many superlative properties and exciting potential scientific applications may have its future determined by the whims of fashion!

Nevertheless, there is a renewed hope that the three ‘killer applications’, electrochemistry, quantum information and high-temperature electronics, along with the huge number of possible diverse applications for CVD diamond that are beginning to find their way to market [5], might be sufficient for diamond research to flourish—despite the uncertainties of the gemstone market. The original review paper in 2000 was entitled: *Diamond—a 21<sup>st</sup>-Century Material*. Maybe that now needs to be qualified somewhat, to: *Diamond—a mid-21<sup>st</sup>-Century Material*, because it may take another 20 years or so before diamond can finally live up to its promise of a ubiquitous wonder material.

**Data accessibility.** Supplementary material is available on the University of Bristol Repository [303].

Supplementary material is also available online [304].

**Declaration of AI use.** We have not used AI-assisted technologies in creating this article.

**Authors’ contributions.** P.M.: conceptualization, project administration, writing—original draft, writing—review and editing; R.Z.: conceptualization, visualization, writing—original draft, writing—review and editing.

Both authors gave final approval for publication and agreed to be held accountable for the work performed therein.

**Conflict of interests.** We declare we have no competing interests.

**Funding.** R.Z. thanks the funding scheme of the Government of the Republic of Kazakhstan under the Bolashak International programme.

**Acknowledgements.** The authors wish to thank Professor Mike Ashfold FRS for carefully proofreading the manuscript and making numerous useful and valuable suggestions.

## References

1. May PW. 2000 Diamond thin films: a 21st-century material. *Phil. Trans. R. Soc. Lond. A* **358**, 473–495. (doi:10.1098/rsta.2000.0542)
2. Onstad E, Clarke D. 2018 How man-made diamonds have grown to threaten natural gems. Reuters Business News. See <https://www.reuters.com/article/idUSKCN10K0N4/> (accessed 7 March 2024).

3. Barkan T. 2019 Graphene: the hype versus commercial reality. *Nat. Nanotechnol.* **14**, 904–906. (doi:10.1038/s41565-019-0556-1)
4. Nebel CE. 2023 CVD diamond: a review on options and reality. *Funct. Diam.* **3**, 2201592. (doi:10.1080/26941112.2023.2201592)
5. Zulkharnay R, May PW. 2024 Applications of diamond films: a review. *Funct. Diam.* **4**, 2410160. (doi:10.1080/26941112.2024.2410160)
6. Dischler B, Wild C (eds). 1998 *Low-pressure synthetic diamond: manufacturing and applications*. Berlin, Germany: Springer. (doi:10.1007/978-3-642-71992-9)
7. Ohtake N, Yoshikawa M. 1990 Diamond film preparation by arc discharge plasma jet chemical vapor deposition in the methane atmosphere. *J. Electrochem. Soc.* **137**, 717–722. (doi:10.1149/1.2086540)
8. Rennick CJ, Ma J, Henney JJ, Wills JB, Ashfold MNR, Orr-Ewing AJ, Mankelevich Y. 2007 Measurement and modeling of Ar/H<sub>2</sub>/CH<sub>4</sub> arc jet discharge chemical vapor deposition reactors. I. intercomparison of derived spatial variations of H atom, C<sub>2</sub>, and CH radical densities. *J. Appl. Phys.* **102**, 063309. (doi:10.1063/1.2783890)
9. Mankelevich Y, Ashfold MNR, Orr-Ewing AJ. 2007 Measurement and modeling of Ar/H<sub>2</sub>/CH<sub>4</sub> arc jet discharge chemical vapor deposition reactors II: modeling of the spatial dependence of expanded plasma parameters and species number densities. *J. Appl. Phys.* **102**, 063310. (doi:10.1063/1.2783891)
10. Ashfold MNR, May PW, Petherbridge JR, Rosser KN, Smith JA, Mankelevich YA, Suetin NV. 2001 Unravelling aspects of the gas phase chemistry involved in diamond chemical vapour deposition. *Phys. Chem. Chem. Phys.* **3**, 3471–3485. (doi:10.1039/b104265n)
11. Lu FX. 2022 Past, present, and the future of the research and commercialization of CVD diamond in China. *Funct. Diam.* **2**, 119–141. (doi:10.1080/26941112.2022.2144769)
12. Lu FX *et al.* 1998 A new type of DC arc plasma torch for low cost large area diamond deposition. *Diam. Relat. Mater.* **7**, 737–741. (doi:10.1016/S0925-9635(97)00180-5)
13. *SEKI Diamond Systems*. See <http://sekiamond.com>.
14. Xuan Z, Yang P, Pu X, Liu E, Qi L, Sun J, Peng H, Hu G, Hou L. 1993 Plasma diagnosis in d.c.-biased hot-filament-assisted chemical vapour deposition by double-probe method. *Diam. Relat. Mater.* **2**, 476–480. (doi:10.1016/0925-9635(93)90103-9)
15. Noguchi H. 2012 *Diamond producing method and dc plasma enhanced CVD apparatus*. Japan Patent JP5842761B2761B2. See <https://patents.google.com/patent/US20140041574A1/en> (accessed 7 March 2024).
16. Bai Y, Jin Z, Lv X, Jiang Z, Wang J, Wu H. 2005 Influence of cathode temperature on gas discharge and growth of diamond films in DC-PCVD processing. *Diam. Relat. Mater.* **14**, 1494–1497. (doi:10.1016/j.diamond.2005.03.005)
17. Chae KW, Baik YJ, Park JK, Lee W. S. 2010 The 8-inch free-standing CVD diamond wafer fabricated by DC-PACVD. *Diam. Relat. Mater.* **19**, 1168–1171. (doi:10.1016/j.diamond.2010.05.002)
18. Baudrillart B, Bénédic F, Chauveau Th, Bartholomot A, Achard J. 2017 Nanocrystalline diamond films grown at very low substrate temperature using a distributed antenna array microwave process: towards polymeric substrate coating. *Diam. Relat. Mater.* **75**, 44–51. (doi:10.1016/j.diamond.2017.01.001)
19. Taylor A, Fendrych F, Fekete L, Vlček J, Řezáčová V, Petrák V, Krucký J, Nesládek M, Liehr M. 2011 Novel high-frequency pulsed MW-linear antenna plasma-chemistry: routes towards large area, low pressure nanodiamond growth. *Diam. Relat. Mater.* **20**, 613–615. (doi:10.1016/j.diamond.2011.01.003)
20. Liehr M, Wieder S, Dieguez-Campo M. 2006 Large area microwave coating technology. *Thin Solid Films* **502**, 9–14. (doi:10.1016/j.tsf.2005.07.226)
21. Gu J, Chen Z, Li R, Zhao X, Das C, Sahnuganathan V, Sudijono J, Lin M, Loh KP. 2021 Nanocrystalline diamond film grown by pulsed linear antenna microwave CVD. *Diam. Relat. Mater.* **119**, 108576. (doi:10.1016/j.diamond.2021.108576)
22. Mehedi HA, Achard J, Rats D, Brinza O, Tallaire A, Mille V, Silva F, Provent Ch, Gicquel A. 2014 Low temperature and large area deposition of nanocrystalline diamond films with distributed antenna array microwave-plasma reactor. *Diam. Relat. Mater.* **47**, 58–65. (doi:10.1016/j.diamond.2014.05.004)

23. Kim J, Tsugawa K, Ishihara M, Koga Y, Hasegawa M. 2010 Large-area surface wave plasmas using microwave multi-slot antennas for nanocrystalline diamond film deposition. *Plasma Sources Sci. Technol.* **19**, 015003. (doi:10.1088/0963-0252/19/1/015003)
24. Tallaire A, Achard J, Silva F, Brinza O, Gicquel A. 2013 Growth of large size diamond single crystals by plasma assisted chemical vapour deposition: recent achievements and remaining challenges. *Comptes Rendus Phys.* **14**, 169–184. (doi:10.1016/j.crhy.2012.10.008)
25. Teraji T *et al.* 2015 Homoepitaxial diamond film growth: high purity, high crystalline quality, isotopic enrichment, and single color center formation. *Phys. Status Solidi* **212**, 2365–2384. (doi:10.1002/pssa.201532449)
26. Baryshev SV, Muehle M. 2024 Scalable production and supply chain of diamond wafers using microwave plasma: a mini-review. *IEEE Trans. Plasma Sci.* 1–22. (doi:10.1109/tps.2023.3339338)
27. Butler JE, Woodin RL. 1993 Thin film diamond growth mechanisms. *Phil. Trans. R. Soc. Lond. A.* **342**, 209–224. (doi:10.1098/rsta.1993.0015)
28. Goodwin DG, Butler JE *et al.* 1997 Theory of diamond chemical vapor deposition. In *Handbook of industrial diamonds and diamond films* (ed. MA Prelas), pp. 527–581. New York, NY, USA: Dekker. (doi:10.1201/9780203752807-11)
29. Butler JE, Mankelevich YA, Cheesman A, Ma J, Ashfold MNR. 2009 Understanding the chemical vapor deposition of diamond: recent progress. *J. Phys.* **21**, 364201. (doi:10.1088/0953-8984/21/36/364201)
30. Ma J, Ashfold MNR, Mankelevich YA. 2009 Validating optical emission spectroscopy as a diagnostic of microwave activated CH<sub>4</sub>/Ar/H<sub>2</sub> plasmas used for diamond chemical vapor deposition. *J. Appl. Phys.* **105**, 043302. (doi:10.1063/1.3078032)
31. Ma J, Richley JC, Ashfold MNR, Mankelevich YA. 2008 Probing the plasma chemistry in a microwave reactor used for diamond chemical vapor deposition by cavity ring down spectroscopy. *J. Appl. Phys.* **104**, 103305. (doi:10.1063/1.3021095)
32. Lombardi G, Hassouni K, Stancu GD, Mechold L, Röpcke J, Gicquel A. 2005 Study of an H<sub>2</sub>/CH<sub>4</sub> moderate pressure microwave plasma used for diamond deposition: modelling and IR tuneable diode laser diagnostic. *Plasma Sources Sci. Technol.* **14**, 440–450. (doi:10.1088/0963-0252/14/3/005)
33. Cheesman A, Smith JA, Ashfold MNR, Langford N, Wright S, Duxbury G. 2006 Application of a quantum cascade laser for time-resolved, in Situ probing of CH<sub>4</sub>/H<sub>2</sub> and C<sub>2</sub>H<sub>2</sub>/H<sub>2</sub> gas mixtures during microwave plasma enhanced chemical vapor deposition of diamond. *J. Phys. Chem.* **110**, 2821–2828. (doi:10.1021/jp056622u)
34. Petherbridge JR, May PW, Pearce SRJ, Rosser KN, Ashfold MNR. 2001 Low temperature diamond growth using CO<sub>2</sub>/CH<sub>4</sub> plasmas: molecular beam mass spectrometry and computer simulation investigations. *J. Appl. Phys.* **89**, 1484–1492. (doi:10.1063/1.1333031)
35. Cheesman A, Harvey JN, Ashfold MNR. 2008 Studies of carbon incorporation on the diamond (100) surface during chemical vapor deposition using density functional theory. *J. Phys. Chem.* **112**, 11436–11448. (doi:10.1021/jp8034538)
36. Rivero P, Shelton W, Meunier V. 2016 Surface properties of hydrogenated diamond in the presence of adsorbates: a hybrid functional DFT study. *Carbon* **110**, 469–479. (doi:10.1016/j.carbon.2016.09.050)
37. Van Regemorter T. 2009 The influence of dopants on the growth of diamond by CVD. PhD Thesis, [Sweden]: Uppsala University. <https://www.diva-portal.org/smash/get/diva2:173161/FULLTEXT01.pdf> (accessed 7 March 2024).
38. Zou Y, Larsson K. 2016 Effect of boron doping on the CVD growth rate of diamond. *J. Phys. Chem. C* **120**, 10658–10666. (doi:10.1021/acs.jpcc.6b02227)
39. Shah ZM, Mainwood A. 2008 A theoretical study of the effect of nitrogen, boron and phosphorus impurities on the growth and morphology of diamond surfaces. *Diam. Relat. Mater.* **17**, 1307–1310. (doi:10.1016/j.diamond.2008.03.028)
40. Richley JC, Harvey JN, Ashfold MNR. 2009 On the role of carbon radical insertion reactions in the growth of diamond by chemical vapor deposition methods. *J. Phys. Chem.* **113**, 11416–11422. (doi:10.1021/jp906065v)
41. Netto A, Frenklach M. 2005 Kinetic Monte Carlo simulations of CVD diamond growth – interplay among growth, etching, and migration. *Diam. Relat. Mater.* **14**, 1630–1646. (doi:10.1016/j.diamond.2005.05.009)

42. Rodgers WJ, May PW, Allan NL, Harvey JN. 2015 Three-dimensional kinetic Monte Carlo simulations of diamond chemical vapor deposition. *J. Chem. Phys.* **142**, 214707. (doi:10.1063/1.4921540)
43. Battaile CC, Srolovitz DJ, Butler JE. 1997 Morphologies of diamond films from atomic-scale simulations of chemical vapor deposition. *Diam. Relat. Mater.* **6**, 1198–1206. (doi:10.1016/S0925-9635(97)00046-0)
44. Gruen DM, Liu S, Krauss AR, Luo J, Pan X. 1994 Fullerenes as precursors for diamond film growth without hydrogen or oxygen additions. *Appl. Phys. Lett.* **64**, 1502–1504. (doi:10.1063/1.111872)
45. Zhou D, McCauley TG, Qin LC, Krauss AR, Gruen DM. 1998 Synthesis of nanocrystalline diamond thin films from an Ar-CH<sub>4</sub> microwave plasma. *J. Appl. Phys.* **83**, 540–543. (doi:10.1063/1.366668)
46. Gruen DM, Redfern PC, Horner DA, Zapol P, Curtiss LA. 1999 Theoretical studies on nanocrystalline diamond: nucleation by dicarbon and electronic structure of planar defects. *J. Phys. Chem. B* **103**, 5459–5467. (doi:10.1021/jp990165y)
47. Rabeau JR, John P, Wilson JIB, Fan Y. 2004 The role of C<sub>2</sub> in nanocrystalline diamond growth. *J. Appl. Phys.* **96**, 6724–6732. (doi:10.1063/1.1810637)
48. May PW, Mankelevich Y. 2006 Experiment and modeling of the deposition of ultrananocrystalline diamond films using hot filament chemical vapor deposition and Ar/CH<sub>4</sub>/H<sub>2</sub> gas mixtures: a generalized mechanism for ultrananocrystalline diamond growth. *J. Appl. Phys.* **100**, 024301. (doi:10.1063/1.2214304)
49. May PW, Harvey JN, Smith JA, Mankelevich Y. 2006 Reevaluation of the mechanism for ultrananocrystalline diamond deposition from Ar/CH<sub>4</sub>/H<sub>2</sub> gas mixtures. *J. Appl. Phys.* **99**, 104907. (doi:10.1063/1.2195347)
50. Ashfold MNR, Goss JP, Green BL, May PW, Newton ME, Peaker CV. 2020 Nitrogen in diamond. *Chem. Rev.* **120**, 5745–5794. (doi:10.1021/acs.chemrev.9b00518)
51. Achard J, Silva F, Brinza O, Tallaire A, Gicquel A. 2007 Coupled effect of nitrogen addition and surface temperature on the morphology and the kinetics of thick CVD diamond single crystals. *Diam. Relat. Mater.* **16**, 685–689. (doi:10.1016/j.diamond.2006.09.012)
52. Jin S, Moustakas TD. 1994 Effect of nitrogen on the growth of diamond films. *Appl. Phys. Lett.* **65**, 403–405. (doi:10.1063/1.112315)
53. Tang CJ, Fernandes AJS, Costa F, Pinto JL. 2011 Effect of microwave power and nitrogen addition on the formation of {100} faceted diamond from microcrystalline to nanocrystalline. *Vacuum* **85**, 1130–1134. (doi:10.1016/j.vacuum.2011.01.024)
54. Ashkinazi E, Khmel'nitskii R, Sedov V, Khomich A, Khomich A, Ralchenko V. 2017 Morphology of diamond layers grown on different facets of single crystal diamond substrates by a microwave plasma CVD in CH<sub>4</sub>-H<sub>2</sub>-N<sub>2</sub> gas mixtures. *Crystals* **7**, 166. (doi:10.3390/cryst7060166)
55. Truscott BS, Kelly MW, Potter KJ, Johnson M, Ashfold MNR, Mankelevich YA. 2015 Microwave plasma-activated chemical vapour deposition of nitrogen-doped diamond, I: N<sub>2</sub>/H<sub>2</sub> and NH<sub>3</sub>/H<sub>2</sub> plasmas. *J. Phys. Chem.* **119**, 12962–12976. (doi:10.1021/acs.jpca.5b09077)
56. Truscott BS, Kelly MW, Potter KJ, Ashfold MNR, Mankelevich YA. 2016 Microwave plasma-activated chemical vapor deposition of nitrogen-doped diamond, II: CH<sub>4</sub>/N<sub>2</sub>/H<sub>2</sub> plasmas. *J. Phys. Chem.* **120**, 8537–8549. (doi:10.1021/acs.jpca.6b09009)
57. Kelly MW, Halliwell SC, Rodgers WJ, Pattle JD, Harvey JN, Ashfold MNR. 2017 Theoretical investigations of the reactions of N- and O-containing species on a C(100):H 2 × 1 reconstructed diamond surface. *J. Phys. Chem.* **121**, 2046–2055. (doi:10.1021/acs.jpca.7b00466)
58. Regemorter TV, Larsson K. 2009 Effect of a NH coadsorbate on the CH<sub>3</sub> (or CH<sub>2</sub>) adsorption to a surface step on diamond (100). *J. Phys. Chem. C* **113**, 19891–19896. (doi:10.1021/jp900853a)
59. Yiming Z, Larsson F, Larsson K. 2014 Effect of CVD diamond growth by doping with nitrogen. *Theor. Chem. Accounts* **133**, 1432. (doi:10.1007/s00214-013-1432-y)
60. May PW, Allan NL, Ashfold MNR, Richley JC, Mankelevich YA. 2009 Simplified Monte Carlo simulations of chemical vapour deposition diamond growth. *J. Phys.* **21**, 364203. (doi:10.1088/0953-8984/21/36/364203)

61. Butler JE, Oleynik I. 2008 A mechanism for crystal twinning in the growth of diamond by chemical vapour deposition. *Phil. Trans. R. Soc. A* **366**, 295–311. (doi:10.1098/rsta.2007.2152)
62. Oberg LM, Batzer M, Stacey A, Doherty MW. 2021 Nitrogen overgrowth as a catalytic mechanism during diamond chemical vapour deposition. *Carbon* **178**, 606–615. (doi:10.1016/j.carbon.2021.03.008)
63. May PW, Harvey JN, Allan NL, Richley JC, Mankelevich Y. 2010 Simulations of chemical vapor deposition diamond film growth using a kinetic Monte Carlo model. *J. Appl. Phys.* **108**, 014905. (doi:10.1063/1.3437647)
64. Ashfold MNR, Mankelevich YuA. 2023 Two-dimensional modeling of diamond growth by microwave plasma activated chemical vapor deposition: effects of pressure, absorbed power and the beneficial role of nitrogen on diamond growth. *Diam. Relat. Mater.* **137**, 110097. (doi:10.1016/j.diamond.2023.110097)
65. Klippenstein SJ, Georgievskii Y, Harding LB. 2006 Predictive theory for the combination kinetics of two alkyl radicals. *Phys. Chem. Chem. Phys.* **8**, 1133–1147. (doi:10.1039/b515914h)
66. Schwaederlé L, Brault P, Rond C, Gicquel A. 2015 Molecular dynamics calculations of CH<sub>3</sub> sticking coefficient onto diamond surfaces. *Plasma Process. Polym.* **12**, 764–770. (doi:10.1002/ppap.201400223)
67. Eckert M, Neyts E, Bogaerts A. 2008 On the reaction behaviour of hydrocarbon species at diamond (100) and (111) surfaces: a molecular dynamics investigation. *J. Phys. D* **41**, 032006. (doi:10.1088/0022-3727/41/3/032006)
68. Teng Y, Zhao W, Tang K, Yang K, Zhao G, Zhu S, Ye J, Gu S. 2023 High efficiency of boron doping and fast growth realized with a novel gas inlet structure in diamond microwave plasma chemical vapor deposition system. *Carbon Lett.* (doi:10.1007/s42823-023-00651-8)
69. Asmusen J. *Process and apparatus for diamond synthesis*. United States Patent: US9732440B2. See <https://patents.google.com/patent/US9732440B2/en> (accessed 22 March 2025).
70. May PW, Ashfold MNR, Mankelevich Y. 2007 Microcrystalline, nanocrystalline, and ultrananocrystalline diamond chemical vapor deposition: experiment and modeling of the factors controlling growth rate, nucleation, and crystal size. *J. Appl. Phys.* **101**, 053115. (doi:10.1063/1.2696363)
71. Butler JE, Sumant AV. 2008 The CVD of nanodiamond materials. *Chem. Vap. Depos.* **14**, 145–160. (doi:10.1002/cvde.200700037)
72. Van der Drift A. 1967 Evolutionary selection, a principle governing growth orientation in vapour-deposited layers. *Philips Res. Rep.* **22**, 267.
73. Wild C, Kohl R, Herres N, Müller-Sebert W, Koidl P. 1994 Oriented CVD diamond films: twin formation, structure and morphology. *Diam. Relat. Mater.* **3**, 373–381. (doi:10.1016/0925-9635(94)90188-0)
74. Schreck M, Gsell S, Brescia R, Fischer M. 2017 Ion bombardment induced buried lateral growth: the key mechanism for the synthesis of single crystal diamond wafers. *Sci. Rep.* **7**, 44462. (doi:10.1038/srep44462)
75. Williams OA. 2011 Nanocrystalline diamond. *Diam. Relat. Mater.* **20**, 621–640. (doi:10.1016/j.diamond.2011.02.015)
76. Xia Y *et al.* 2023 Application of nano-crystalline diamond in tribology. *Materials* **16**, 2710. (doi:10.3390/ma16072710)
77. Shenderova OA, Gruen DM (eds). 2012 *Ultrananocrystalline diamond: synthesis, properties and applications*. Amsterdam, The Netherlands: Elsevier.
78. Auciello O. 2022 Science and technology of a transformational multifunctional ultrananocrystalline diamond (UNCD™) coating. *Funct. Diam.* **2**, 1–24. (doi:10.1080/26941112.2022.2033606)
79. Kovalchenko AM, Elam JW, Erdemir A, Carlisle JA, Auciello O, Libera JA, Pellin MJ, Gruen DM, Hryn JN. 2011 Development of ultrananocrystalline diamond (UNCD) coatings for multipurpose mechanical pump seals. *Wear* **270**, 325–331. (doi:10.1016/j.wear.2010.10.059)
80. Skoog SA, Kumar G, Zheng J, Sumant AV, Goering PL, Narayan RJ. 2016 Biological evaluation of ultrananocrystalline and nanocrystalline diamond coatings. *J. Mater. Sci.* **27**. (doi:10.1007/s10856-016-5798-y)

81. Birrell J, Gerbi JE, Auciello O, Gibson JM, Gruen DM, Carlisle JA. 2003 Bonding structure in nitrogen doped ultrananocrystalline diamond. *J. Appl. Phys.* **93**, 5606–5612. (doi:10.1063/1.1564880)
82. Auciello O (ed). 2022 *Ultrananocrystalline diamond coatings for next-generation high-tech and medical devices*. Cambridge, UK: Cambridge University Press. (doi:10.1017/9781316105177)
83. Das D, Singh RN. 2007 A review of nucleation, growth and low temperature synthesis of diamond thin films. *Int. Mater. Rev.* **52**, 29–64. (doi:10.1179/174328007x160245)
84. Li X, He L, Li Y, Yang Q. 2020 Diamond deposition on iron and steel substrates: a review. *Micromachines* **11**, 719. (doi:10.3390/mi11080719)
85. Haque A, Gupta S, Narayan J. 2020 Characteristics of diamond deposition on Al<sub>2</sub>O<sub>3</sub>, diamond-like carbon, and Q-carbon. *ACS Appl. Electron. Mater.* **2**, 1323–1334. (doi:10.1021/acsaem.0c00106)
86. Saw KG, Andrienko I, Cimmino A, Spizzirri P, Prawer S, du Plessis J. 2003 Growth of diamond on  $\alpha$ -(0001) sapphire substrates. *Diam. Relat. Mater.* **12**, 1663–1669. (doi:10.1016/S0925-9635(03)00189-4)
87. Malakoutian M. 2021 Polycrystalline diamond growth on  $\beta$ -Ga<sub>2</sub>O<sub>3</sub> for thermal management. *Appl. Phys. Express* **14**, 055502. (doi:10.35848/1882-0786/abf4f1)
88. Chalker PR, Johnston C, Romani S, Ayres CF, Buckley-Golder IM. 1994 Nucleation and growth of CVD diamond on magnesium oxide (100) and titanium nitride-magnesium oxide (100) surfaces. *Diam. Relat. Mater.* **3**, 393–397. (doi:10.1016/0925-9635(94)90191-0)
89. Lu YG. 2012 Analytical TEM study of CVD diamond growth on TiO<sub>2</sub> sol–gel layers. *Diam. Relat. Mater.* **23**, 93–99. (doi:10.1016/j.diamond.2012.01.022)
90. Liu JW, Liao MY, Imura M, Oosato H, Watanabe E, Tanaka A, Iwai H, Koide Y. 2013 Interfacial band configuration and electrical properties of LaAlO<sub>3</sub>/Al<sub>2</sub>O<sub>3</sub>/hydrogenated-diamond metal-oxide-semiconductor field effect transistors. *J. Appl. Phys.* **114**. (doi:10.1063/1.4819108)
91. Yao Y, Sang D, Duan S, Wang Q, Liu C. 2021 Review on the properties of boron-doped diamond and one-dimensional-metal-oxide based P-N heterojunction. *Molecules* **26**, 17. (doi:10.3390/molecules26010071)
92. Crawford KG, Qi D, McGlynn J, Ivanov TG, Shah PB, Weil J, Tallaire A, Ganin AY, Moran DAJ. 2018 Thermally stable, high performance transfer doping of diamond using transition metal oxides. *Sci. Rep.* **8**, 3342. (doi:10.1038/s41598-018-21579-4)
93. Polo MC, Sánchez G, Wang WL, Esteve J, Andújar JL. 1997 Growth of diamond films on boron nitride thin films by bias-assisted hot filament chemical vapor deposition. *Appl. Phys. Lett.* **70**, 1682–1684. (doi:10.1063/1.118668)
94. Argoitia A, Angus JC, Ma JS, Wang L, Pirouz P, Lambrecht WRL. 1994 Heteroepitaxy of diamond on c-BN: growth mechanisms and defect characterization. *J. Mater. Res.* **9**, 1849–1865. (doi:10.1557/jmr.1994.1849)
95. Zhang XW, Boyen HG, Deyneka N, Ziemann P, Banhart F, Schreck M. 2003 Epitaxy of cubic boron nitride on (001)-oriented diamond. *Nat. Mater.* **2**, 312–315. (doi:10.1038/nmat870)
96. Pearton SJ, Ren F, Zhang AP, Lee KP. 2000 Fabrication and performance of GaN electronic devices. *Mater. Sci. Eng.* **30**, 55–212. (doi:10.1016/s0927-796x(00)00028-0)
97. Mishra UKShenLKazior TEWuYF2008 GaN-based RF power devices and amplifiers. *Proc. IEEE* **96**, 287–305. (doi:10.1109/JPROC.2007.911060)
98. Bar-Cohen A, Maurer JJ, Altman DH. 2019 Embedded cooling for wide bandgap power amplifiers: a review. *J. Electron. Packag.* **141**, 040803. (doi:10.1115/1.4043404)
99. Oba M, Sugino T. 2001 Oriented growth of diamond on (0001) surface of hexagonal GaN. *Diam. Relat. Mater.* **10**, 1343–1346. (doi:10.1016/S0925-9635(00)00448-9)
100. May PW, Tsai HY, Wang WN, Smith JA. 2006 Deposition of CVD diamond onto GaN. *Diam. Relat. Mater.* **15**, 526–530. (doi:10.1016/j.diamond.2005.11.036)
101. Pomeroy JW, Bernardoni M, Dumka DC, Fanning DM, Kuball M. 2014 Low thermal resistance GaN-on-diamond transistors characterized by three-dimensional Raman thermography mapping. *Appl. Phys. Lett.* **104**, 083513. (doi:10.1063/1.4865583)
102. Sun H, Simon RB, Pomeroy JW, Francis D, Faili F, Twitchen DJ, Kuball M. 2015 Reducing GaN-on-diamond interfacial thermal resistance for high power transistor applications. *Appl. Phys. Lett.* **106**, 111906. (doi:10.1063/1.4913430)

103. Mandel S *et al.* 2019 Thick, adherent diamond films on AlN with low thermal barrier resistance. *ACS Appl. Mater. Interfaces* **11**, 40826–40834. (doi:10.1021/acsami.9b13869)
104. Catledge SA, Vohra YK. 2000 Interfacial oxide and carbide phases in the deposition of diamond films on beryllium metal. *Diam. Relat. Mater.* **9**, 1327–1330. (doi:10.1016/S0925-9635(00)00246-6)
105. Chung HK, Sung JC. 2001 The rapid growth of thin transparent films of diamond. *Mater. Chem. Phys.* **72**, 130–132. (doi:10.1016/s0254-0584(01)00421-7)
106. Polini R, Barletta M, Rubino G, Vesco S. 2012 Recent advances in the deposition of diamond coatings on Co-cemented tungsten carbides. *Adv. Mater. Sci. Eng.* **2012**, 1–14. (doi:10.1155/2012/151629)
107. Mukherjee D. 2020 Deposition of diamond films on single crystalline silicon carbide substrates. *Diam. Relat. Mater.* **101**, 107625. (doi:10.1016/j.diamond.2019.107625)
108. Tucker DA, Seo DK, Whangbo MH, Sivazlian FR, Stoner BR, Bozeman SP, Sowers AT, Nemanich RJ, Glass JT. 1995 Comparison of silicon, nickel, and nickel silicide (Ni<sub>3</sub>Si) as substrates for epitaxial diamond growth. *Surf. Sci.* **334**, 179–194. (doi:10.1016/0039-6028(95)00469-6)
109. Chen MR, Chang L, Chang DF, Chen HG. 2001 Diamond growth on CoSi<sub>2</sub>/Si by bias-enhanced microwave plasma chemical vapor deposition method. *Mater. Chem. Phys.* **72**, 172–175. (doi:10.1016/s0254-0584(01)00430-8)
110. Singh J, Vellaikal M. 1994 Microstructural evolution of diamond growth on iron silicide/silicon substrates by hot filament chemical vapor deposition. *Surf. Coatings Technol.* **64**, 131–137. (doi:10.1016/0257-8972(94)90099-x)
111. Lyu JL, Bai H, Yu JH, Xue C, Nishimura K, Li H, Jiang N. 2015 High thermal conductivity diamond coated graphite by microwave plasma chemical vapour deposition. *Mater. Sci. Technol.* **31**, 1919–1924. (doi:10.1179/1743284715y.0000000047)
112. Li Z, Wang L, Suzuki T, Argoitia A, Pirouz P, Angus JC. 1993 Orientation relationship between chemical vapor deposited diamond and graphite substrates. *J. Appl. Phys.* **73**, 711–715. (doi:10.1063/1.353327)
113. Orwa JO *et al.* 2021 Growth of diamond coating on carbon fiber: relationship between fiber microstructure and stability in hydrogen plasma. *Diam. Relat. Mater.* **115**, 108349. (doi:10.1016/j.diamond.2021.108349)
114. Haubner R, Lessiak M. 2017 Deposition of CVD diamond coatings on carbon fiber composite substrates. *Key Eng. Mater.* **742**, 419–426. (doi:10.4028/www.scientific.net/kem.742.419)
115. Zanin H, May PW, Harniman RL, Risbridger T, Corat EJ, Fermin DJ. 2015 High surface area diamond-like carbon electrodes grown on vertically aligned carbon nanotubes. *Carbon* **82**, 288–296. (doi:10.1016/j.carbon.2014.10.073)
116. Mahi C, Brinza O, Issaoui R, Achard J, Bénédict F. 2022 Synthesis of high quality transparent nanocrystalline diamond films on glass substrates using a distributed antenna array microwave system. *Coatings* **12**, 1375. (doi:10.3390/coatings12101375)
117. Ficek M, Niedziałkowski P, Smietana MJ, Kob M. 2017 Linear antenna microwave chemical vapour deposition of diamond films on long-period fiber gratings for bio-sensing applications. *Opt. Mater. Express* **7**, 3952. (doi:10.1364/OME.7.003952)
118. Tsugawa K, Ishihara M, Kim J, Koga Y, Hasegawa M. 2010 Nanocrystalline diamond film growth on plastic substrates at temperatures below 100°C from low-temperature plasma. *Phys. Rev. B* **82**, 125460. (doi:10.1103/PhysRevB.82.125460)
119. Izak T, Babchenko O, Potocky S, Remes Z, Kozak H, Verveniotis E, Rezek B, Kromka A. 2014 Low temperature diamond growth. In *Nanodiamond* (ed. O Williams), pp. 290–342. London, UK: The Royal Society of Chemistry. (doi:10.1039/9781849737616-00290)
120. Mandal S. 2021 Nucleation of diamond films on heterogeneous substrates: a review. *RSC Adv.* **11**, 10159–10182. (doi:10.1039/d1ra00397f)
121. Nunn N, Torelli M, McGuire G, Shenderova O. 2017 Nanodiamond: a high impact nanomaterial. *Curr. Opin. Solid State Mater. Sci.* **21**, 1–9. (doi:10.1016/j.cossms.2016.06.008)
122. Mochalin VN, Shenderova O, Ho D, Gogotsi Y. 2012 The properties and applications of nanodiamonds. *Nat. Nanotechnol.* **7**, 11–23. (doi:10.1038/nnano.2011.209)

123. Dolmatov VYu, Veretennikova MV, Marchukov VA, Sushchev VG. 2004 Currently available methods of industrial nanodiamond synthesis. *Phys. Solid State* **46**, 611–615. (doi:10.1134/1.1711434)
124. Krueger A, Ozawa M, Jarre G, Liang Y, Stegk J, Lu L. 2007 Deagglomeration and functionalisation of detonation diamond. *Phys. Status Solidi* **204**, 2881–2887. (doi:10.1002/pssa.200776330)
125. Barnard AS, Russo SP, Snook IK. 2003 Coexistence of bucky diamond with nanodiamond and fullerene carbon phases. *Phys. Rev. B* **68**, 073406. (doi:10.1103/physrevb.68.073406)
126. Krueger A, Lang D. 2012 Functionality is key: recent progress in the surface modification of nanodiamond. *Adv. Funct. Mater.* **22**, 890–906. (doi:10.1002/adfm.201102670)
127. Say JM, van Vreden C, Reilly DJ, Brown LJ, Rabeau JR, King NJC. 2011 Luminescent nanodiamonds for biomedical applications. *Biophys. Rev.* **3**, 171–184. (doi:10.1007/s12551-011-0056-5)
128. Fu CC *et al.* 2007 Characterization and application of single fluorescent nanodiamonds as cellular biomarkers. *Proc. Natl Acad. Sci. USA* **104**, 727–732. (doi:10.1073/pnas.0605409104)
129. Fox OJL, Holloway JOP, Fuge GM, May PW, Ashfold MNR. 2009 Electro spray deposition of diamond nanoparticle nucleation layers for subsequent CVD diamond growth. *MRS Online Proceedings Library* **1203**, 1727–1737. (doi:10.1557/PROC-1203-J17-27)
130. Schreck M. 2009 Heteroepitaxial growth. In *CVD diamond for electronic devices and sensors* (ed. R Sussmann), pp. 125–161. Hoboken, NJ: John Wiley & Sons. (doi:10.1002/9780470740392)
131. Wang W, Liu B, Zhang L, Han J, Liu K, Dai B, Zhu J. 2022 Heteroepitaxy of diamond semiconductor on iridium: a review. *Funct. Diam.* **2**, 215–235. (doi:10.1080/26941112.2022.2162348)
132. Fischer M, Gsell S, Schreck M, Brescia R, Stritzker B. 2008 Preparation of 4-inch Ir/YSZ/Si(001) substrates for the large-area deposition of single-crystal diamond. *Diam. Relat. Mater.* **17**, 1035–1038. (doi:10.1016/j.diamond.2008.02.028)
133. Audiatac (Augsburg Diamond Technology GmbH). See <https://www.audiatac.de/en/> (accessed 22 March 2025).
134. Gajewski W, chatz PA, Williams OA, Haenen K, Bustarret E, Stutzmann M, Garrido JA. 2009 Electronic and optical properties of boron-doped nanocrystalline diamond films. *Phys. Rev. B* **79**, 045206. (doi:10.1103/physrevb.79.045206)
135. May PW, Ludlow WJ, Hannaway M, Heard PJ, Smith JA, Rosser KN. 2008 Raman and conductivity studies of boron doped microcrystalline diamond, faceted nanocrystalline diamond and cauliflower diamond films. *Diam. Relat. Mater.* **17**, 105–117. (doi:10.1016/j.diamond.2007.11.005)
136. Ekimov EA, Sidorov VA, Bauer ED, Mel'nik NN, Curro NJ, Thompson JD, Stishov SM. 2004 Superconductivity in diamond. *Nature* **428**, 542–545. (doi:10.1038/nature02449)
137. Zhang G *et al.* 2023 Unconventional giant 'magnetoresistance' in bosonic semiconducting diamond nanorings. *Adv. Mater.* **35**, 2211129. (doi:10.1002/adma.202211129)
138. Wort CJH, Balmer RS. 2008 Diamond as an electronic material. *Mater. Today* **11**, 22–28. (doi:10.1016/s1369-7021(07)70349-8)
139. Macpherson JV. 2015 A practical guide to using boron doped diamond in electrochemical research. *Phys. Chem. Chem. Phys.* **17**, 2935–2949. (doi:10.1039/c4cp04022h)
140. Kalish R. 2001 The search for donors in diamond. *Diam. Relat. Mater.* **10**, 1749–1755. (doi:10.1016/S0925-9635(01)00426-5)
141. Kalish R, Uzan-Saguy C, Philosoph B, Richter V, Lagrange JP, Gheeraert E, Deneuille A, Collins AT. 1997 Nitrogen doping of diamond by ion implantation. *Diam. Relat. Mater.* **6**, 516–520. (doi:10.1016/s0925-9635(96)00657-7)
142. Pinault-Thaury MA, Temgoua S, Gillet R, Bensalah H, Stenger I, Jomard F, Issaoui R, Barjon J. 2019 Phosphorus-doped (113) CVD diamond: a breakthrough towards bipolar diamond devices. *Appl. Phys. Lett.* **114**, 112106. (doi:10.1063/1.5079924)
143. May PW, Davey M, Rosser KN, Heard PJ. 2008 Arsenic and Antimony Doping: An Attempt to Deposit n-Type CVD diamond. In *Mater. Res. Soc. Symp. Proc.* vol. **1039**. (doi:10.1557/PROC-1039-P15-01)

144. Khmel'nitsky RA, Saraykin VV, Dravin VA, Zavedeyev EV, Makarov SV, Bronsky VS, Gippius AA. 2016 Lithium implanted into diamond: regular trends and anomalies. *Surf. Coat. Tech.* **307**, 236–242. (doi:10.1016/j.surfcoat.2016.08.047)
145. Prawer S, Uzan-Saguy C, Braunstein G, Kalish R. 1993 Can *n*-type doping of diamond be achieved by Li or Na ion implantation? *Appl. Phys. Lett.* **63**, 2502–2504. (doi:10.1063/1.110462)
146. Sakaguchi I, N.-Gamo M, Kikuchi Y, Yasu E, Haneda H, Suzuki T, Ando T. 1999 Sulfur: a donor dopant for *n*-type diamond semiconductors. *Phys. Rev. B* **60**, R2139–R2141. (doi:10.1103/physrevb.60.r2139)
147. Kalish R, Reznik A, Uzan-Saguy C, Cytermann C. 2000 Is sulfur a donor in diamond? *Appl. Phys. Lett.* **76**, 757–759. (doi:10.1063/1.125885)
148. Wu Y *et al.* 2021 N-type diamond semiconductor induced by co-doping selenium and boron. *Comput. Mater. Sci.* **196**, 110515. (doi:10.1016/j.commatsci.2021.110515)
149. Halliwell SC, May PW, Fox NA, Othman MZ. 2017 Investigations of the co-doping of boron and lithium into CVD diamond thin films. *Diam. Relat Mater* **76**, 115–122. (doi:10.1016/j.diamond.2017.05.001)
150. Conejeros S, Othman MZ, Croot A, Hart JN, O'Donnell KM, May PW, Allan NL. 2020 Hunting the elusive shallow *n*-type donor – an *ab initio* study of Li and N co-doped diamond. *Carbon* **171**, 857–868. (doi:10.1016/j.carbon.2020.09.065)
151. Li R. 2005 A molecular dynamics study of boron and nitrogen in diamond. *Solid State Commun.* **135**, 155–157. (doi:10.1016/j.ssc.2005.04.019)
152. Fan K, Tang K, Zhang M, Wu K, Zhao G, Huang Y, Zhu S, Ye J, Gu S. 2023 The boron-phosphorous co-doping scheme for possible *n*-type diamond from first principles. *Comput. Mater. Sci.* **222**, 112113. (doi:10.1016/j.commatsci.2023.112113)
153. Strobel P, Riedel M, Ristein J, Ley L. 2004 Surface transfer doping of diamond. *Nature* **430**, 439–441. (doi:10.1038/nature02751)
154. Crawford KG, Maini I, Macdonald DA, Moran DAJ. 2021 Surface transfer doping of diamond: a review. *Prog Surf Sci* **96**, 100613. (doi:10.1016/j.progsurf.2021.100613)
155. Nebel CE. 2007 Surface-conducting diamond. *Science* **318**, 1391–1392. (doi:10.1126/science.1151314)
156. Ren Z, Zhang J, Zhang J, Zhang C, Chen D, Yang P, Li Y, Hao Y. 2017 Polycrystalline diamond MOSFET with MoO<sub>3</sub> gate dielectric and passivation layer. *IEEE Electron Dev Lett* **38**, 1302–1304. (doi:10.1109/LED.2017.2727879)
157. Jelezko F, Wrachtrup J. 2006 Single defect centres in diamond: a review. *Phys. Status Solidi* **203**, 3207–3225. (doi:10.1002/pssa.200671403)
158. Kurtsiefer C, Mayer S, Zarda P, Weinfurter H. 2000 Stable solid-state source of single photons. *Phys. Rev. Lett.* **85**, 290–293. (doi:10.1103/physrevlett.85.290)
159. Prawer S, Greentree AD. 2008 Diamond for quantum computing. *Science* **320**, 1601–1602. (doi:10.1126/science.1158340)
160. Dobrovitski VV, Fuchs GD, Falk AL, Santori C, Awschalom DD. 2013 Quantum control over single spins in diamond. *Annu. Rev. Condens. Matter Phys.* **4**, 23–50. (doi:10.1146/annurev-conmatphys-030212-184238)
161. Gruber A, Dräbenstedt A, Tietz C, Fleury L, Wrachtrup J, Borczykowski C von. 1997 Scanning confocal optical microscopy and magnetic resonance on single defect centers. *Science* **276**, 2012–2014. (doi:10.1126/science.276.5321.2012)
162. Schirhagl R, Chang K, Loretz M, Degen CL. 2014 Nitrogen-vacancy centers in diamond: nanoscale sensors for physics and biology. *Annu. Rev. Phys. Chem.* **65**, 83–105. (doi:10.1146/annurev-physchem-040513-103659)
163. Wrachtrup J, Jelezko F, Grotz B, McGuinness L. 2013 Nitrogen-vacancy centers close to surfaces. *MRS Bull.* **38**, 149–154. (doi:10.1557/mrs.2013.22)
164. Dolde F *et al.* 2013 Room-temperature entanglement between single defect spins in diamond. *Nat. Phys.* **9**, 139–143. (doi:10.1038/nphys2545)
165. Barson MSJ, Krausz E, Manson NB, Doherty MW. 2019 The fine structure of the neutral nitrogen-vacancy center in diamond. *Nanophotonics* **8**, 1985–1991. (doi:10.1515/nanoph-2019-0142)

166. Neu E, Steinmetz D, Riedrich-Möller J, Gsell S, Fischer M, Schreck M, Becher C. 2011 Single photon emission from silicon-vacancy colour centres in chemical vapour deposition nano-diamonds on iridium. *New J. Phys.* **13**, 025012. (doi:10.1088/1367-2630/13/2/025012)
167. Becker JN, Neu E. 2020 The silicon vacancy center in diamond. *Semiconductors and Semimetals* **103**, 201–235. (doi:10.1016/bs.semsem.2020.04.001)
168. Nguyen M, Nikolay N, Bradac C, Kianinia M, Ekimov EA, Mendelson N, Benson O, Aharonovich I. 2019 Photodynamics and quantum efficiency of germanium vacancy color centers in diamond. *Adv. Photon.* **1**, 066002. (doi:10.1117/1.AP.1.6.066002)
169. Görlitz J *et al.* 2022 Coherence of a charge stabilised tin-vacancy spin in diamond. *Npj Quantum Inf.* **8**, 45. (doi:10.1038/s41534-022-00552-0)
170. Trusheim ME *et al.* 2019 Lead-related quantum emitters in diamond. *Phys. Rev. B* **99**, 075430. (doi:10.1103/physrevb.99.075430)
171. Rodgers LVH, Hughes LB, Xie M, Maurer PC, Kolkowitz S, Bleszynski Jayich AC, de Leon NP. 2021 Materials challenges for quantum technologies based on color centers in diamond. *MRS Bull.* **46**, 623–633. (doi:10.1557/s43577-021-00137-w)
172. CVD Lab-grown Diamonds Market. MarketsandMarkets. See <https://www.marketsandmarkets.com/Market-Reports/cvd-lab-grown-diamonds-market-11040749.html> (accessed 22 March 2025).
173. Liang Q, Yan CS, Meng Y, Lai J, Krasnicki S, Mao HK, Hemley RJ. 2009 Recent advances in high-growth rate single-crystal CVD diamond. *Diam. Relat. Mater.* **18**, 698–703. (doi:10.1016/j.diamond.2008.12.002)
174. Fisher D, Spits RA. 2000 Spectroscopic evidence of GE POL HPHT-treated natural type IIa diamonds. *Gems Gemol.* **36**, 42–49. (doi:10.5741/gems.36.1.42)
175. Eaton-Magana S, Shigley JE. 2016 Observations on CVD-grown synthetic diamonds: a review. *Gems Gemol.* **52**, 222–245. (doi:10.5741/GEMS.52.3.222)
176. Infi Advanced Materials Co.,Ltd, China. See <https://www.lab-diamond.cn/> (accessed 22 March 2025).
177. Smithsonian Museum. *History of the Hope Diamond*. See <https://www.si.edu/spotlight/hope-diamond/history> (accessed 7 March 2024).
178. Heyer S, Janssen W, Turner S, Lu YG, Yeap WS, Verbeeck J, Haenen K, Krueger A. 2014 Toward deep blue nano hope diamonds: heavily boron-doped diamond nanoparticles. *ACS Nano* **8**, 5757–5764. (doi:10.1021/nn500573x)
179. Tallaire A, Mille V, Brinza O, Tran Thi TN, Brom JM, Loguinov Y, Katruscha A, Koliadin A, Achard J. 2017 Thick CVD diamond films grown on high-quality type IIa HPHT diamond substrates from New Diamond Technology. *Diam. Relat. Mater.* **77**, 146–152. (doi:10.1016/j.diamond.2017.07.002)
180. Friel I, Clewes SL, Dhillon HK, Perkins N, Twitchen DJ, Scarsbrook GA. 2009 Control of surface and bulk crystalline quality in single crystal diamond grown by chemical vapour deposition. *Diam. Relat. Mater.* **18**, 808–815. (doi:10.1016/j.diamond.2009.01.013)
181. Umezawa H, Tatsumi N, Kato Y, Shikata SI. 2013 Leakage current analysis of diamond Schottky barrier diodes by defect imaging. *Diam. Relat. Mater.* **40**, 56–59. (doi:10.1016/j.diamond.2013.09.011)
182. Li D, Wang Q, Lv X, Li L, Zou G. 2023 Reduction of dislocation density in single crystal diamond by Ni-assisted selective etching and CVD regrowth. *J. Alloy. Compd.* **960**, 170890. (doi:10.1016/j.jallcom.2023.170890)
183. Achard J, Silva F, Brinza O, Bonnin X, Mille V, Issaoui R, Kasu M, Gicquel A. 2009 Identification of etch-pit crystallographic faces induced on diamond surface by H<sub>2</sub>/O<sub>2</sub> etching plasma treatment. *Phys. Status Solidi* **206**, 1949–1954. (doi:10.1002/pssa.200982210)
184. Stehl C, Fischer M, Gsell S, Berdermann E, Rahman MS, Traeger M, Klein O, Schreck M. 2013 Efficiency of dislocation density reduction during heteroepitaxial growth of diamond for detector applications. *Appl. Phys. Lett.* **103**, 151905. (doi:10.1063/1.4824330)
185. Kono S, Teraji T, Kodama H, Sawabe A. 2015 Imaging of diamond defect sites by electron-beam-induced current. *Diam. Relat. Mater.* **59**, 54–61. (doi:10.1016/j.diamond.2015.09.006)
186. Umezawa H, Ikeda K, Tatsumi N, Ramanujam K, Shikata S i. 2009 Device scaling of pseudo-vertical diamond power Schottky barrier diodes. *Diam. Relat. Mater.* **18**, 1196–1199. (doi:10.1016/j.diamond.2009.04.013)

187. Umezawa H, Mokuno Y, Yamada H, Chayahara A, Shikata S. 2010 Characterization of Schottky barrier diodes on a 0.5-inch single-crystalline CVD diamond wafer. *Diam. Relat. Mater.* **19**, 208–212. (doi:10.1016/j.diamond.2009.11.001)
188. Shikata S. 2016 Single crystal diamond wafers for high power electronics. *Diam. Relat. Mater.* **65**, 168–175. (doi:10.1016/j.diamond.2016.03.013)
189. Achard J, Tallaire A, Mille V, Naamoun M, Brinza O, Boussadi A, William L, Gicquel A. 2014 Improvement of dislocation density in thick CVD single crystal diamond films by coupling H<sub>2</sub>/O<sub>2</sub> plasma etching and chemo-mechanical or ICP treatment of HPHT substrates. *Phys. Status Solidi* **211**, 2264–2267. (doi:10.1002/pssa.201431181)
190. Kato Y, Umezawa H, Yamaguchi H, Shikata S. 2012 Structural analysis of dislocations in type-IIa single-crystal diamond. *Diam. Relat. Mater.* **29**, 37–41. (doi:10.1016/j.diamond.2012.07.008)
191. Tang YH, Golding B. 2016 Stress engineering of high-quality single crystal diamond by heteroepitaxial lateral overgrowth. *Appl. Phys. Lett.* **108**, 052101. (doi:10.1063/1.4941291)
192. Ohmagari S, Yamada H, Tsubouchi N, Umezawa H, Chayahara A, Mokuno Y, Takeuchi D. 2019 Toward high-performance diamond electronics: control and annihilation of dislocation propagation by metal-assisted termination. *Phys. Status Solidi* **216**, 00498. (doi:10.1002/pssa.201900498)
193. Mehmel L *et al.* 2021 Dislocation density reduction using overgrowth on hole arrays made in heteroepitaxial diamond substrates. *Appl. Phys. Lett.* **118**, 061901. (doi:10.1063/5.0033741)
194. Mokuno Y, Kato Y, Tsubouchi N, Chayahara A, Yamada H, Shikata S. 2014 A nitrogen doped low-dislocation density free-standing single crystal diamond plate fabricated by a lift-off process. *Appl. Phys. Lett.* **104**, 252109. (doi:10.1063/1.4885552)
195. Oliffe A. 2023 *Record-breaking 34.59-carat CVD lab-grown diamond examined*. Jewellery Monthly Magazine. See <https://www.jewellerymonthly.com/record-breaking-lab-grown-diamond-unveiled/> (accessed 22 March 2025).
196. Eaton-Magana S, Breeding CM. 2018 Features of synthetic diamonds. *Gems Gemol.* **54**, 202–204. (doi:10.5741/gems.54.2.202)
197. Shigley J. 2016 *HPHT and CVD diamond growth processes: making lab-grown diamonds*. *GIA Research News*. GIA. See <https://www.gia.edu/hpht-and-cvd-diamond-growth-processes> (accessed 22 March 2025).
198. Breeding CM, Shen AH, Eaton-Magaña S, Rossman GR, Shigley JE, Gilbertson A. 2010 Developments in gemstone analysis techniques and instrumentation during the 2000s. *Gems Gemol.* **46**, 241–257. (doi:10.5741/gems.46.3.241)
199. D’Haenens-Johansson UFS, Butler JE, Katruscha AN. 2022 Synthesis of diamonds and their identification. *Rev. Mineral. Geochem.* **88**, 689–754. (doi:10.2138/rmg.2022.88.13)
200. Sumiya H. 2014 HPHT Synthesis of Large, High-Quality, Single Crystal Diamonds. In *Comprehensive hard materials* (ed. CE Nebel), pp. 9780–444, vol. 3. London, UK: Elsevier. (doi:10.1016/B978-0-08-096527-7.00046-5)
201. Gicquel A, Hassouni K, Silva F, Achard J. 2001 CVD diamond films: from growth to applications. *Curr. Appl. Phys.* **1**, 479–496. (doi:10.1016/s1567-1739(01)00061-x)
202. Tabakoya T *et al.* 2019 High-rate growth of single-crystalline diamond (100) films by hot-filament chemical vapor deposition with tantalum filaments at 3000°C. *Phys. Status Solidi Appl. Mater. Sci.* **216**, 00244. (doi:10.1002/pssa.201900244)
203. van Enckevort WJP, Janssen G, Schermer JJ, Giling LJ. 1995 Step-related growth phenomena on exact and misoriented {001} surfaces of CVD-grown single-crystal diamonds. *Diam. Relat. Mater.* **4**, 250–255. (doi:10.1016/0925-9635(94)05201-8)
204. Yamanaka S, Watanabe H, Masai S, Kawata S, Hayashi K, Takeuchi D, Okushi H, Kajimura K. 1998 Junction properties of homoepitaxial diamond films grown by step-flow mode. *J. Appl. Phys.* **84**, 6095–6099. (doi:10.1063/1.368922)
205. Fischer AM, Bhattacharya A, Hardy A, Grotjohn TA, Ponce FA. 2023 The effect of step-flow growth on the surface morphology and optical properties of thick diamond films. *Diam. Relat. Mater.* **140B**, 110507. (doi:10.1016/j.diamond.2023.110507)
206. Yamada H, Chayahara A, Umezawa H, Tsubouchi N, Mokuno Y, Shikata S. 2012 Fabrication and fundamental characterizations of tiled clones of single-crystal diamond with 1-inch size. *Diam. Relat. Mater.* **24**, 29–33. (doi:10.1016/j.diamond.2011.09.007)

207. Parikh NR, Hunn JD, McGucken E, Swanson ML, White CW, Rudder RA, Malta DP, Posthill JB, Markunas RJ. 1992 Single-crystal diamond plate liftoff achieved by ion implantation and subsequent annealing. *Appl. Phys. Lett.* **61**, 3124–3126. (doi:10.1063/1.107981)
208. Hrdlička V, Matvieiev O, Navrátil T, Šelešovská R. 2023 Recent advances in modified boron-doped diamond electrodes: a review. *Electrochimica Acta* **456**, 142435. (doi:10.1016/j.electacta.2023.142435)
209. Einaga Y, Foord JS, Swain GM. 2014 Diamond electrodes: diversity and maturity. *MRS Bull.* **39**, 525–532. (doi:10.1557/mrs.2014.94)
210. Einaga Y. 2010 Diamond electrodes for electrochemical analysis. *J. Appl. Electrochem.* **40**, 1807–1816. (doi:10.1007/s10800-010-0112-z)
211. May PW *et al.* 2016 Diamond-coated ‘black silicon’ as a promising material for high-surface-area electrochemical electrodes and antibacterial surfaces. *J. Mater. Chem. B* **4**, 5737–5746. (doi:10.1039/c6tb01774f)
212. Yu Y, Wu L, Zhi J. 2014 Diamond nanowires: fabrication, structure, properties, and applications. *Angew. Chem. Int. Ed.* **53**, 14326–14351. (doi:10.1002/anie.201310803)
213. Varga M, Stehlik S, Kaman O, Izak T, Domonkos M, Lee DS, Kromka A. 2017 Templated diamond growth on porous carbon foam decorated with polyvinyl alcohol-nanodiamond composite. *Carbon* **119**, 124–132. (doi:10.1016/j.carbon.2017.04.022)
214. Petrák V *et al.* 2017 Fabrication of porous boron-doped diamond on SiO<sub>2</sub> fiber templates. *Carbon* **114**, 457–464. (doi:10.1016/j.carbon.2016.12.012)
215. Manivannan A, Seehra MS, Tryk DA, Fujishima A. 2002 Electrochemical detection of ionic mercury at boron-doped diamond electrodes. *Anal. Lett.* **35**, 355–368. (doi:10.1081/al-120002535)
216. Zazoua A, Khedimallah N, Jaffrezic-Renault N. 2018 Electrochemical determination of cadmium, lead, and nickel using a polyphenol-polyvinyl chloride-boron-doped diamond electrode. *Anal. Lett.* **51**, 336–347. (doi:10.1080/00032719.2017.1310879)
217. Ivandini TA, Sato R, Makide Y, Fujishima A, Einaga Y. 2006 Electrochemical detection of arsenic(III) using iridium-implanted boron-doped diamond electrodes. *Anal. Chem.* **78**, 6291–6298. (doi:10.1021/ac0519514)
218. Berek J, Fischer J, Navrátil T, Pecková K, Yosypchuk B, Zima J. 2007 Nontraditional electrode materials in environmental analysis of biologically active organic compounds. *Electroanalysis* **19**, 2003–2014. (doi:10.1002/elan.200703918)
219. Wang J, Chen G, Chatrathi MP, Fujishima A, Tryk DA, Shin D. 2003 Microchip capillary electrophoresis coupled with a boron-doped diamond electrode-based electrochemical detector. *Anal. Chem.* **75**, 935–939. (doi:10.1021/ac0262053)
220. Rivera-Utrilla J, Sánchez-Polo M, Ferro-García MÁ, Prados-Joya G, Ocampo-Pérez R. 2013 Pharmaceuticals as emerging contaminants and their removal from water: a review. *Chemosphere* **93**, 1268–1287. (doi:10.1016/j.chemosphere.2013.07.059)
221. Park J, Quaiserová-Mocko V, Patel BA, Novotný M, Liu A, Bian X, Galligan JJ, Swain GM. 2008 Diamond microelectrodes for *in vitro* electroanalytical measurements: current status and remaining challenges. *Anal.* **133**, 17–24. (doi:10.1039/b710236b)
222. Park J, Galligan JJ, Fink GD, Swain GM. 2006 *In vitro* continuous amperometry with a diamond microelectrode coupled with video microscopy for simultaneously monitoring endogenous norepinephrine and its effect on the contractile response of a rat mesenteric artery. *Anal. Chem.* **78**, 6756–6764. (doi:10.1021/ac060440u)
223. Patel BA, Bian X, Quaiserová-Mocko V, Galligan JJ, Swain GM. 2007 *In vitro* continuous amperometric monitoring of 5-hydroxytryptamine release from enterochromaffin cells of the guinea pig ileum. *Anal.* **132**, 41–47. (doi:10.1039/b611920d)
224. Fan B. 2020 Flexible, diamond-based microelectrodes fabricated using the diamond growth side for neural sensing. *Microsystems Nanoeng.* **6**, 42. (doi:10.1038/s41378-020-0155-1)
225. Yang N, Foord JS, Jiang X. 2016 Diamond electrochemistry at the nanoscale: a review. *Carbon* **99**, 90–110. (doi:10.1016/j.carbon.2015.11.061)
226. Kondo T. 2022 Recent electroanalytical applications of boron-doped diamond electrodes. *Curr. Opin. Electrochem.* **32**, 100891. (doi:10.1016/j.coelec.2021.100891)

227. Song MJ, Kim JH, Lee SK, Lim DS. 2011 Fabrication of Pt nanoparticles-decorated CVD diamond electrode for biosensor applications. *Anal. Sci.* **27**, 985–989. (doi:10.2116/analsci.27.985)
228. Shahrokhian S, Ranjbar S, Ghalkhani M. 2016 Modification of the electrode surface by Ag nanoparticles decorated nano diamond - graphite for voltammetric determination of ceftizoxime. *Electroanalysis* **28**, 469–476. (doi:10.1002/elan.201500377)
229. Song MJ, Lee SK, Lee JY, Kim JH, Lim DS. 2012 Electrochemical sensor based on Au nanoparticles decorated boron-doped diamond electrode using ferrocene-tagged aptamer for proton detection. *J. Electroanal. Chem.* **677**, 139–144. (doi:10.1016/j.jelechem.2012.05.019)
230. Li H, Qin J, Li M, Li C, Xu S, Qian L, Yang B. 2020 Gold-nanoparticle-decorated boron-doped graphene/BDD electrode for tumor marker sensor. *Sensors Actuators B* **302**, 127209. (doi:10.1016/j.snb.2019.127209)
231. McLaughlin MHS, Pakpour-Tabrizi AC, Jackman RB. 2021 A detailed EIS study of boron doped diamond electrodes decorated with gold nanoparticles for high sensitivity mercury detection. *Sci. Rep.* **11**, 9505. (doi:10.1038/s41598-021-89045-2)
232. Subramanian P, Motorina A, Yeap WS, Haenen K, Coffinier Y, Zaitsev V, Niedziolka-Jonsson J, Boukherroub R, Szunerits S. 2014 An impedimetric immunosensor based on diamond nanowires decorated with nickel nanoparticles. *Anal.* **139**, 1726–1731. (doi:10.1039/c3an02045b)
233. Marton M, Michniak P, Behul M, Rehacek V, Vojs Stanova A, Redhammer R, Vojs M. 2019 Bismuth modified boron doped diamond electrode for simultaneous determination of Zn, Cd and Pb ions by square wave anodic stripping voltammetry: influence of boron concentration and surface morphology. *Vacuum* **167**, 182–188. (doi:10.1016/j.vacuum.2019.06.012)
234. Yang N, Gao F, Nebel CE. 2013 Diamond decorated with copper nanoparticles for electrochemical reduction of carbon dioxide. *Anal. Chem.* **85**, 5764–5769. (doi:10.1021/ac400377y)
235. Verlato E, Barison S, Einaga Y, Fasolin S, Musiani M, Nasi L, Natsui K, Paolucci F, Valenti G. 2019 CO<sub>2</sub> reduction to formic acid at low overpotential on BDD electrodes modified with nanostructured CeO<sub>2</sub>. *J. Mater. Chem.* **7**, 17896–17905. (doi:10.1039/C9TA01000A)
236. Jiwanti PK, Einaga Y. 2020 Further study of CO<sub>2</sub> electrochemical reduction on palladium modified BDD electrode: influence of electrolyte. *Chem. Asian J.* **15**, 910–919. (doi:10.1002/asia.201901669)
237. Jiwanti PK, Ichzan AM, Dewandaru RKP, Atriardi SR, Einaga Y, Ivandini TA. 2020 Improving the CO<sub>2</sub> electrochemical reduction to formic acid using iridium-oxide-modified boron-doped diamond electrodes. *Diam. Relat. Mater.* **106**, 107874. (doi:10.1016/j.diamond.2020.107874)
238. Jiwanti PK, Natsui K, Nakata K, Einaga Y. 2018 The electrochemical production of C<sub>2</sub>/C<sub>3</sub> species from carbon dioxide on copper-modified boron-doped diamond electrodes. *Electrochimica Acta* **266**, 414–419. (doi:10.1016/j.electacta.2018.02.041)
239. Bossel U, Eliasson B. 2003 *Energy and the Hydrogen Economy, AFDC Report (2003)*. See [https://afdc.energy.gov/files/pdfs/hyd\\_economy\\_bossel\\_eliasson.pdf](https://afdc.energy.gov/files/pdfs/hyd_economy_bossel_eliasson.pdf) (accessed 22 March 2025).
240. Brillas E, Martínez-Huitle CA. 2011 *Synthetic diamond films: preparation, electrochemistry, characterization, and applications*. New York, NY: Wiley-Blackwell.
241. He Y, Lin H, Guo Z, Zhang W, Li H, Huang W. 2019 Recent developments and advances in boron-doped diamond electrodes for electrochemical oxidation of organic pollutants. *Sep. Purif. Technol.* **212**, 802–821. (doi:10.1016/j.seppur.2018.11.056)
242. Al-Abdallat Y, Jumah I, Jumah R, Ghanem H, Telfah A. 2020 Catalytic electrochemical water splitting using boron doped diamond (BDD) electrodes as a promising energy resource and storage solution. *Energies* **13**, 5265. (doi:10.3390/en13205265)
243. Geiger S, Kasian O, Mingers AM, Nicley SS, Haenen K, Mayrhofer KJJ, Cherevko S. 2017 Catalyst stability benchmarking for the oxygen evolution reaction: the importance of backing electrode material and dissolution in accelerated aging studies. *ChemSusChem* **10**, 4140–4143. (doi:10.1002/cssc.201701523)

244. Ashcheulov P *et al.* 2018 Nanocrystalline boron-doped diamond as a corrosion-resistant anode for water oxidation via Si photoelectrodes. *ACS Appl. Mater. Interfaces* **10**, 29552–29564. (doi:10.1021/acsami.8b08714)
245. Behúl M *et al.* 2020 Nanostructured boron doped diamond enhancing the photoelectrochemical performance of TiO<sub>2</sub>/BDD heterojunction anodes. *Vacuum* **171**, 109006. (doi:10.1016/j.vacuum.2019.109006)
246. Mavrokefalos CK, Hasan M, Rohan JF, Compton RG, Foord JS. 2017 Electrochemically deposited Cu<sub>2</sub>O cubic particles on boron doped diamond substrate as efficient photocathode for solar hydrogen generation. *Appl. Surf. Sci.* **408**, 125–134. (doi:10.1016/j.apsusc.2017.02.148)
247. Qiu Y, Pan Z, Chen H, Ye D, Guo L, Fan Z, Yang S. 2019 Current progress in developing metal oxide nanoarrays-based photoanodes for photoelectrochemical water splitting. *Sci. Bull.* **64**, 1348–1380. (doi:10.1016/j.scib.2019.07.017)
248. Clematis D, Panizza M. 2021 Application of boron-doped diamond electrodes for electrochemical oxidation of real wastewaters. *Curr. Opin. Electrochem.* **30**, 100844. (doi:10.1016/j.coelec.2021.100844)
249. Martínez-Huitle CA, Brillas E. 2021 A critical review over the electrochemical disinfection of bacteria in synthetic and real wastewaters using a boron-doped diamond anode. *Curr. Opin. Solid State Mater. Sci.* **25**, 100926. (doi:10.1016/j.cossms.2021.100926)
250. Brosler P, Girão AV, Silva RF, Tedim J, Oliveira FJ. 2023 In-house vs. commercial boron-doped diamond electrodes for electrochemical degradation of water pollutants: a critical review. *Front. Mater.* **10**. (doi:10.3389/fmats.2023.1020649)
251. Li D, Qu J. 2009 The progress of catalytic technologies in water purification: a review. *J. Environ. Sci.* **21**, 713–719. (doi:10.1016/s1001-0742(08)62329-3)
252. De Luna Y, Bensalah N. 2022 Review on the electrochemical oxidation of endocrine-disrupting chemicals using BDD anodes. *Curr. Opin. Electrochem.* **32**, 100900. (doi:10.1016/j.coelec.2021.100900)
253. La Merrill MA *et al.* 2020 Consensus on the key characteristics of endocrine-disrupting chemicals as a basis for hazard identification. *Nat. Rev. Endocrinol.* **16**, 45–57. (doi:10.1038/s41574-019-0273-8)
254. Enozo. See <https://enozo.com/> (accessed 22 March 2025).
255. Nebel CE. 2013 A source of energetic electrons. *Nat. Mater.* **12**, 780–781. (doi:10.1038/nmat3714)
256. Hamers RJ, Bandy JA, Zhu D, Zhang L. 2014 Photoemission from diamond films and substrates into water: dynamics of solvated electrons and implications for diamond photoelectrochemistry. *Faraday Discuss* **172**, 397–411. (doi:10.1039/c4fd00039k)
257. Raymakers J, Haenen K, Maes W. 2019 Diamond surface functionalization: from gemstone to photoelectrochemical applications. *J. Mater. Chem. C* **7**, 10134–10165. (doi:10.1039/c9tc03381e)
258. Christianson JR, Zhu D, Hamers RJ, Schmidt JR. 2014 Mechanism of N<sub>2</sub> reduction to NH<sub>3</sub> by aqueous solvated electrons. *J. Phys. Chem. B* **118**, 195–203. (doi:10.1021/jp406535p)
259. Zhu D, Zhang L, Ruther RE, Hamers RJ. 2013 Photo-illuminated diamond as a solid-state source of solvated electrons in water for nitrogen reduction. *Nat. Mater.* **12**, 836–841. (doi:10.1038/nmat3696)
260. Zhu D, Bandy JA, Li S, Hamers RJ. 2016 Amino-terminated diamond surfaces: photoelectron emission and photocatalytic properties. *Surf. Sci.* **650**, 295–301. (doi:10.1016/j.susc.2016.01.003)
261. Li S, Bandy JA, Hamers RJ. 2018 Enhanced photocatalytic activity of diamond thin films using embedded Ag nanoparticles. *ACS Appl. Mater. Interfaces* **10**, 5395–5403. (doi:10.1021/acsami.7b13821)
262. Zhang L, Zhu D, Nathanson GM, Hamers RJ. 2014 Selective Photoelectrochemical Reduction of Aqueous CO<sub>2</sub> to CO by Solvated Electrons. *Angew. Chem. Int. Ed.* **53**, 9746–9750. (doi:10.1002/anie.201404328)
263. Bachman BF, Zhu D, Bandy J, Zhang L, Hamers RJ. 2022 Detection of aqueous solvated electrons produced by photoemission from solids using transient absorption measurements. *ACS Meas. Sci. Au* **2**, 46–56. (doi:10.1021/acsmesuresciau.1c00025)

264. Sussmann R (ed). 2009 *CVD diamond for electronic devices and sensors*. Chichester, West Sussex, UK: Wiley. (doi:10.1002/9780470740392)
265. Donato N, Rouger N, Pernot J, Longobardi G, Udrea F. 2020 Diamond power devices: state of the art, modelling, figures of merit and future perspective. *J. Phys. D* **53**, 093001. (doi:10.1088/1361-6463/ab4eab)
266. Araujo D, Suzuki M, Lloret F, Alba G, Villar P. 2021 Diamond for electronics: materials, processing and devices. *Materials* **14**, 7081. (doi:10.3390/ma14227081)
267. Koizumi S, Umezawa H, Pernot J, Suzuki M (eds). 2018 *Power electronics device applications of diamond semiconductors*. Cambridge, UK: Woodhead Publishing. (Woodhead Publishing Series in Electronic and Optical Materials).
268. Statista. Electricity lost in transmission in the United Kingdom (UK) in selected years from 1970 to 2021. See <https://www.statista.com/statistics/550583/electricity-losses-in-transmission-uk/> (accessed 22 March 2025).
269. Gurbuza Y, Esame O, Tekin I, Kang WP, Davidson JL. 2005 Diamond semiconductor technology for RF device applications. *Solid State Electron.* **49**, 1055–1070. (doi:10.1016/j.sse.2005.04.005)
270. Bormashov VS, Terentiev SA, Buga SG, Tarelkin SA, Volkov AP, Teteruk DV, Kornilov NV, Kuznetsov MS, Blank VD. 2017 Thin large area vertical Schottky barrier diamond diodes with low on-resistance made by ion-beam assisted lift-off technique. *Diam. Relat. Mater.* **75**, 78–84. (doi:10.1016/j.diamond.2017.02.006)
271. Traoré A, Muret P, Fiori A, Eon D, Gheeraert E, Pernot J. 2014 Zr/oxidized diamond interface for high power Schottky diodes. *Appl. Phys. Lett.* **104**, 052105. (doi:10.1063/1.4864060)
272. Saremi M, Hathwar R, Dutta M, Koeck FAM, Nemanich RJ, Chowdhury S, Goodnick SM. 2017 Analysis of the reverse I-V characteristics of diamond-based PIN diodes. *Appl. Phys. Lett.* **111**, 043507. (doi:10.1063/1.4986756)
273. Liu J, Koide Y. 2018 An overview of high-k oxides on hydrogenated-diamond for metal-oxide-semiconductor capacitors and field-effect transistors. *Sensors* **18**, 1813. (doi:10.3390/s18061813)
274. Pham TT, Maréchal A, Muret P, Eon D, Gheeraert E, Rouger N, Pernot J. 2018 Comprehensive electrical analysis of metal/Al<sub>2</sub>O<sub>3</sub>/O-terminated diamond capacitance. *J. Appl. Phys.* **123**, 161523. (doi:10.1063/1.4996114)
275. Matsumoto T, Kato H, Oyama K, Makino T, Ogura M, Takeuchi D, Inokuma T, Tokuda N, Yamasaki S. 2016 Inversion channel diamond metal-oxide-semiconductor field-effect transistor with normally off characteristics. *Sci. Rep.* **6**, 31585. (doi:10.1038/srep31585)
276. Butler JE. 2017 Nanometric diamond delta doping with boron. *Phys. Status Solidi RRL* **11**, 1600329. (doi:10.1002/pssr.201600329)
277. Kawarada H *et al.* 2017 Durability-enhanced two-dimensional hole gas of C-H diamond surface for complementary power inverter applications. *Sci. Rep.* **7**, 42368. (doi:10.1038/srep42368)
278. Praver S, Aharonovich I (eds). 2014 *Quantum information processing with diamond: principles and applications*. Cambridge, UK: Elsevier, Woodhead.
279. Nebel CE. 2020 Nitrogen-vacancy doped CVD diamond for quantum applications: a review. *Semicond. Semimetals* **103**, 73–136. (doi:10.1016/bs.semsem.2020.03.004)
280. Thiering G, Gali A. 2020 Color centers in diamond for quantum applications. *Semicond. Semimetals* **103**, 1–36. (doi:10.1016/bs.semsem.2020.03.001)
281. Jeske J *et al.* 2017 Stimulated emission from nitrogen-vacancy centres in diamond. *Nat. Commun.* **8**, 14000. (doi:10.1038/ncomms14000)
282. Arute F *et al.* 2019 Quantum supremacy using a programmable superconducting processor. *Nature* **574**, 505–510. (doi:10.1038/s41586-019-1666-5)
283. Togan E *et al.* 2010 Quantum entanglement between an optical photon and a solid-state spin qubit. *Nature New Biol.* **466**, 730–735. (doi:10.1038/nature09256)
284. Liu S, Yu R, Li J, Wu Y. 2013 Creation of quantum entanglement with two separate diamond nitrogen vacancy centers coupled to a photonic molecule. *J. Appl. Phys.* **114**, 244306. (doi:10.1063/1.4856935)
285. Bernien H *et al.* 2013 Heralded entanglement between solid-state qubits separated by three metres. *Nature* **497**, 86–90. (doi:10.1038/nature12016)

286. Hensen B *et al.* 2015 Loophole-free Bell inequality violation using electron spins separated by 1.3 kilometres. *Nature* **526**, 682–686. (doi:10.1038/nature15759)
287. Bradley CE, Randall J, Abobeih MH, Berrevoets RC, Degen MJ, Bakker MA, Markham M, Twitchen DJ, Taminiou TH. 2019 A ten-qubit solid-state spin register with quantum memory up to one minute. *Phys. Rev. X* **9**, 031045. (doi:10.1103/physrevx.9.031045)
288. van der Sar T *et al.* 2012 Decoherence-protected quantum gates for a hybrid solid-state spin register. *Nature* **484**, 82–86. (doi:10.1038/nature10900)
289. Neumann P, Beck J, Steiner M, Rempp F, Fedder H, Hemmer PR, Wrachtrup J, Jelezko F. 2010 Single-shot readout of a single nuclear spin. *Science* **329**, 542–544. (doi:10.1126/science.1189075)
290. Liu K *et al.* 2021 Tailoring of typical color centers in diamond for photonics. *Adv. Mater.* **33**, e2000891. (doi:10.1002/adma.202000891)
291. Nakazato T, Reyes R, Imaiike N, Matsuda K, Tsurumoto K, Sekiguchi Y, Kosaka H. 2022 Quantum error correction of spin quantum memories in diamond under a zero magnetic field. *Commun. Phys.* **5**, 102. (doi:10.1038/s42005-022-00875-6)
292. Pezzagna S, Meijer J. 2021 Quantum computer based on color centers in diamond. *Appl. Phys. Rev.* **8**, 011308. (doi:10.1063/5.0007444)
293. Beveratos A, Brouri R, Gacoin T, Villing A, Poizat JP, Grangier P. 2002 Single photon quantum cryptography. *Phys. Rev. Lett.* **89**, 187901. (doi:10.1103/physrevlett.89.187901)
294. Kucsko G, Maurer PC, Yao NY, Kubo M, Noh HJ, Lo PK, Park H, Lukin MD. 2013 Nanometre-scale thermometry in a living cell. *Nature* **500**, 54–58. (doi:10.1038/nature12373)
295. Balasubramanian G *et al.* 2008 Nanoscale imaging magnetometry with diamond spins under ambient conditions. *Nature* **455**, 648–651. (doi:10.1038/nature07278)
296. Degen CL. 2008 Scanning magnetic field microscope with a diamond single-spin sensor. *Appl. Phys. Lett.* **92**, 243111. (doi:10.1063/1.2943282)
297. Taylor JM, Cappellaro P, Childress L, Jiang L, Budker D, Hemmer PR, Yacoby A, Walsworth R, Lukin MD. 2008 High-sensitivity diamond magnetometer with nanoscale resolution. *Nat. Phys.* **4**, 810–816. (doi:10.1038/nphys1075)
298. QDTI. See <https://qdti.com/> (accessed 22 March 2025).
299. Nvision. See <https://www.nvision-imaging.com/> (accessed 22 March 2025).
300. Qnami. See <https://qnami.ch/> (accessed 22 March 2025).
301. Zimmisky P. 2022 *What a Mature Lab-Grown Diamond Jewelry Market Could Look Like*. Paul Zimmisky Diamond Analytics website. See <https://www.paulzimmisky.com/What-a-Mature-Lab-Grown-Diamond-Jewelry-Market-Could-Look-Like/> (accessed 22 March 2025).
302. Drucker R. 2023 *Gem Focus - August 2023 - Featuring Lab-Grown Diamonds: the topic that consumes us*. Gemworld International. See <https://www.gemguide.com/gem-focus-august-2023-featuring-lab-grown-diamonds-the-topic-that-consumes-us/> (accessed 22 March 2025).
303. May PW, Zulkharnay R. 2025 Supplementary material for: Diamond thin films: a 21st century material. Part 2: a new hope. University of Bristol Repository. (doi:10.5523/bris.1x6x8faofwfyf2s2jgdjclw683)
304. May PW, Zulkharnay R. 2025 Supplementary material from: Diamond thin films: a twenty-first century material. Part 2: a new hope. Figshare. (doi:10.6084/m9.figshare.c.7766570)